Kunal Kumar Mishra

GAS SENSOR BASED ON EPITAXIAL GRAPHENE FOR NO_2 SENSING

Thesis submitted in partial fulfillment of the requirements for the degree of Master of Science in Technology.

Espoo, 16.07.2014

Supervisor:

Hele Savin
Assistant Professor

Instructor:

Serguei Novikov
Senior Researcher

Aalto University
School of Electrical
Engineering

AALTO UNIVERSITY SCHOOL OF ELECTRICAL ENGINEERING
Department of Micro and Nano-sciences
ABSTRACT OF THE MASTER´S THESIS

Author: Kunal Kumar Mishra

Subject of the thesis:
Gas sensor based on epitaxial graphene for NO_2 sensing

Number of pages: 9 + 73	Date: 16.7.2014
Professorship: Micro and Nanoelectronics	Code of professorship: S-69
Supervisor: Assistant Professor Hele Savin	
Instructor: Senior Researcher Serguei Novikov	

Graphene based gas sensor has been a major trend in the field of scientific research for gas detection. The stable two-dimensional structure, outstanding electronic properties and compatibility with CMOS processing makes it an ideal candidate for a cheap, effective ultrasensitive gas sensor. The purpose of this thesis is to investigate the sensitivity of the epitaxial graphene based gas sensor at low concentrations of NO_2 gas. It also studies the effect of humidity and temperature on the sensitivity of the sensor for its practical application.

An epitaxial graphene layer was grown on 4H-SiC substrate at temperature suitable for monolayer graphene. The graphene layer was characterized using Atomic force Microscope (AFM) for surface morphology and Auger Electron Spectroscopy (AES) for number of graphene layers. Six sensors samples were fabricated using the grown epitaxial graphene layer for evaluating the stability in the sensitivity of the sensors to NO_2 exposure. The sensitivity was calculated as the relative change in their resistance on the detection of a test gas. Initially, the drifts of the sensors were measured and the effects of temperature and humidity on their drifts were also evaluated. They were then exposed to four different lower concentrations of NO_2 gas i.e. 0.1 ppb, 0.2 ppb, 0.5ppb and 1ppb. The sensitivities of the sensors were found to be proportional to the concentration of NO_2 gas.

The effect of humidity on the sensitivity of the sensor has been outlined by comparing the sensor responses with exposure to NO_2 in dry carrier gas (Relative Humidity, RH=0.02%) and the NO_2 gas in humidified carrier gas (RH=50%). It has been observed that increase in humidity causes improvement in the sensitivity of the sensors at low NO_2 concentrations. There was 2.725% improvement in the sensitivity at 1ppb NO_2 concentration under humid condition. Similarly, the effect of temperature on the sensitivity has been ascertained by comparing the measurements at room temperature and at an elevated temperature. At the elevated temperature (110°C), the sensitivities of the sensors decreased compared to their responses at room temperature (20°C). There was 2.86% decrease in the sensitivity at 1ppb NO_2 concentration at elevated temperature.

Keywords: Gas sensor, NO_2, Epitaxial graphene, Monolayer, Ultra-sensitive, Low concentration, High temperature, Humidity, Selectivity	Publishing language: English

Preface

This Master's Thesis has been conducted in Micronova as a project of Electron Physics Group in Department of Micro and Nano-sciences, Aalto University School of Electrical Engineering.

First of all, I express sincere gratitude to my Thesis supervisor, Prof. Hele Savin for providing me an opportunity to work on this interesting topic. I am very grateful to my Thesis instructor, Dr. Serguei Novikov for his inspiring guidance, insightful advices and genuine support. His invaluable experience and critical feedbacks helped me gain better understanding about the critical aspects of graphene and gas sensors.

I extend my thanks to Henri Jusilla for providing me training on operation of Atomic Force Microscope. Lots of thanks go to Natalia Lebedeva for all her helps during the fabrication, experiments and documentation processes. I also want to thank Ville Vähänissi for his technical support and advices regarding the thesis work. I would like to express my warmest appreciation to all my colleagues of Electron Physics Group who has directly or indirectly helped me during my stay.

Mere words are not enough to express my gratitude to my parents, my sisters and my brother for their love and encouragement in every step of my life.

Espoo, 16th July, 2014

Kunal Kumar Mishra

Table of Contents

List of Symbols and Abbreviations:

AES	Auger Electron Spectroscopy
AFM	Atomic Force Microscope
Ar	Argon
Au	Gold
C	Carbon
cm	centimeter
CMA	Cylindrical Mirror Analyzer
CMOS	Complementary Metal Oxide Semiconductor
CNT	Carbon Nano-Tubes
Co	Cobalt
CO_2	Carbon dioxide
Cu	Copper
CVD	Chemical Vapor Deposition
^{O}C	Degree Celsius
EBES	Electron Beam Evaporation System
eV	electron volt
FET	Field Effect Transistor
FIB	Focused Ion Beam
FLG	Few Layer Graphene
H	Hydrogen
H_2O	Hydrogen Dioxide
H_2O_2	Hydrogen Peroxide
HCl	Hydrogen Chloride
HF	Hydrogen Fluoride
HNO_3	Hydrogen Nitrate (also known as Nitric acid)
HOMO	Highest Occupied Molecular Orbital
In_2O_3	Indium (III) Oxide
Ir	Iridium
KHz	Kilo Hertz
LDA	Local Density Approximation
LEED	Low Energy Electron Diffraction

LUMO	Lowest Unoccupied Molecular Orbital
MFC	Mass Flow Controller
mm	millimeter
N_2	Nitrogen
NH_3	Ammonia
NH_4OH	Ammonium Hydroxide
Ni	Nickel
nm	nanometer
O_2	Oxygen
OTG	Ozone Treated Graphene
Pd	Palladium
ppm	Parts Per Million
ppb	Parts Per Billion
ppt	Parts Per Trillion
Pt	Platinum
PVD	Physical Vapor Deposition
RCA-1	Radio Corporation of America-1 (also known as Standard Clean-1 (SC-1))
Rh	Rhodium
RH	Relative Humidity
RHEED	Reflection High Energy Electron Diffraction
RIE	Reactive Ion Etching
Ru	Ruthenium
sccm	Standard Cubic Centimeters per Minute
Si	Silicon
SiC	Silicon Carbide
SLG	Single Layer Graphene
SnO_2	Tin Oxide
Ti	Titanium
UHV	Ultra High Vacuum
UV	Ultra-Violet
µm	Micrometer
WO_3	Tungsten Trioxide
ZnO	Zinc Oxide

List of Figures:

List of Tables:

1. Introduction to Graphene based gas sensors

1.1 Gas Sensors

Now-a-days, gas sensors are prevalent in various forms for the detection of combustible, flammable and toxic gases. With the growing concerns of environment pollution and its hazardous effects, the role of cost effective, highly sensitive and selective gas sensors for detection of these gaseous elements is growing rapidly. Especially in the case of harmful gases like NO_2, there has been a constant, continuous effort to detect their lowest possible concentration. NO_2 is an important indicator of environment pollution. Only one percent of NO_2 is formed naturally; ninety nine percent are produced as a by-product of fuel consumption. In atmosphere, it reacts with water molecules to form nitric acid. Nitric acid causes acid rain which is detrimental to the environment. As per European Commission Air Quality Standards, NO_2 concentration in atmosphere should not exceed the limit of 30ppb over an average period of one year. In order to detect such a low concentration, we need a smaller, cheaper and portable ultrasensitive gas sensor.

Electro-chemical gas sensors are small, portable and power efficient sensors which detects through the electrochemical reaction between the sensing electrode and target gas. Electrochemical reaction leads to cross sensitivity, poor selectivity and negatively impacts the lifetime of the sensor device. Infrared gas sensor utilizes adsorption of IR radiation at specific molecular vibrational frequencies to detect target gas in proportion to their concentration. They are more sensitive with longer lifetimes (more than ten years), but are more expensive, cumbersome and sensitive to temperature variation. Traditionally, transition metal oxides such as In_2O_3, SnO_2, ZnO and WO_3 based gas sensors have been also used for NO_2 detection [1]. However, these sensors suffered from lower concentration detection and the sensing response being dependent on the growth process and process conditions. Carbon Nano-tubes (CNTs) based gas sensors have exhibited fast responses and high sensitivity for detection of small concentrations of toxic gases at room temperature but their uses were limited by precision degradation by noise signal and performance reduction in networks [2, 3]. Recently, the researchers have successfully demonstrated the graphene based gas sensors which are cheaper, stable and have potential to trace gases at extremely low concentration [4]. Schedin et al. have

mentioned that graphene inserted in a multi-terminal Hall bars device can even detect a single molecule of NO_2. So, this work primarily focuses on the detection of a very low concentration of NO_2 gas using epitaxial graphene based gas sensor.

Graphene is a two dimensional layer carbon atoms arranged in honey comb structure. It is available in monolayer, bi-layer, few layers or multiple layer form. The two dimensional structure of graphene allows full exposure of its atoms to the adsorbing gaseous molecules. As a result, the electrical properties of graphene are strongly affected by adsorption of gaseous molecules. The graphene also possess inherently low electrical noise due to quality of crystal lattice and low charge fluctuation [5]. In addition, graphene allows integration at wafer scale using the conventional lithographic approaches with potential of a rapid and low cost production of sensors at low power consumption. Hence, the high surface to volume ratio, low electrical noise, high charge transport properties and compatibility with CMOS processing have made graphene suitable for making an ultrasensitive gas sensor [4].

1.2 Background of the Graphene based sensor for NO_2 detection

This section provides a summarized description of the results of some important researches in the field of graphene based NO_2 sensing. It highlights and briefly discusses those progresses that have been done and could prove as a corner stone for the further research.

To begin with, the study of ultrasensitive NO_2 detection by epitaxially grown graphene by R. Pearce et al. [6] shows that graphene grown on SiC substrate possess n-type characteristics due to transfer of electrons from SiC to graphene. The characteristics of graphene layer depend on the substrate over which it is fabricated. Upon high concentration of NO_2 exposure, there is transition from n-type conductivity of graphene layer to p-type due to electron with drawing nature of NO_2; making holes a majority carrier on graphene surface and leading to decrease in resistance of graphene layer at further exposure. The response and recovery time improve with increase in temperature. Also, the response of single layer graphene sensor is better than the multilayer graphene sensor due to the screening effect i.e. current passing through the non-exposed layers of multilayer graphene.

Chen et al. [4] performed experiment in inert condition using Ar and N_2 gas to study the intrinsic sensing potential of graphene and the effect of UV light illumination. The conductance of the

sensor increases by ~1% upon the exposure of 40 ppt of NO_2 for 5 min in a N_2 flow. It also shows ultra sensitivity along with excellent reversibility and reproducibility. The change in resistance or conductance of the sensor is proportional to the concentration of NO_2 gas. The detection limit is estimated to be 2.06 ppt. The UV light illumination plays a role of cleaning the graphene surface during the course of detection.

S. Novikov et al. [7] studied the difference in the sensitivity of the graphene obtained using 4HSiC and CVD grown graphene. He also found that the resistance of both the sensors decreased with exposure to NO_2. However, the former shows higher response even in low concentration. With increase in concentration, the sensitivity reduces due to the saturation of graphene surface with the exposed concentration of NO_2. There is increase in sensitivity of NO_2 detection under heating or UV light illumination or in presence of humid air. For 4HSiC sample, heating was proved to be the best way to increase the sensitivity.

Essore Massera et al. [5] performed comparison between the performances of graphene based sensor manufactured using two different approaches i.e. exfoliated graphene from scotch tape method placed in chemi-resistor architecture and graphene sheet obtained from chemical exfoliation method deposited on Au transducers for NO_2 detection. They found that the first method was unsuitable for sensor fabrication as the electrode deposition by FIB caused damage the crystal lattice of the graphene layer and produces the characteristic different from the reported one. The later produced coherent characteristic and was used to study the effects of humidity on NO_2 detection. They concluded that the increase in humidity level in the carrier produces increase in the device conductance proportional to the measured humidity level.

Nomani et al. [8] studied the sensitivity of graphene sensor for NO_2 detection using two different sensors made up of graphene grown on Si and C face of SiC substrate. It was found that the overall sensitivity of both the sensors was better than the sensitivity obtained using the sensors with graphene obtained from exfoliated method and reduction of graphene oxide. The opposite conductance change was observed using Si and C face graphene sensor. For Si-face sensor, the increase in conductance indicated the p-type nature of the graphene, while for C-face sensor; the decrease in conductance indicated the n-type nature of the graphene. The role of temperature for NO_2 sensing was also studied for both the sensors. Both these sensors showed faster responses and shorter recovery times at high temperature. The shorter recovery time was attributed to the

faster desorption of NO_2 molecules. The change in conductance of Si-face sensor reached saturation at 300°C and the response time was smaller than that of C-face sensor. The reason for the appearance of kinks in the response of both the sensors at higher temperature at the initial stage of NO_2 flow remains unknown. The selectivity of NO_2 detection under interfering gases was studied by applying a series of gases such as N_2, NH_3, CO_2, O_2 and H_2O along with NO_2 on the Si-face sensor at 300°C. It was found that the response on NO_2 detection was in opposite direction and transient time faster than the responses of other gases. The Si-face sensor exhibited sufficient selectivity and stability under constant operating conditions confirming its usability in sensing application.

F. Schedin et al. [9] also studied the graphene based gas sensor for NO_2 detection and found that the changes in the conductivity of the graphene layer on exposure to NO_2 gas are quantized with each event representing adsorption or desorption of a single NO_2 molecule.

There are several other studies done for graphene based NO_2 sensing in modified condition:

Chung et al. [10] studied NO_2 detection using ozone treated graphene sensor (OTG). In comparison to a pristine graphene sensor, the use of OTG sensor showed the percentage response improved by a factor of 2 and response time by a factor of 8 when it was exposed to 200 ppm concentration of NO_2 at room temperature. This improvement in the response is caused by oxygen groups from ozone treatment which increases the number of favorable sites for NO_2 adsorption. While a pristine graphene sensor could not detect NO_2 molecules below 10ppm concentration, the detection limit of OTG sensor was estimated to be 1.3 ppb. The NO_2 molecules are adsorbed at the low energy binding sites of graphene or on high energy binding sites of the oxygen in ozone. While the response time in case of pristine graphene sensor is recoverable; upon the exposure of graphene to ozone, the high energy binding sites are tightly held by NO_2 molecules resulting in non-recoverable response.

While investigating graphene based back gated field effect transistor for NO_2 detection, A. K. Singh et al. [11] proposed that the electrical tunability of the graphene and hence the sensitivity of the graphene based FETs can be controlled with appropriate back gate bias. Since the carrier concentration changes and the Fermi level movement acts together to enhance the detection

sensitivity, the sensitivity of p-type graphene can be better than the n-type graphene for the detection of electron withdrawing NO_2 gas.

The encouraging results of the above researches provided a strong motivation and a crucial basis for studying and understanding the characteristics of the epitaxial based graphene sensor at lower concentrations of NO_2 gas.

1.3 Structure of the thesis

The thesis report starts with the introduction about the gas sensor and its various types. It highlights the importance of ultrasensitive graphene based NO_2 sensor, gives the background of the researches in this field and discusses the organization of the report in chapter 1. Chapter 2 focuses on understanding of the graphene and its electronic properties. It discusses various available methods for graphene layer fabrication with their pros and cons. Description of the working principle of the graphene based gas sensors, and the impacts of temperature and humidity on their sensing responses are also provided. Chapter 3 presents the details about processes involved in fabrication of the sensor device and working principles of those processes. Chapter 4 includes the description of the measurement set up used for examining the responses of the sensor samples. Details about the softwares included in managing and controlling the devices, and explanation about the approaches involved during the measurement are given. Chapter 5 presents the results of the studies of the characterization of the fabricated sensor samples. It also deals with the measurement of the sensitivities of the epitaxial graphene sensors and the effect of temperature and humidity on their responses. Finally, chapter 6 talks about the conclusion of this thesis work and provide the possible grounds for further research in this field.

2. Graphene

Graphene is a two dimensional layer (2D) allotrope of carbon with single atomic layer thickness. The carbons atoms are arranged in hexagonal structure and can be considered as benzene stripped out of their hydrogen atoms. It is the basic structural element for the formation of other carbon allotropes. Fullerenes are formed by wrapping up of graphene. Carbon nanotubes, CNTs (1D) are obtained by folding graphene layer in cylindrical form with varying diameter and length. Graphite (3D) consists of multiple graphene layers deposited one on the other, weakly coupled by van der Waals force. Graphene has a high electron mobility of ~200000 cm^2/Vs, a carrier density of ~$10^{12}/cm^2$ and a corresponding resistivity of ~10^{-6} Ω-cm [4]. It is good conductor of heat and electricity. It is transparent and biocompatible. Mechanical flexing or strain does not degrade the electronic properties of graphene offering an advantage of flexible sensors which can be integrated with numerous smart systems [12]. The distinctive mechanical, thermal and electrical properties of graphene have invited strong interest among the researchers.

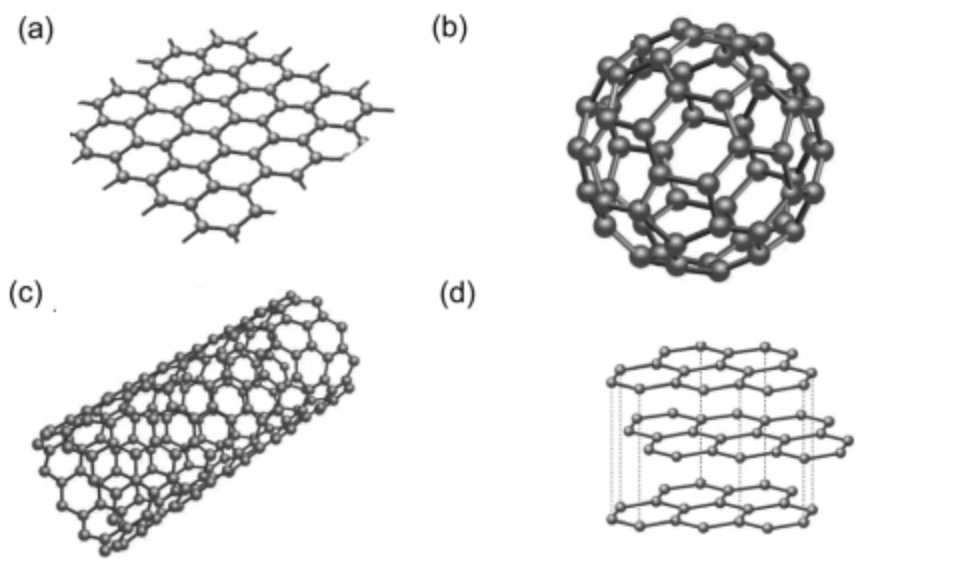

Figure 2-1: Allotropes of carbon (a) graphene, (b) fullerene, (c) carbon nano-tube (CNT), and (d) graphite [13]

2.1 Electronic Structure of Graphene

Honey comb structure of graphene is formed by sp^2 hybridized carbon atoms. C atom ($1s^2$ $2s^2$ $2p^2$) has two core electrons in 1s orbital and 4 valence electrons in 2s, $2p_x$, $2p_y$ and $2p_z$ orbitals.

With sp^2 hybridization, 2s, $2p_x$ and $2p_y$ (assume) forms a triangular planer structure of 3 σ-orbitals with mutual angle of 120^o in x-y plane and the remaining un-hybridized $2p_z$ orbital is perpendicular to the plane. The 3 σ-orbitals form strong σ-bonds with three adjacent C atoms and the un-hybridized $2p_z$ orbital forms the π bond with an adjacent C atom. The tight σ-bonds provide structural rigidity but σ-electrons do not contribute to conduction. However, the π and π* orbitals, formed from one of the p-orbital that remains unaffected, behave as valence band and conduction band respectively and contribute to conduction. The graphene lattice structure consists of two atoms (A and B) per unit cell. The valence bands and conduction bands come in close contact at six points within the Brillouin zone where the low energy dispersion relations are almost linear and have zero effective mass. The electrons in these low energy regions behave as relativistic quasi particles or "Dirac fermions" that follow Dirac equations. Dirac points, the points (K and K') where the conduction bands and the valence bands meet, results in zero bandgap making graphene layer to behave as a semi-metal [14, 15]. Since the Fermi level is located at the converging point of the bi-conical structure, it leads to a low conductivity of intrinsic graphene. A very high conductivity can be achieved by varying Fermi level under the influence of electric field and changing the nature of graphene to either n-type or p-type.

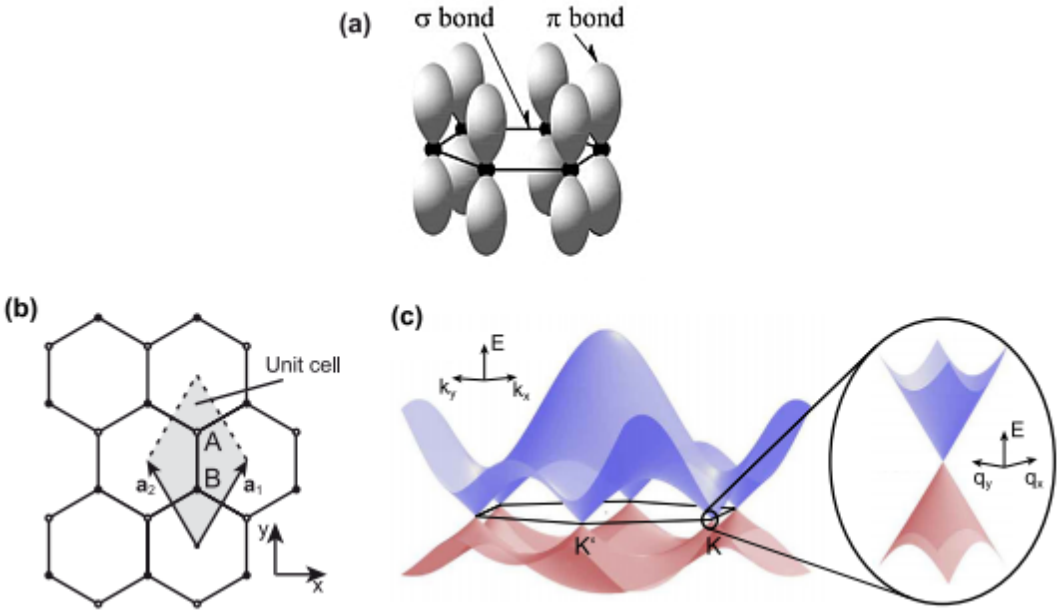

Figure 2-2: (a) Bond structure in graphene, (b) Graphene lattice structure, and (c) Electronic dispersion of graphene [16]

2.2 Epitaxial Graphene

A convenient method for mass production of graphene layer has been a challenge for graphene based devices. Several methods have already been developed to produce single layer graphene (SLG) as well as few layer graphene (FLG) sheets. When graphene was discovered by Andre Geim and Kostya Novoselov in 2004 at University of Manchester, they used scotch tape method to obtain graphene layers and then transferred them from the tape onto small pieces of Si substrate with few nanometers of oxide layer. This method possesses no control on the number of layers and is an inefficient process that is unsuitable for large-scale production. Graphene production from the reduction of graphene oxide has also been reported. However, Hydrazine, a toxic chemical used in the decomposition introduces extra nitrogen which can affect the sensing response [17].

Other methods like chemical exfoliation, unzipping of carbon nano-tubes also exit. One of the prevalent methods for graphene production is epitaxial graphene growth using chemical vapor deposition (CVD): Thermal CVD and plasma enhanced CVD. The plasma enhanced CVD process is suitable for low temperature synthesis. In CVD method, the growth of graphene takes place on metals Co, Ni, Cu, or sometimes noble metals like Ru, Rh, Pd, Ir and Pt. These metals act as a catalyst for the thermal decomposition of carbon source, usually some gas containing carbon atoms. However, the control of temperature, gaseous flow rate and transfer of graphene layer have been challenging for the deposition of SLG and FLG.

The most popular method for production of a high quality epitaxial graphene layer is graphitization. The thermal treatment of epitaxially matched surface like silicon carbide (SiC) takes place at ~1500^{o}C under vacuum which results in sublimation of silicon atoms while the carbon enriched surface undergoes a reorganization leading to graphitization. The number and quality of graphene layer deposition depends on various factors such as surface cleaning of SiC substrate, decomposition temperature, duration of annealing, etc. Atomic Force Microscopy (AFM) is used to analyze the surface topology and Raman Spectrum analysis is used to determine the crystal coherence length and the thickness of epitaxial graphene.

The growth of epitaxial graphene is not uniform along all the faces of SiC substrate. The graphene growth on the Si side of SiC substrate is slow and continues only for small span of time leading to a thin layer. However, the growth on C side of SiC substrate does not limit and produces a thick layer of epitaxial graphene [6]. For graphene layer grown on SiC substrate, the

first layer acts as a buffer and the subsequent layer behave n-type due to the transfer of electrons from SiC substrate to the graphene layer. There is a decrease in the bandgap energy of 0.26 eV with each subsequent layer closet to SiC substrate due to shielding effect between surface of graphene and SiC [6, 18, 19].

2.2.1 Effect of temperature on the resistance of epitaxial graphene

With the increase in temperature, there is increase in the number of thermally generated electron-hole pairs in graphene layer. It causes decrease in its resistance and creates a negative coefficient of resistance of graphene which is similar to intrinsic semi-conductors. The change in resistance for a single layer graphene sensor is slower and takes a longer time to stabilize than the multi layer graphene sensor [6].

2.2.2 Effect of humidity on the resistance of epitaxial graphene

The position and orientation of H_2O molecules determine the effect of humidity on the resistance of the epitaxial graphene. When H_2O interacts with O-atom pointing towards the graphene surface, there is a small transfer of electrons to graphene while when the interaction takes place with H–atom pointing towards the graphene surface, there is a small transfer of charge to H_2O molecule. This is due to the relative position of HOMO and LUMO with respect to Dirac point. HOMO is completely located on O atom and the LUMO is mostly located on H atoms. The three different orientations are: starting with O-atom and O-H bonds pointing up (a), O-H bonds pointing down (b), and O-H bonds parallel to the graphene surface (c). In case of orientation (a), HOMO plays a predominant role. There is a small transfer of charge to graphene through mixing with graphene orbitals above Fermi level. There is also mixing of orbitals below the Dirac point, but there is no transfer of charges due to filled orbitals. In case of orientations (b) and (c), LUMO plays the dominant role and accepts some charge from graphene through mixing with graphene orbitals below Dirac point. Mixing of orbitals also takes place above the Dirac point but there is no transfer of charge due to all empty orbitals. Generally, it is found that the acceptor nature of H_2O with graphene is favorable [20].

2.3 Working principle of NO_2 graphene sensor

The working principle of graphene based gas sensor is based on the change in the electrical conductivity of graphene surface due to the absorption/desorption of gaseous molecules, which may act as donors or acceptors [8]. A monolayer graphene sheet acts as n-type by adsorbing

electron with-drawing NO_2 gas and p-type by adsorbing electron donating NH_3 gas on its surface. Its two dimensional physical structure maximizes the effect as the whole volume is available for interaction with adsorbents. It also exhibits metallic conductivity such that Johnson noise, even in the limit of no charge carriers, causes considerable relative change in carrier concentration. The inherent fewer crystal defects ensure a low excess noise by thermal switching. These features maximize the signal to noise ratio to a level sufficient for detecting changes by a single electron charge at room temperature [9].

During NO_2 gas detection, when graphene layer is exposed to NO_2 molecules, they are adsorbed on the graphene surface. Since NO_2 acts as an electron acceptor, the electron charge transfer occurs from graphene to NO_2 molecule due to its electron withdrawing power [10]. This causes accumulation of hole charge carriers on the surface of graphene layer, resulting in decrease in its resistance i.e. increase in its conductance. This is generally in the case of multilayered graphene layer. In case of single layer of graphene, there is transfer of electrons to the graphene surface from the SiC substrate and there is decrease in conductance i.e. increase in resistance with NO_2 detection.

The contamination of graphene surface of sensor with gas molecules can be reversed back to the initial stage. A short time UV light illumination can be used to clean the graphene surface by the photo-induced molecular desorption of the molecules [8]. Thermal treatment has also been used effectively for annealing graphene surface back to its pristine state [21].

2.3.1 NO_2 interaction with epitaxial graphene

When epitaxial graphene is exposed to NO_2 gas, the interaction between NO_2 and epitaxial graphene depends upon the orientation of triangular shaped NO_2 molecule and the presence of numerous adsorption sites on graphene surface. The three major adsorption configurations proposed are shown in figure 2-3. When the NO_2 molecule is bonded to the graphene surface with the nitrogen end, it is referred to as Nitro configuration. Similarly, when it is bonded to graphene surface using a single Oxygen end, the configuration is referred to as Nitrite configuration and when two Oxygen ends are involved in bonding, it is referred to as Cyclo-addition configuration. At Local Density Approximation (LDA) level, the binding energy of the adsorption structure is given by,

$$\Delta E = E(\text{absorption structure}) - E(\text{epitaxial graphene}) - E(NO_2),$$

where E(absorption structure), E(epitaxial graphene) and E(NO_2) are the total energies of fully relaxed configuration of absorption structure, epitaxial graphene and NO_2 respectively.

Due to the electron rich nature of oxygen atoms in NO_2, the binding energy of oxygen end structures is slightly higher than the nitrogen end structure. Chemical bonding with a Nitro configuration with the formation of C-N bond is the most common interaction process. This chemisorption process is endothermic and the C atom is slightly pulled up from the graphene surface. NCC bond angles are 107.4° while the third one is 103.3°. In case of CCC, two of the bond angles are 114.5° and the third one is 109°. The weak C-N bond is due to the deviation of some bond angles from the tetrahedron angle of 109.5°. Chemisorption of NO_2 on graphene surface in Nitro configuration is a reversible process as both the adsorption and desorption barrier energies are low. Hence, the recovery of a clean graphene surface is feasible. The chemisorption process in Nitrite and Cyclo-addition configurations is endothermic. There is an increase in the energy barrier due to rearrangement of the N-O bonds in NO_2 group.

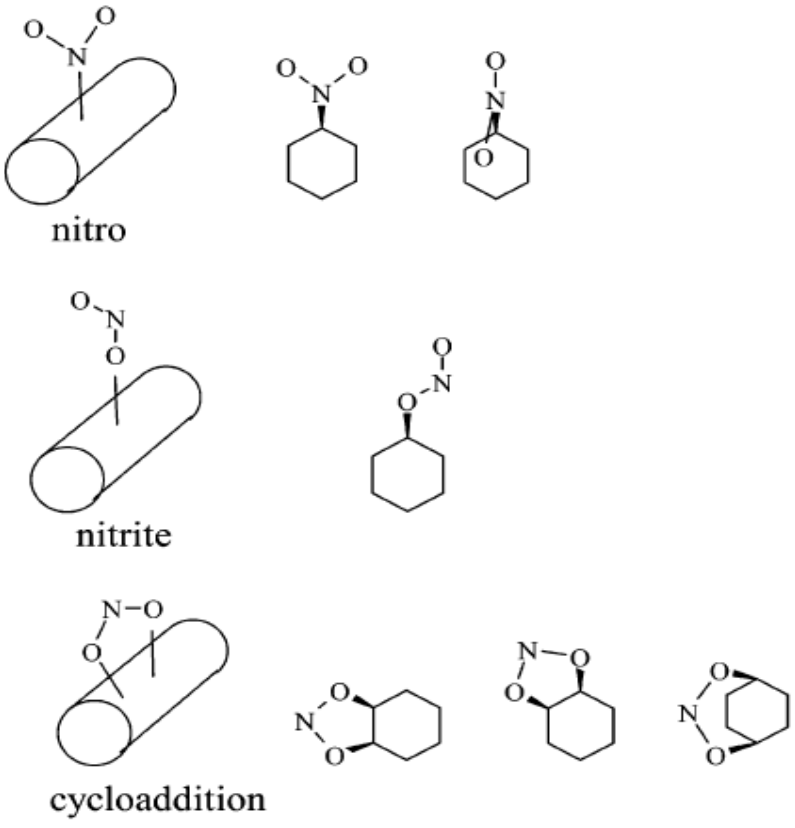

Figure 2-3: Different structures of NO_2 absorption on rolled up graphene surfaces in nitro, nitrite and cyclo-addition configuration [22]

Multiple adsorptions of NO_2 molecules are possible because of the presence of numerous adsorption sites. Specially, after the adsorption of the first NO_2 group, the structure contains an unpaired electron which can pair with another NO_2 group. There are also other positions (meta-, para-, ortho-, etc) on the hexagonal C structure of graphene surface for the adsorption of second NO_2 molecule discussed in detail in [22]. The interaction of two NO_2 groups in Nitrite configuration is more stable than the Nitro configuration. Rearrangement in the N-O bond during nitrite adsorption also produces larger reaction barrier than in the Nitro configuration. The adsorption of two NO_2 groups increases the desorption barrier especially in the case of Nitrite configuration and the recovery of pure graphene surface becomes difficult.

The study of interaction effects of N_2O_4 on graphene surface is equally important. Generally, in the gaseous phase, NO_2 remains in equilibrium with N_2O_4. Among the various isomers of N_2O_4, [15, 22] discusses the interaction of O_2N- NO_2. The interaction of N_2O_4 with graphene surface produces two chemisorbed NO_2 groups. Similarly, two adsorbed NO_2 groups may also desorb from the surface to form N_2O_4. Since the equilibrium N-N distance (1.83Å) is larger than the C-N distance (0.7Å), the N-N interaction is weak with little stabilization effect. Hence, the probability of direct adsorption of N_2O_4 to produce two adsorbed NO_2 groups is higher than vice-versa.

Interaction of NO_2 with epitaxial graphene also depends upon the factor that whether it has been fabricated on Si face or C-face of SiC substrate. This has been attributed to the presence of large number of graphene layers on the C-face of the substrate than the Si-face [8]. With the ambi-polar presence of charge carriers, the p-type or n-type characteristic of graphene is determined by the charge carrier playing the dominant role [8, 23]. As a strong oxidizer, NO_2 withdraws electrons from the surface of substrate on which it gets adsorbed. This results in the increase in the number of holes on the substrate. The decrease in conductance with NO_2 adsorption confirms the n-type nature of Si-face fabricated epitaxial graphene while the increase in the conductance with NO_2 adsorption confirms the p-type nature of C-face fabricated epitaxial graphene. The n-type nature of monolayer of graphene on Si-face is due to transfer of electrons from the SiC substrate with a small carrier concentration and thus, provides larger response. However, the p-type nature on multiple graphene layers on C-face arises due to the screening effect of the

intermediate layers between the top layer of graphene and the SiC substrate with higher carrier concentration, and thus, produces smaller response [6, 18, 19]. In the present work, the epitaxial graphene grown on Si-face of SiC substrate has been used to perform the experiments.

At elevated temperature, the C-N bonding between graphene and NO_2 molecules is weakened. This results in reduced interaction and decreases the response of the sensor. Higher temperature assists desorption of NO_2 from the graphene surface. Hence the sensors at higher temperature exhibit shorter recovery times [8]. The effects of temperature on NO_2 detection of epitaxial graphene have been studied in detail in results section.

Humidity plays an important role in NO_2 sensing characteristics of graphene sensor. In the presence of humidity, nitrogen dioxide reacts with water to form nitric acid. The nitric acid formed is capable of causing oxidation of graphene to produce defect sites on the graphene sensing surface [25]. The multiple defect sites enhance the interaction of graphene surface with NO_2 molecules and increases the sensitivity of the sensor [26]. The effects of humidity on NO_2 detection of epitaxial graphene have been studied in detail in results section.

3. Fabrication of NO_2 Gas sensor

The fabrication of a NO_2 gas sensor involves fabrication of epitaxial graphene layer, characterization of the epitaxial graphene layer, photolithography, metallization and formation of contacts. Graphene was grown on a 5mm*5mm SiC substrate. It is known that the growth of graphene on Si-terminated face of SiC substrate is slower than the C-terminated face. So, Si-terminated face was chosen for the growth of monolayer of graphene. The sample was immersed in a glass beaker with acetone solution to remove the protection layer of photoresist.

Cleaning of the SiC substrate surface is utmost necessary to get the desired monolayer of graphene. The beaker containing the sample was placed on ultrasonic bath for 5 minutes to remove the dust particles from the sample surfaces. The sample was then treated with RCA-1 solution (NH_4OH:H_2O_2:H_20 1:1:3) in a quartz beaker, placed on a hot plate for 5 minutes in order to remove the organic contaminations. The oxygen atoms produced in the RCA-1 solution oxidize the organic contaminants present on the surfaces of the sample. In the process, it also oxidizes the silicon and leaves a thin oxide layer on the surface of the substrate. The sample thus was placed in the 10% HF solution for 3-5 seconds to remove the oxide from the surface of the substrate. The cleaned SiC substrate was dried using nitrogen flow and the sample was ready for graphene growth.

3.1 Epitaxial graphene fabrication technology

The graphene growth principle is based on the thermal decomposition of silicon carbide. At very high temperature, the Si atoms in SiC layer escapes leaving behind only C atoms leading to graphene layer formation. This process is called graphitization. The high annealing time increases the number of liberated carbon atoms and as a result, also increases the number of graphene layers. In this work, graphitization has been done at atmospheric pressure. However, it can be carried out at low pressure to increase the growth rate and lower the graphitization temperature. Also, graphitization has linear dependence on temperature and the growth rate is slow. The SiC surface must be cleaned by hydrogen etching to remove the damaged SiC layer [28, 31].

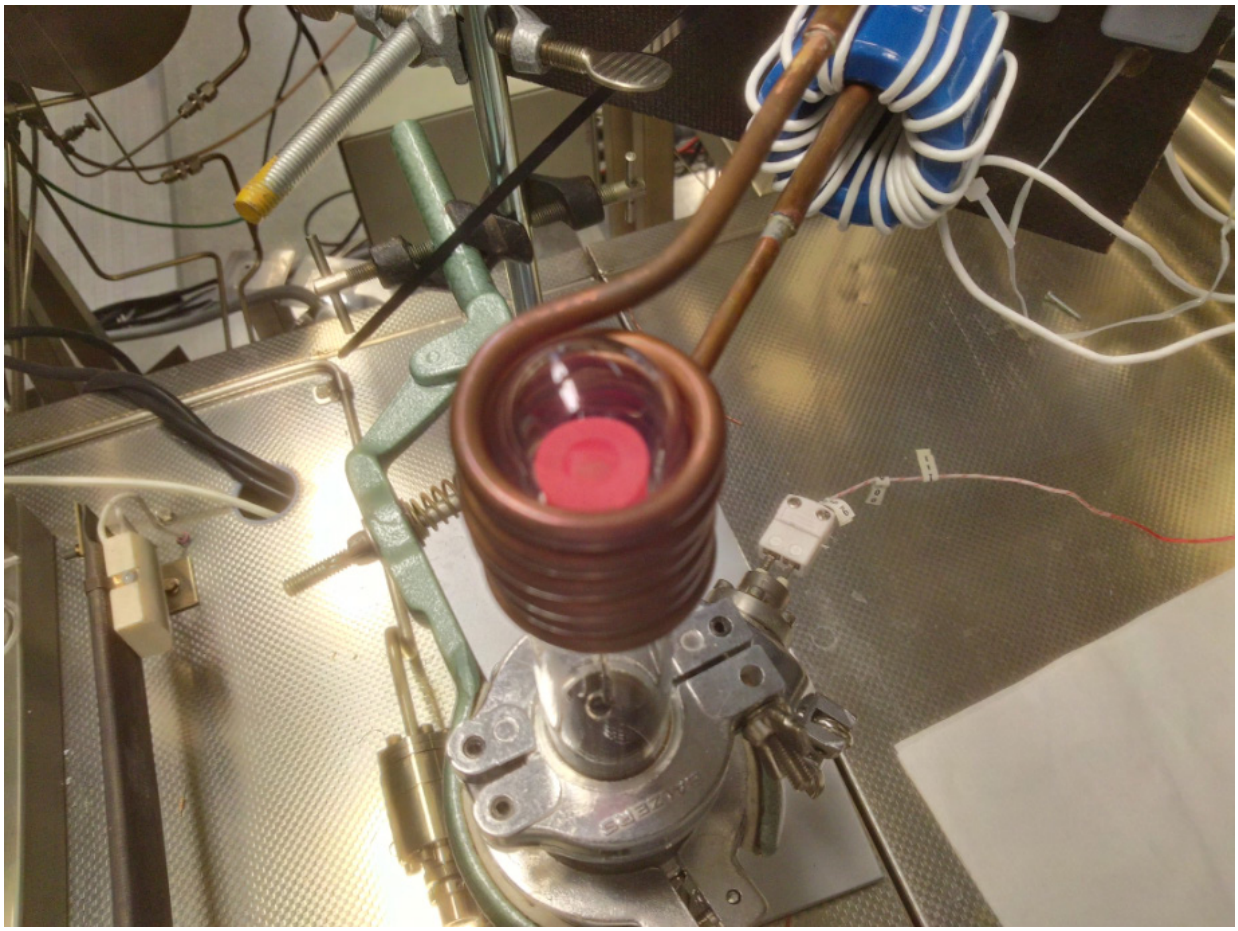

Figure 3-1: Gas chamber for graphene fabrication. The chamber is heated using inductive coil. Fan and water supply are used as cooling of the heating system.

The fabrication gas chamber is shown above in figure 3-1. The cleaned and dry SiC substrate was placed in the graphite holder of the fabrication chamber with the Si-terminated surface facing upward. The chamber was purged with 200 sccm and 2000 sccm of H_2 and Ar gas flows respectively. The graphite holder was then inductively heated at 1450 ^oC with power of 2 kW for 2 minutes to remove the damaged carbide layer. After that the Ar and H_2 gases were pumped out from the chamber and only 2000 sccm of Ar gas was flown through the chamber. The sample was heated at 1560 ^oC with power of 2kW for 5 minutes to form the layer of graphene on the top surface of silicon carbide.

3.2 Operating principle of Auger Electron Spectroscopy

Auger Electron Spectroscopy is a surface sensitive analytical technique used for investigating the composition of thin films as well as compositional distribution of elements in multi-layered films

along depth direction [29]. The identity and quantity of the element is determined from the kinetic energy and intensity peaks of Auger electrons. The principle of AES is shown in figure 3-2 below. In AES, under ultra high vacuum, the incident radiation causes ejection of an electron from the K-shell of an atom. The ionized atom becomes highly unstable and there is a radiation-less transition of an electron from higher energy level (say, L-shell) occupying the hole position in the K-shell. The energy emitted during this transition is transferred to an electron in the higher energy shell (M-shell) causing its emission. These emitted electrons are known as Auger electrons. The kinetic energy, E_k associated with an Auger electron is given as

$E_k = E_K - E_L - E_M$; where E_K, E_L and E_M are the energies associated with K-shell, L-shell and M-shell electrons respectively.

Energy related to Auger electrons is specific to an element and its electronic structure. An Auger electron from Si atom possesses energy of 92 eV and that coming from C possesses 272 eV.

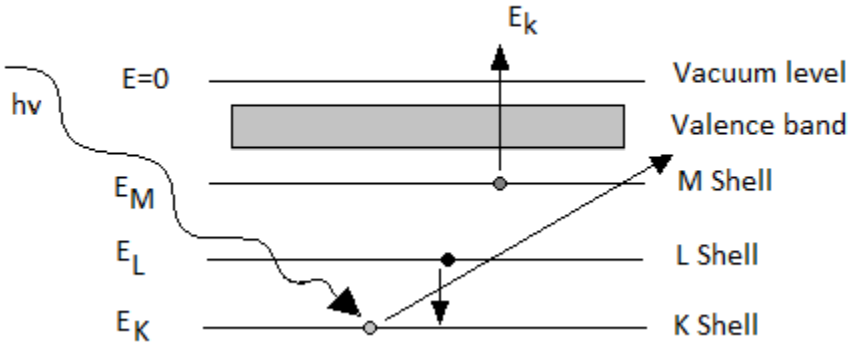

Figure 3-2: Principle of Auger Electron Spectroscopy

In this experiment, AES was used to determine the number of graphene layers on the surface of SiC substrate. The measurement setup consists of an electron gun, a Cylindrical Mirror Analyzer (CMA), and a computer for data processing as shown in figure 3-2. The cylindrical mirror analyzer includes an electron detector, a photomultiplier, a signal modulation circuit, a lock-in amplifier, an oscilloscope and a spectrometer. In an Ultra High Vacuum (UHV) condition; an electron beam, accelerated by a power supply of 4.5 keV, was bombarded on the sample surface at an angle of 15^o. The emitted Augur electrons beam at an angle θ was detected by CMA and

the measured spectrum was forwarded to the computer for further processing. The computer determined the derivative of the number of Augur electrons (N) as a function of their kinetic energy and provides the silicon-carbon peak-to-peak ratio. This ratio was used to determine the number of graphene layers in the epitaxial graphene thin film fabricated on the sample surface.

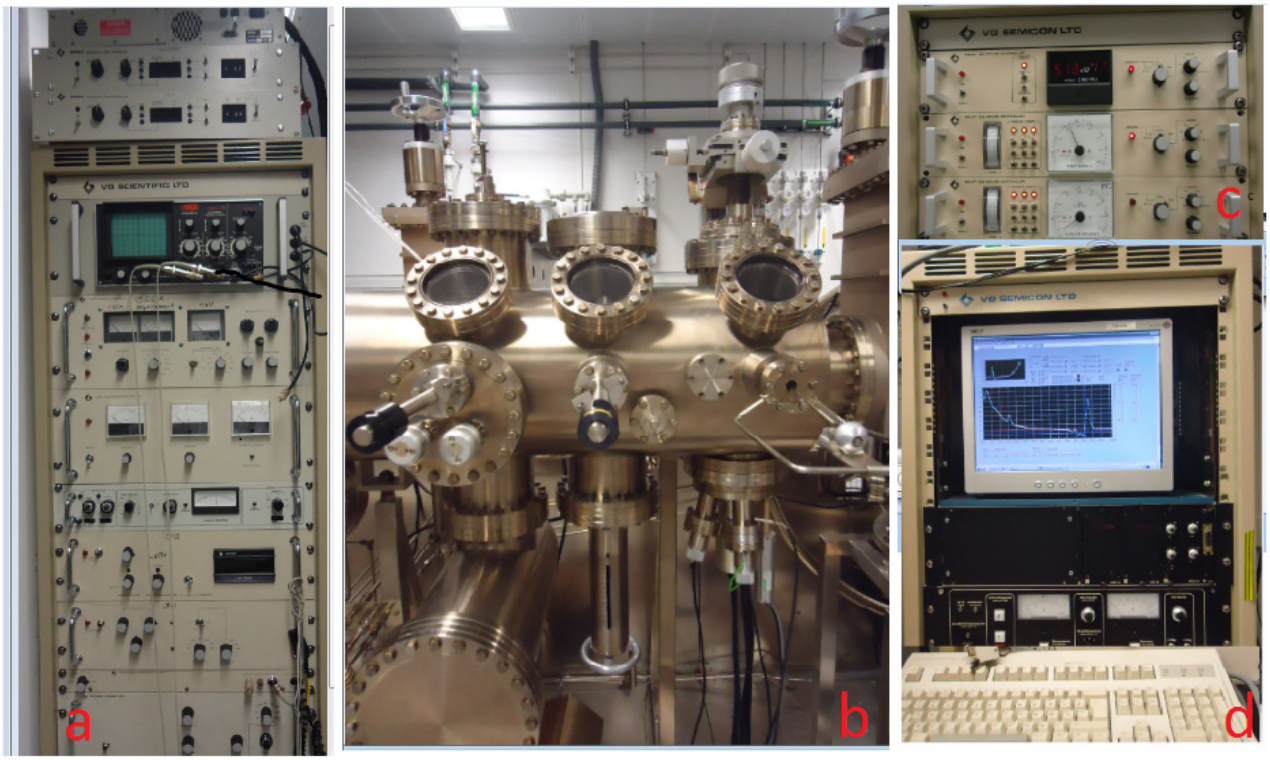

Figure 3-3: AES experimental setup (a) Voltage control panel, (b) Main Auger measurement apparatus, (c) Pressure monitor panel, and (d) Computer system for Auger spectrum measurement

The angle θ for the emitted Augur electrons beam is found to be 42° for CMA analyzers [30, 31].

3.3 Operating principle of Atomic Force Microscope

Atomic Force Microscope is an instrument used to measure nano-scale surface features of conducting, semiconducting and insulator materials. When cantilever tip, made up of Silicon or Silicon Nitride, approaches the sample; it interacts with the sample surface due to van der Waals Force. This causes bending of cantilever tip which is measured by the deflected laser light. The 4-segment photodiode system captures the deflected laser light and produces an equivalent

electrical signal. The feedback circuit utilizes the electrical signal to adjust the voltage affecting piezo scanner and adjusts its position along xyz direction. The operating principle of AFM is shown in figure 3-4 below. AFM can be operated in contact mode and semi-contact mode. In contact mode, the distance between the tip and the sample is < 0.5nm. There is a strong interaction between the tip and the sample surface as the tip comes in mechanical contact with the surface. Though it provides fast scanning, the contact between the tip and the surface may sometime damage the sample or tip or both. In semi-contact mode, the distance between the tip and the sample is 0.1-10 nm. There is a weak interaction between the tip and the surface as the tip does not touch the surface but oscillates with resonant frequency. It does not cause any damage but provides low resolution images of the sample surface than the contact mode.

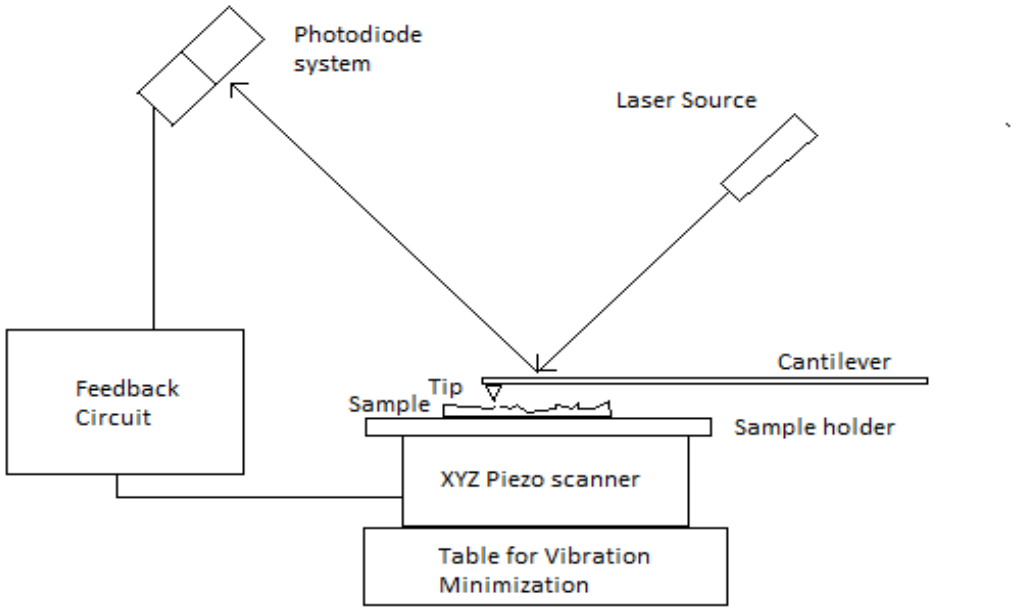

Figure 3-4: Principle of operation of AFM

AFM was used to measure the surface morphology (i.e. height variation) of the fabricated graphene samples. During the measurement, semi-contact method was used. The oscillation frequency of the cantilever tip was 141.7 KHz. The feedback gain was set as 0.2 and the set point voltage was kept at half of the oscillation magnitude. The oscillation magnitude should be adjusted between 20 and 25. While scanning the sample, the cantilever tip interacts with the sample surface by the force determined by the set-point voltage. The deflection of the tip is

measured using 4-segment photodiode. The feedback circuit calculates the corresponding voltage and compares it with the set-point voltage. In the case of mismatch, the feedback circuit makes correction which causes piezoelectric elements to expand or to contract. As a result, the sample holder moves so that the interaction force corresponds to the set point voltage. The sample then moves in x-y direction for actual scanning of the sample. A 14μm*14μm and a 5μm*5μm size images were taken for the analysis of the sample.

3.4 Photolithography

Photolithography is a micro-fabrication technique used to transfer geometrical patterns present in a mask to the surface of the substrate. It involves several steps such as surface cleaning, photo-resist coating, alignment and optical exposure, development and etching. Surface cleaning is an important step in the photolithography to remove any traces of organic, ionic and metallic impurities from the surface of the substrate. Photo-resist is a light sensitive polymer used for pattern formation and layer protection. In positive photo-resist, a photon breaks up the chain that forms the polymer, often releasing the acid groups [32]. Laser has been used as the source of illumination. After exposure, the substrate is developed in a developer solution where the photo-resist with broken chains gets dissolved. Etching is the process of removal of materials from the exposed portion of thin film present on the substrate and thus, creates the necessary geometrical patterns on it.

Laser writing was used as photolithography method to form the metal contacts and graphene channels in the sensors sample without the physical mask. The sample was first cleaned in acetone, iso-propanol and then in water. The sample was dried in a spin dryer and a thin layer of a positive photoresist AZ 5214 E was spin-coated over the fabricated graphene layer by high-speed centrifugal resist spinner of the substrate. The sample was soft baked at 90^{o} C for 20 minutes and then placed on the laser writer. The mask layout used for laser illumination is shown in figure 3-6.

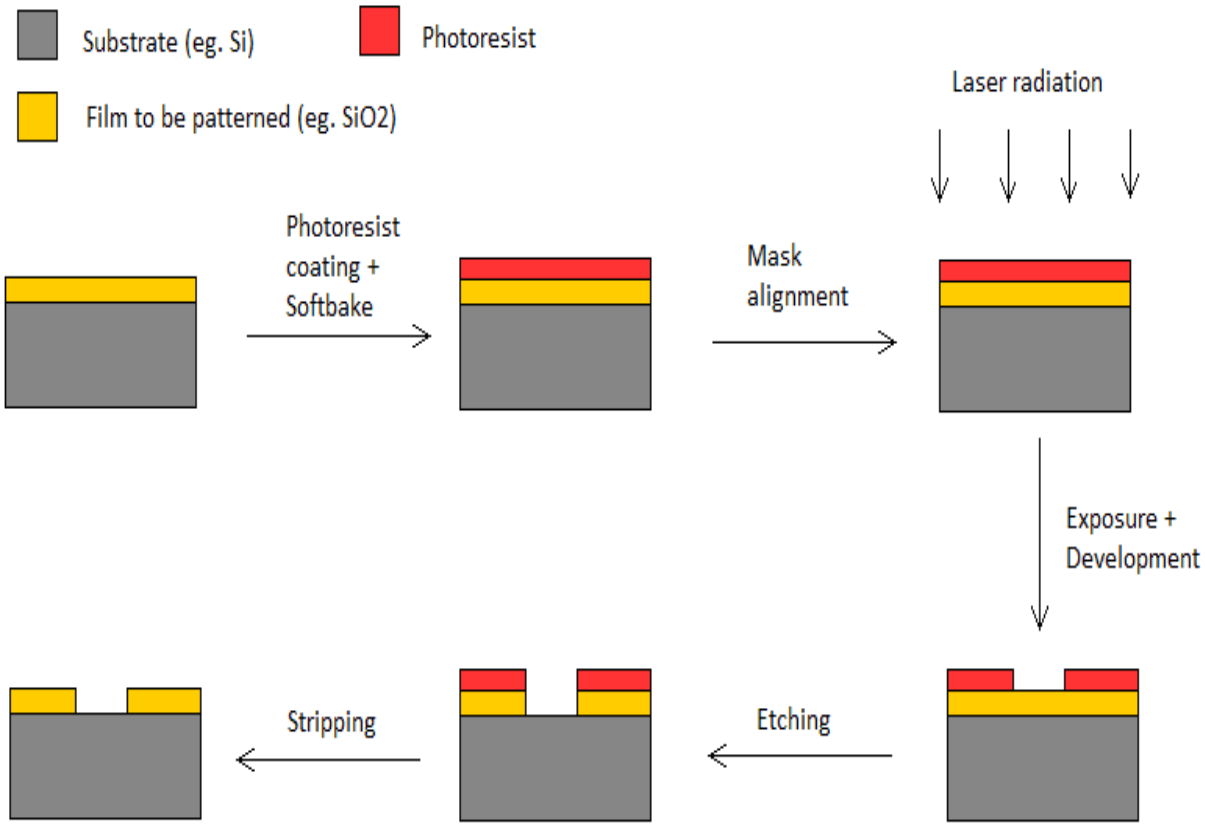

Figure 3-5: Principle of Photolithography

There are 10 sensors structures present on the masks. However, only six of them will be finally used for NO_2 sensing. Layer 0 mask defines the shape of graphene channel of the sensor. Layer 1 helps to generate geometrical patterns for first layer of metallization. Layer 3 helps to establish connection between graphene channel and first layer of metallization. Alignment in a particular plane was achieved by defining two types of alignment marks. Depending upon the pattern on the mask layer L0, the laser light was scanned over the photo-resist causing the breakdown of the bonds in the irradiated region of photo-resist polymer. After laser exposure, the sample was immersed in AZ 351B Developer solution for 1 minute during which the portion of photoresist affected by the light got dissolved. The graphene layer, not coated with photoresist, was then removed by Reactive Ion Etching (RIE) using oxygen recipe as etchant.

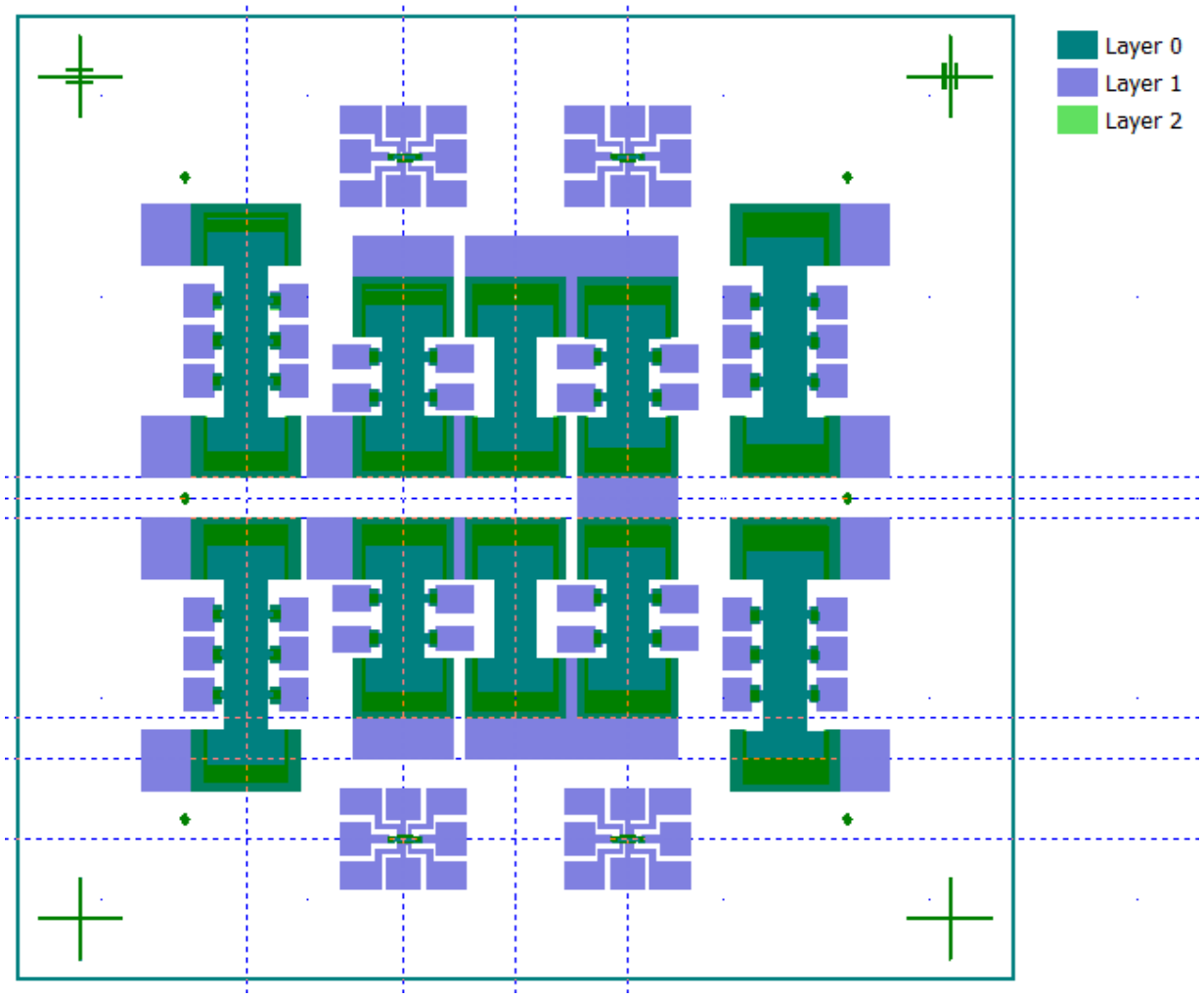

Figure 3-6: Layout for Laser Writing

3.5 Operating principle of Electron Beam Evaporation System (EBES)

EBES is a type of PVD used for depositing thin film of materials using an electron beam gun. The operating principle of EBES is shown in figure 3-7. The material to be deposited, acts as an anode, is placed on a crucible within the water cooled hearth. A tungsten filament, acts as a cathode, upon heating emits a high flux of electrons under vacuum which are accelerated by high voltage and focused on the crucible containing the source material by a magnetic system. The electron beam causes atoms from the source material to evaporate into the gaseous phase. These atoms then precipitate into solid form, coating everything in the vacuum chamber within the line of sight with a thin layer of anode material. A shutter, placed above the crucible, is generally kept in closed position during the evaporant being conditioned, degassed and monitored prior to

running actual thin film deposition. This technique provides uniform coating, precise layer monitoring and efficient deposition of evaporated material to the substrate. The deposition rate varies from as low as 1nm per minute to few micrometers per minute. Due to very high deposition rate, this technique is more prevalent in the industrial applications.

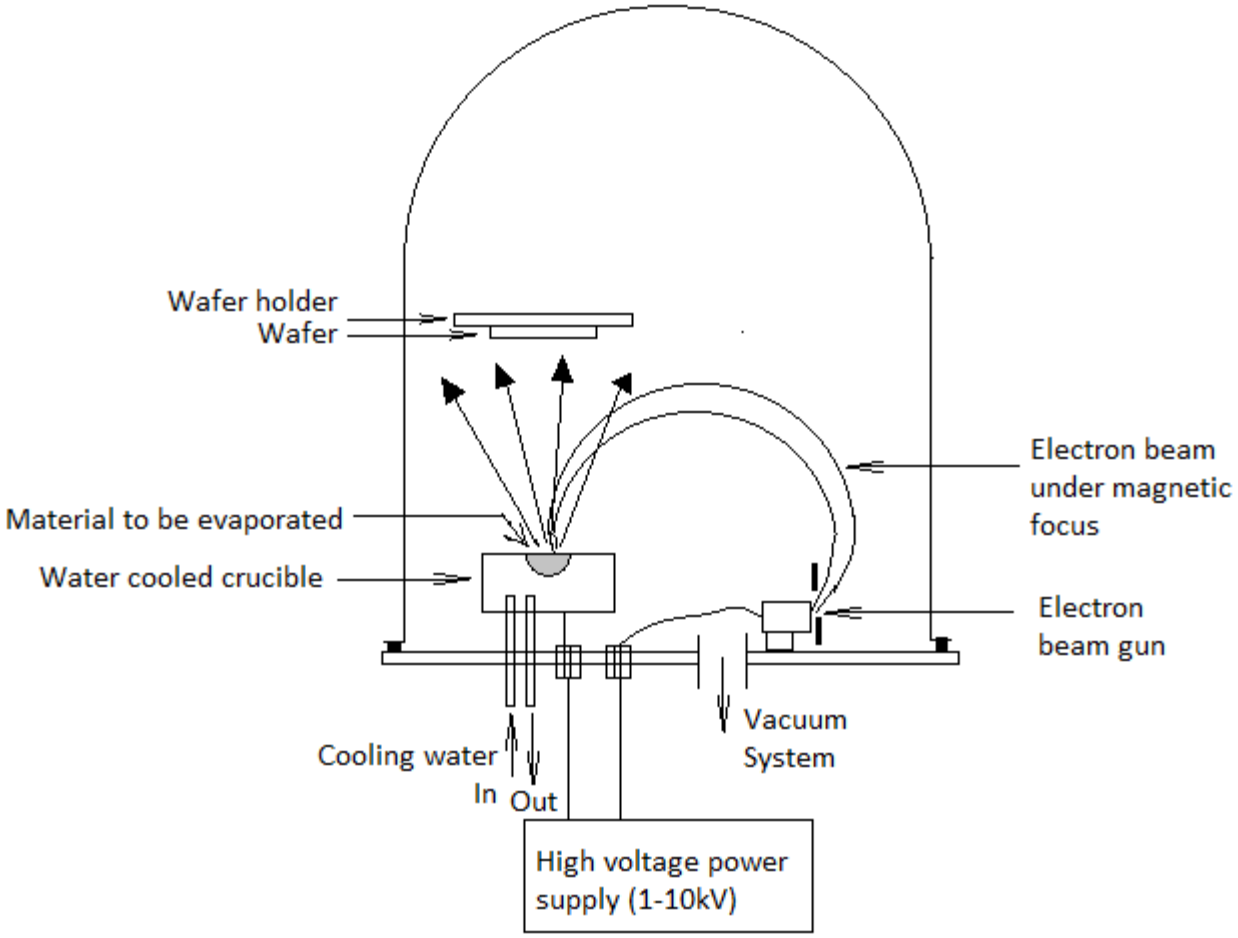

Figure 3-7: Operating principle of Electron Beam Evaporation System

EBES was used for the deposition of a thin metal layer of Titanium (Ti) followed by Gold (Au). Small Ti metal pellets were loaded in the crucible placed at the base. The sensor sample was placed right above the base such that the front face of the sample was placed right above the crucible containing Ti metal sheet. A high voltage of 4 kV was applied to the filament generating the high energy electron beam. The bulk density of Titanium was set as 4.56g.cm^{-3} and Z-factor as 0.6. After the deposition of 5nm of Titanium, the process was stopped. The position of the crucible was then changed to Au and the same procedures were followed for the deposition of

20nm of Gold. The corresponding bulk density of Au was set as 19.3g.cm^{-3}.and Z-factor as 0.381. After the metal deposition, the sample was immersed in acetone solution for lift-off. The jet of acetone solution was pumped using a pipette on the surface of the sample so that the metal deposited over the substrate remains unaffected and that deposited over the photoresist is removed.

The sample containing the sensor devices was glued on a sample holder and baked for an hour at 150^{o}C for curing. The sample holder contains a platinum heating element, on the backside of the sample, used to vary the temperature of the sensors by applying voltage across the platinum resistor. The fabricated sensor device and the Teflon chamber are shown in figure 3-8 below. The sensor device was then placed in a special Teflon enclosure for the measurement of its responses to test gases. The connections were maintained through a hermetic 16-pin connector. The enclosure consisted of two pipe connections, one for gas let-in and other for gas let-out.

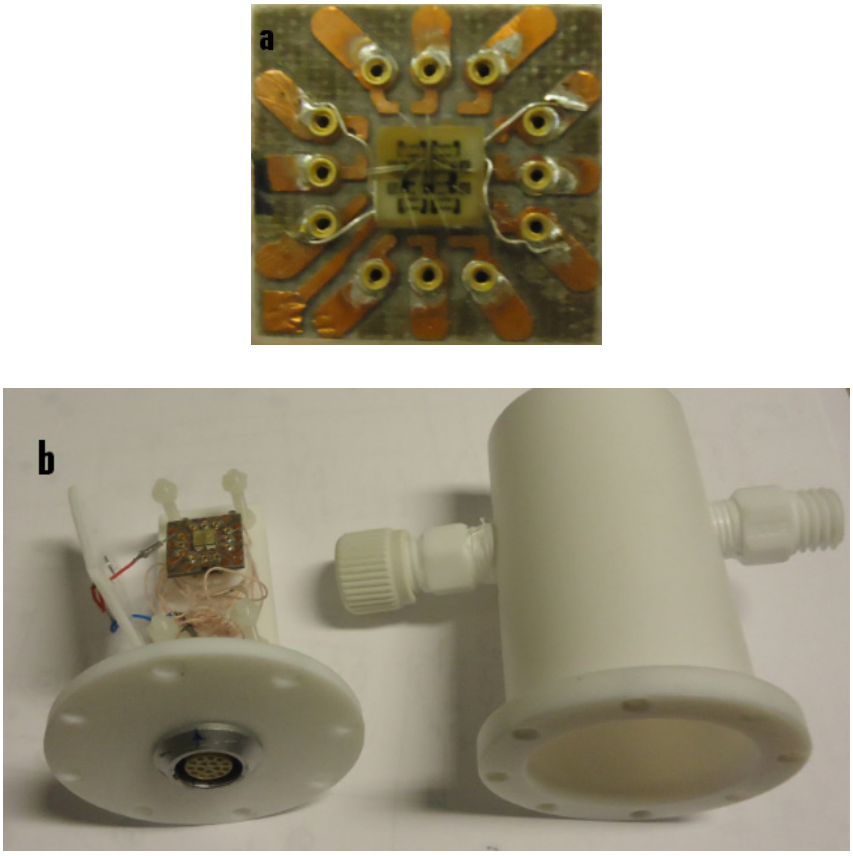

Figure 3-8: (a) Fabricated sensor device on a sample holder (b) Teflon chamber with sample holder

4. Experimental Setup

The gas sensing mechanism is based on the change in conductivity of the graphene layer upon the interaction with the test gases. The sensor devices are connected to the measurement system using co-axial wires. The desired concentration of the test gas is achieved by mixing it with air or purified N_2 gas at specific ratios using mass flow controllers. The changes in the resistances of the sensors upon the interaction with the test gases are recorded at defined interval of time. The sensor response is calculated as the percentage change in the resistances of the sensors upon detection of the test gas. During the experiment, the measurement of voltage (U) and current (I) across each sensor are monitored using Keithley 2700 Multimeter/ Data Acquisition System Unit. The resistance across a particular sensor is calculated as

$$\text{Resistance (R)} = \frac{\text{Voltage across the sensor (U)}}{\text{Current flowing through the sensor (I)}}$$

The schematic diagram for measuring the responses of epitaxial gas sensors to NO_2 gas is shown in the figure 4-1. In the setup, the air first passes through the filter where the moisture and chemical contaminants are removed. The dry air is then used as a carrier. The carrier can be humidified later using manual valves by passing it through a glass washing bottle filled with de-ionized water known as the humidifier of the system. Mass flow controllers MFC1 and MFC2, which are controlled by LabVIEW, provides the supply of dry or humid carrier gas. Pneumatic valves are also controlled by LabVIEW software. This setup can be used to study two different test gases using the Mass flow controllers MFC7 and MFC8. However, it has been used to study only NO_2 as a test gas. The test gas is mixed with the carrier gas in certain ratios to obtain the desired concentration of the test gas which is directed towards the sensor chamber. To achieve low concentrations, NO_2 gas undergoes through two dilution steps. A humidity and temperature sensor is placed in the incoming path to the sensor chamber which provides the temperature and relative humidity of the incoming test gas.

The concentration limit of the measurement setup is between 0.1ppb - 10ppm.

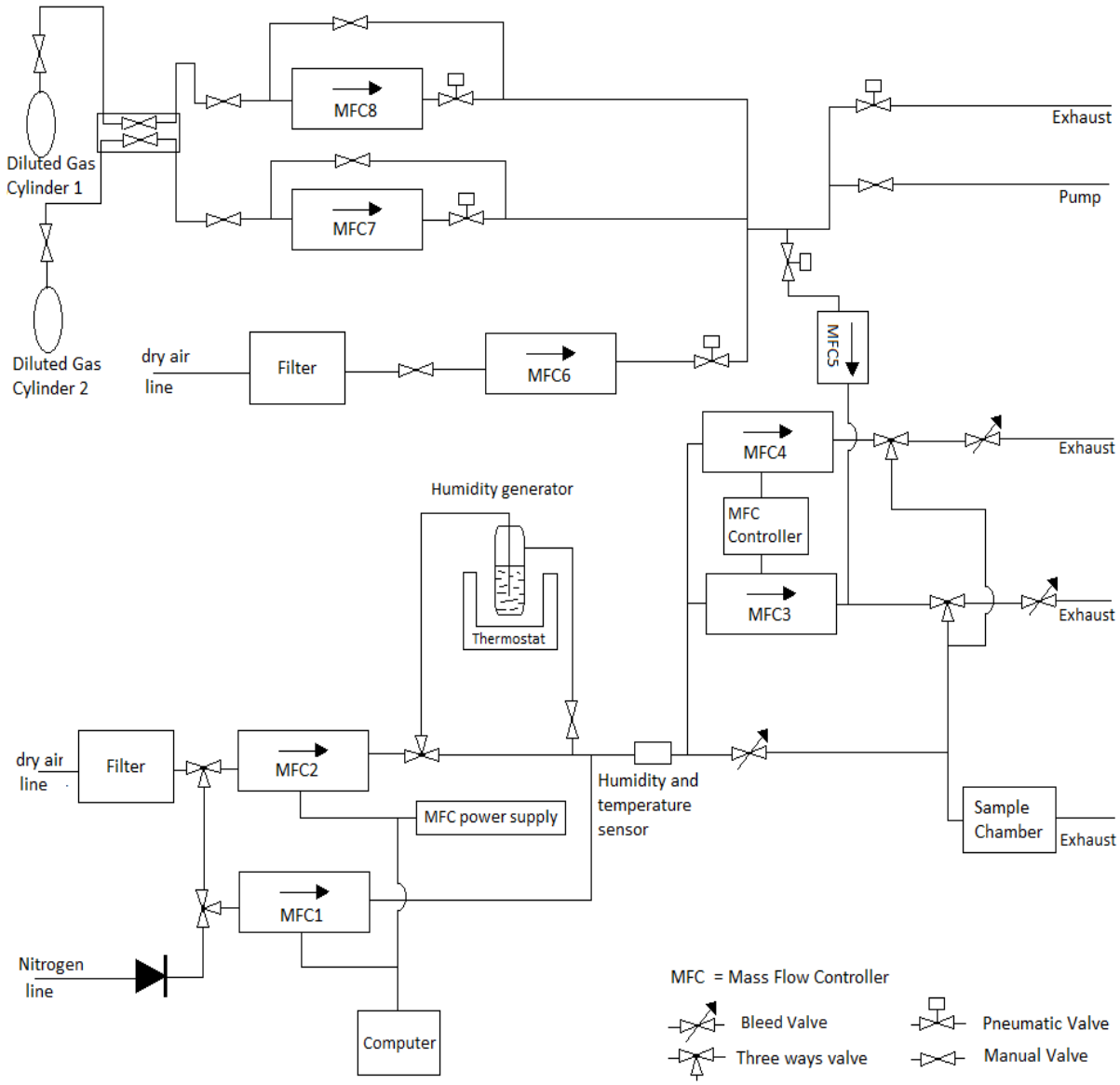

Figure 4-1: A Schematic Diagram of Experimental Setup

The concentration levels of gas flow, operating temperature and humidity conditions are controlled using LabVIEW software and some gas measurement programs. "ke27xx continuous multi read.vi" is the main program which is used to control the beginning and end of the measurements. It also presents the graphical displays of the sensors' responses. The graphs of the responses can be saved along with the measured data. At the end of the each measurement cycle, it provides two options: "Continue carrier gas flow" and "Ventilate". When "Continue carrier gas flow" is chosen, dry or humid carrier gas continue to flow, NO_2 gas valve is closed and a

complete new measurement cycle can be resumed. However, when “Ventilate” is chosen, it purges out any residual NO_2 gas by excess carrier gas flow and then closes all the pneumatic valves. The sensor chamber can then be opened and the samples can be changed. "Vapor generation system with global.vi" program is used to control the flow of carrier gases to the sensor chamber. "Gas system 4 stage heating.vi" program is used to vary the concentration of the test gas, supply time duration, cleaning of the graphene surface through heating and removal of the gas from the chamber containing the sensors. “Keithley 228- Set values and operate.vi” program is used to control supply voltage to the heater. "Serial Clear Error.vi" program is run to remove any error in the main carrier gas supply control panel. More details on the operation of LabVIEW software and simulations of gas measurements programs are provided in the reference [33].

Table 1: Typical time intervals used in gas response measurements

Time intervals	Description	Duration(s)
Preheating time	In, the initial phase of measurement, the sample are heated for this duration.	60
Stabilizing time	The sample gas is directed to second dilution stage bypassing the sample chamber.	60
Sample delay	The sample gas bypasses the second dilution stage and only pure carrier gas flows through the sensor chamber.	1200
Stage time	The carrier gas mixed with NO_2 gas is introduced to the sensor sample in this duration.	3600
Ventilate time	The sample gas is OFF and only the pure carrier gas flows through the chamber.	1200
Annealing time	During this period, the sensors are heated in order to clean the graphene surface.	3600

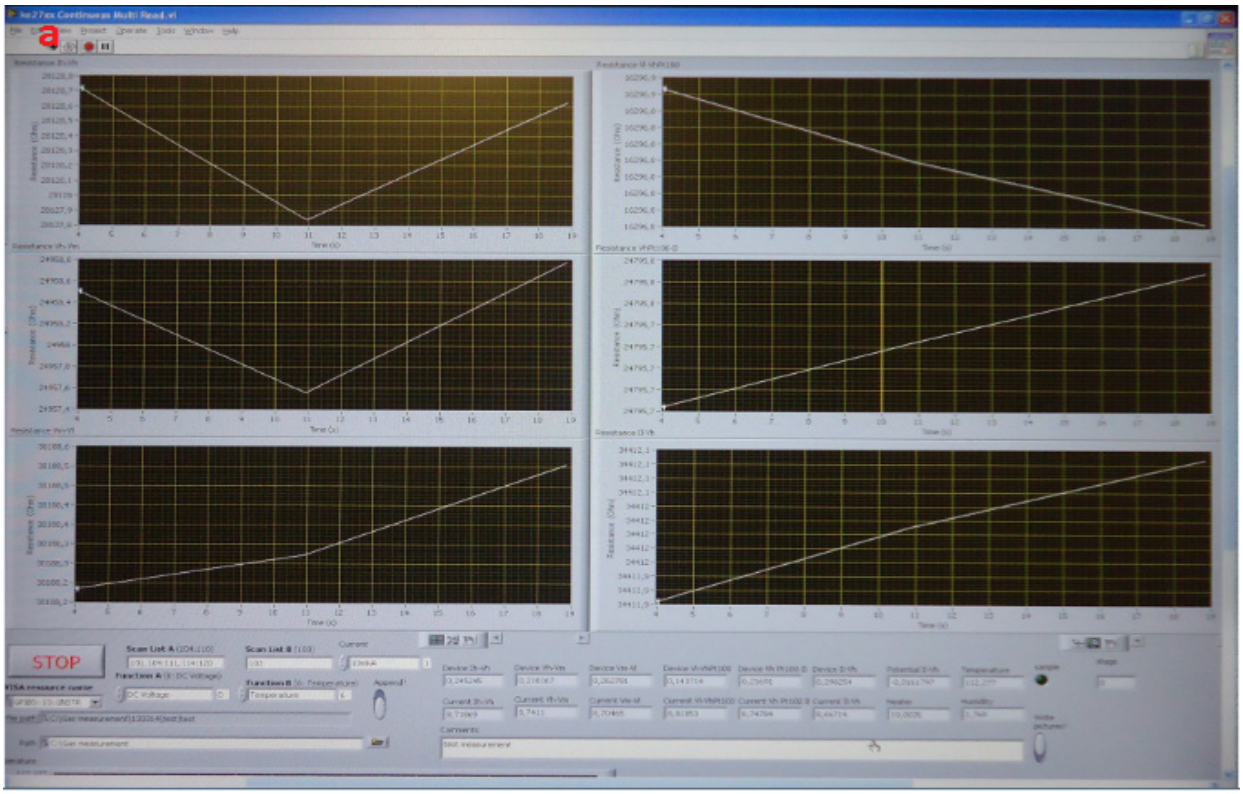
a
STOP

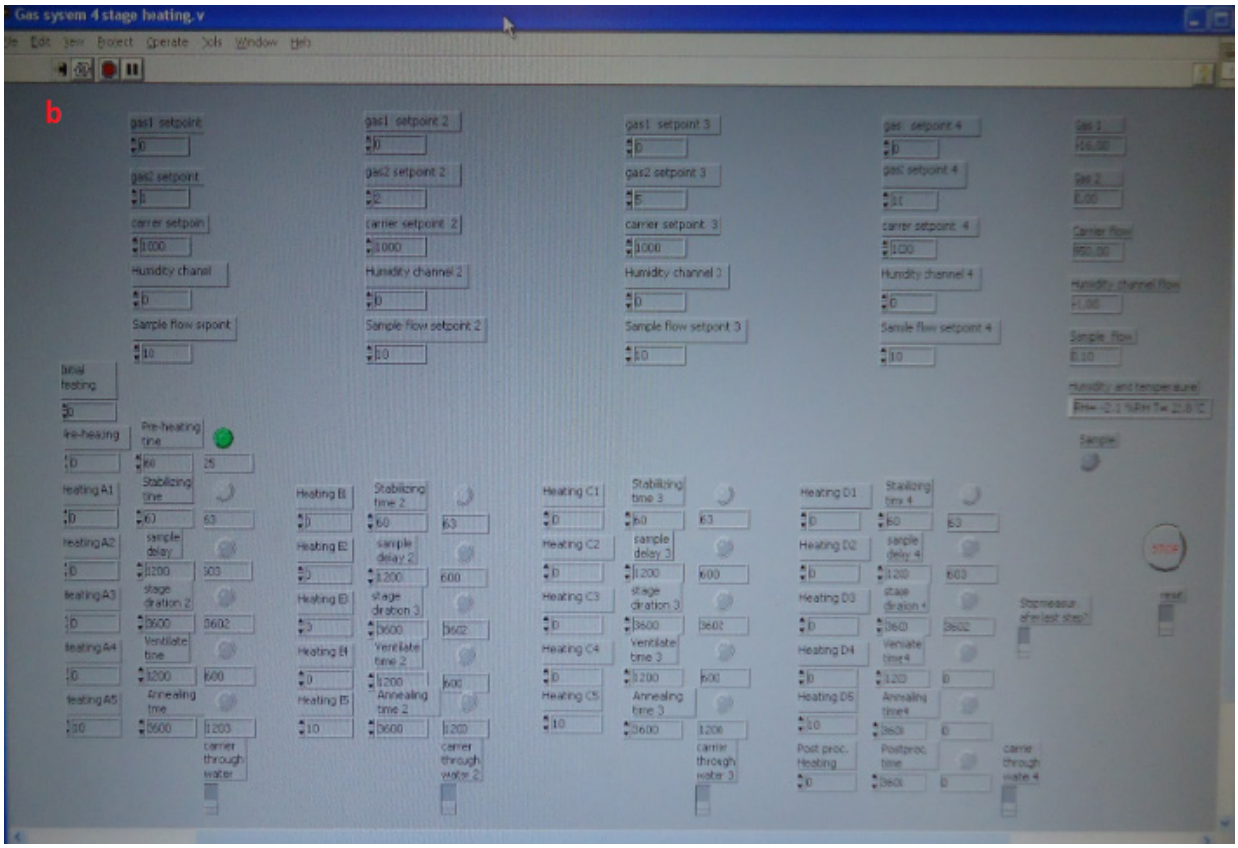
Gas sysem 4 stage heating.v
b
gas1 setpoint
gas2 setpoint
carrier setpoin
Humidity chanal
Sample flow sipoint
gas1 setpoint 2
gas2 setpoint 2
carrier setpoint 2
Humidity channel 2
Sample flow setpoint 2
gas1 setpoint 3
gas2 setpoint 3
carrier setpoint 3
Humidity channel 3
Sample flow setpoint 3
gas setpoint 4
gas2 setpoint 4
carrier setpoint 4
Humidity channel 4
Sample flow setpoint 4
Initial heating
Pre-heating
Pre-heating time
Heating A1
Heating A2
Heating A3
Heating A4
Heating A5
Stabilizing time
sample delay
stage duration 2
Ventilate time
Annealing time
carrier through water
Heating B1
Heating B2
Heating B3
Heating B4
Heating B5
Stabilizing time 2
sample delay 2
stage duration 3
Ventilate time 2
Annealing time 2
carrier through water 2
Heating C1
Heating C2
Heating C3
Heating C4
Heating C5
Stabilizing time 3
sample delay 3
stage duration 3
Ventilate time 3
Annealing time 3
carrier through water 3
Heating D1
Heating D2
Heating D3
Heating D4
Heating D5
Stabilizing time 4
sample delay 4
stage duration 4
Ventilate time 4
Annealing time 4
Post proc. Heating
Postproc. time
carrie through water 4
STOP
reset

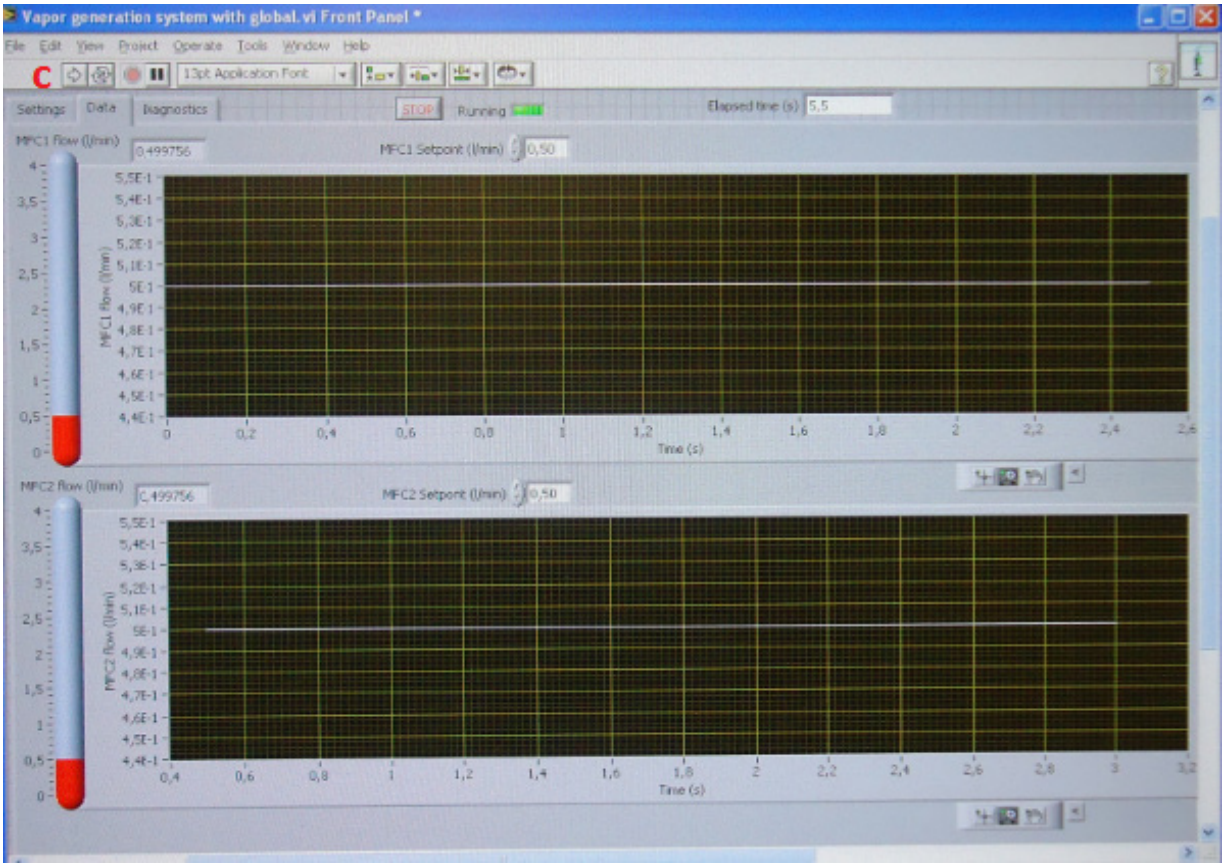
Vapor generation system with global.vi Front Panel *
File Edit View Project Operate Tools Window Help
13pt Application Font
Settings
Data
Diagnostics
STOP
Running
Elapsed time (s)
5,5
MFC1 Flow (l/min)
0,499756
MFC1 Setpoint (l/min)
0,50
MFC1 Flow (l/min)
Time (s)
MFC2 Flow (l/min)
0,499756
MFC2 Setpoint (l/min)
0,50
MFC2 Flow (l/min)
Time (s)

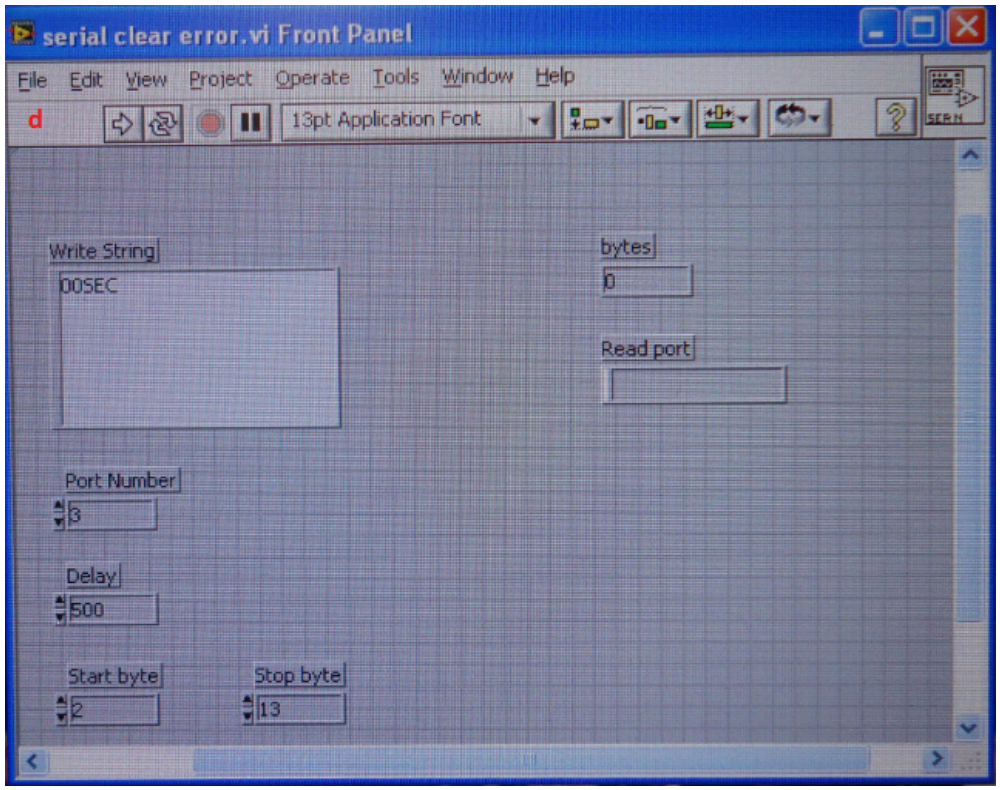
serial clear error.vi Front Panel
File Edit View Project Operate Tools Window Help
13pt Application Font
Write String
00SEC
bytes
0
Read port
Port Number
3
Delay
500
Start byte
2
Stop byte
13

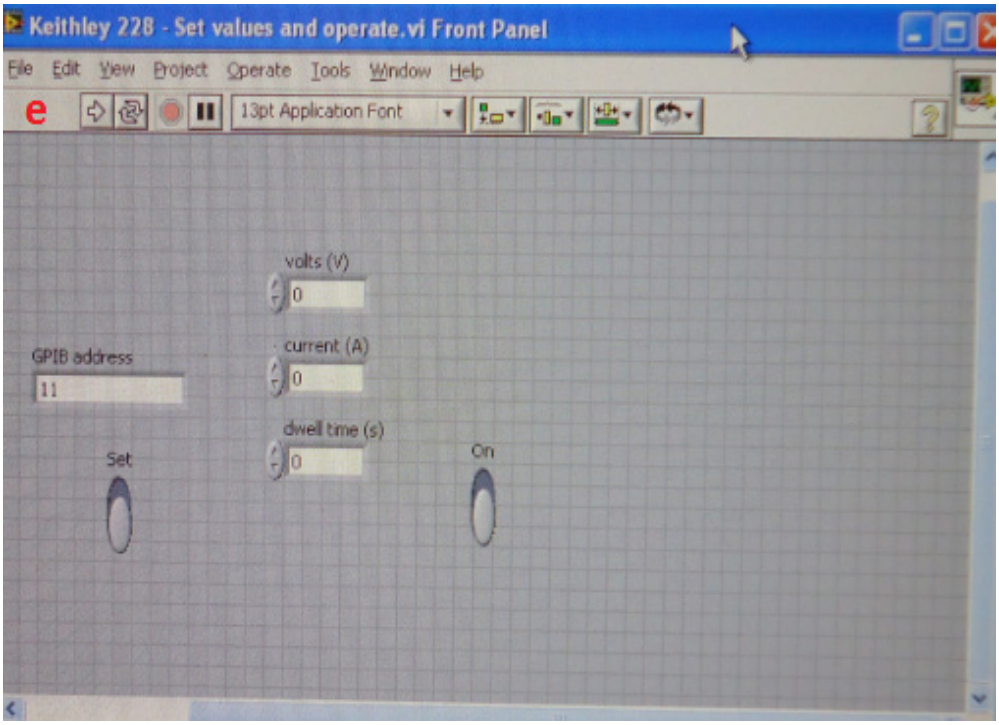

Figure 4-2: Screen shots of the LabVIEW panels. (a) ke27xx continuous multi read.vi, (b) Gas system 4 stage heating.vi, (c) Vapor generation system with global.vi, (d) Serial Clear Error.vi, and (e) Keithley 228- Set values and operate.vi

The actual concentration of NO_2 gas is calculated as

$$\text{Concentration, } C = \frac{\text{Flow of } NO_2}{\text{Flow of carrier gas} + \text{Flow of } NO_2}$$

$$\approx \frac{\text{Flow of } NO_2}{\text{Flow of carrier gas}} \ldots \text{(since Flow of } NO_2 \text{ <<< Flow of carrier gas)}$$

$$\text{Concentration at first dilution, } C_1 = \frac{\text{Initial conc. of } NO_2 * 1^{st} \text{ setpoint of } NO_2}{1^{st} \text{ setpoint for carrier gas}}$$

$$\text{Concentration at second dilution, } C_2 = \frac{\text{Initial conc. of } NO_2 * 2^{nd} \text{ setpoint of } NO_2}{2^{nd} \text{ setpoint for carrier gas}}$$

Percentage response is defined as the change in resistance when exposed to a test gas and is expressed in terms of percentage.

$$\text{Response, } r = \frac{R_0 - R_g}{R_0} * 100\%$$

where R_0 and R_g are the resistances of the sensor before and after the exposure to a test gas respectively.

To compare the responses of the sensors, the rate of responses is calculated as

$$\text{Rate of response} = \frac{r_f - r_i}{t_f - t_i}$$

where (t_f - t_i) denotes the exposure interval and, r_i and r_f are the responses of the sensors at the start and end of the exposure interval.

Table 2: Calculations of different concentrations of NO_2 in a measurement cycle

Initial concentration of NO_2 gas = 10 ppm						
	Setpoint 1 (NO_2) sccm	Setpoint 1 (Air) sccm	Concentration after first dilution	Setpoint 2 (NO_2) sccm	Setpoint 2 (Air) sccm	Concentration after second dilution
Step1	10	1000	0.1ppm	1	1000	0.1ppb
Step2	10	1000	0.1ppm	2	1000	0.2ppb
Step3	10	1000	0.1ppm	5	1000	0.5ppb
Step4	10	1000	0.1ppm	10	1000	1ppb

5. Results

This section contains the experimental results of the study of fabricated graphene film and the responses of epitaxial graphene sensors to carrier gas and NO_2 under varying ambient conditions. Characterization of fabricated epitaxial graphene layer includes measurements of its thickness using Auger Electron Spectroscopy (AES) and surface topology measurements using Atomic Force Microscope (AFM).

Several experiments were carried out for measuring the drift of sensors and the effects of temperature and humidity on their drifts. Different low concentration levels of NO_2 gas were applied on the sensors to measure their corresponding responses. First, the sensor samples are exposed to 0.1ppb concentration level, followed by 0.2ppb, 0.5ppb and 1ppb concentration levels of NO_2 gas. Recovery of pristine graphene layer at room temperature is a slow process. Thermal annealing was used to obtain graphene surface back to original state before exposing to the next concentration level of NO_2 gas. During the practical application, the gas sensors have to operate under humid condition or at elevated temperature. Thus, the effects of humidity and temperature on NO_2 sensing responses of the sensors were also measured. The results of these experiments have been described in detail under characterization of sensor responses. The responses were tested using six graphene sensors referred here as sensor1, sensor2, sensor3, sensor4, sensor5 and sensor6. The responses of these sensors have been named against their measured date. Some of the responses of sensors containing undesirable noise were removed and the most reliable responses of these sensors have been included.

5.1 Characterization of fabricated epitaxial graphene layer

The silicon-carbon peak-to-peak ratio was calculated from the Auger electron spectrum shown in the figure 5-1. It was compared with the "Silicon-carbon Auger intensity ratio Vs Number of graphene layers" graph [27]. The number of graphene layers in the epitaxial film was found to be 0.8 (< 1). Hence, the fabricated epitaxial layer can be considered as a monolayer graphene.

The topography measurement of the graphene surface level using AFM in the figure 5-2 shows that the surface of the graphene is covered with regular network of mono-atomic steps. The color scale height variation is between 0 to 3.8 nm. Since the decomposition for SiC is not a self limit-

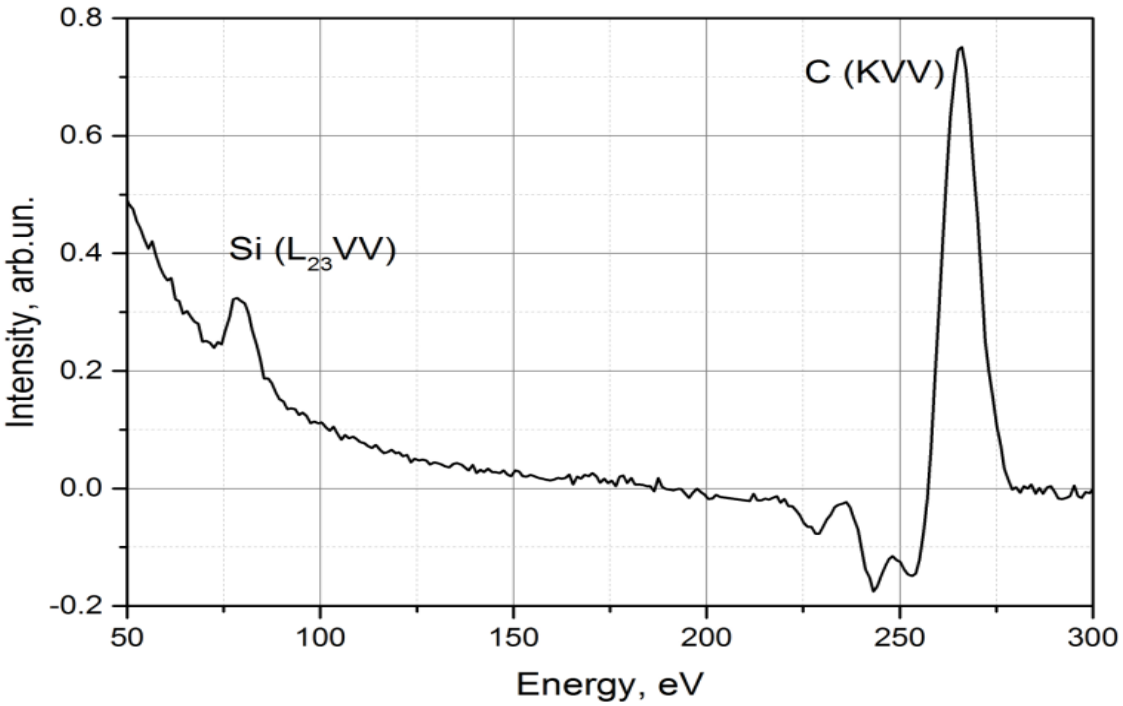

Figure 5-1: Auger Electron Spectroscopy Image of epitaxial graphene layer

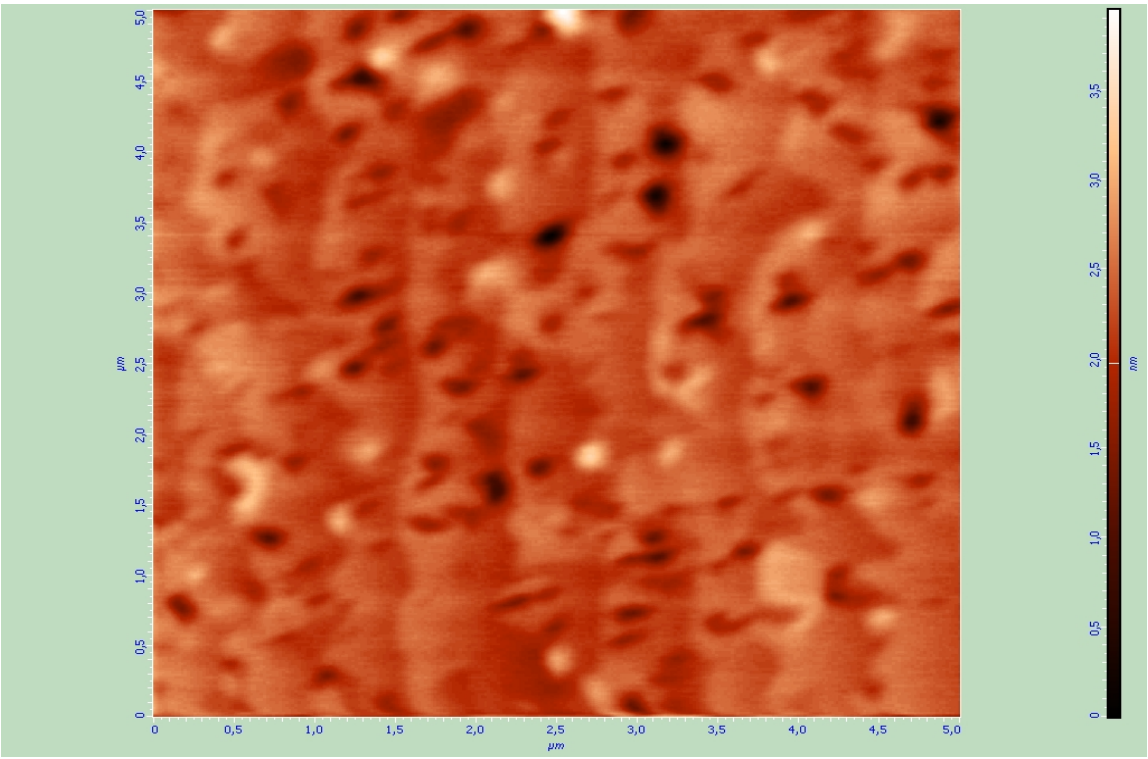

Figure 5-2: Image of the epitaxial graphene surface under AFM

ing process, the graphene film of different thicknesses and surface coverage exist together [31]. The bright spots may be SiC bi-layer or graphene, orange regions may be monolayer of graphene, while the black granules present in the image may be more holes on the surface formed during graphene growth.

5.2 Characterization of graphene sensors' responses

It covers the responses of the graphene sensors under varying ambient conditions. The dry air was used as carrier gas to measure the drift responses of the sensors. In each measurement cycle, four low level concentrations of NO_2 i.e. 0.1ppb, 0.2ppb, 0.5ppb and 1ppb were passed over the sensors to record their respective responses. After exposure to each concentration of NO_2, annealing was carried out at 110^oC to increase the responses at subsequent low concentration levels. Temperature was changed between room temperature and an elevated temperature (110^oC) to measure the corresponding changes in the drifts and responses of the sensors. Similarly, the variations in their drifts and responses due to the change in humidity level between RH=0.02% and RH=50% were also examined.

5.2.1 Sensor's drift

During the drift measurement of the graphene sensors, 1000 sccm of dry air was passed over the sensors at room temperature and the change in their resistances were measured as their drifts. The drifts of sensor1 collected for two measurement cycles are shown in the figure 5-3.

During the first measurement cycle, the resistance of the graphene sensor1 decreased non-linearly from 29.6 kΩ to 24.9 kΩ. There was initial sharp decrease in the resistance, which may be probably due to desorption of electron acceptors impurity species present in the dry air from the graphene surface. Desorption of the interfering gases causes increase in the carrier concentration of the sensor. In the later part of the measurement, the decrease in its resistance was relatively slow due to slower desorption of the residual contamination. During the second measurement as a continuation of the first, the resistance of sensor1 decreased from 24.9 kΩ to 23.7 kΩ and the dependence of the change in resistance approached towards linearity. There was overall decrease in the resistances of all the sensors in the dry air carrier gas. The drifts of sensors 2-6 are attached in the Appendix 3.

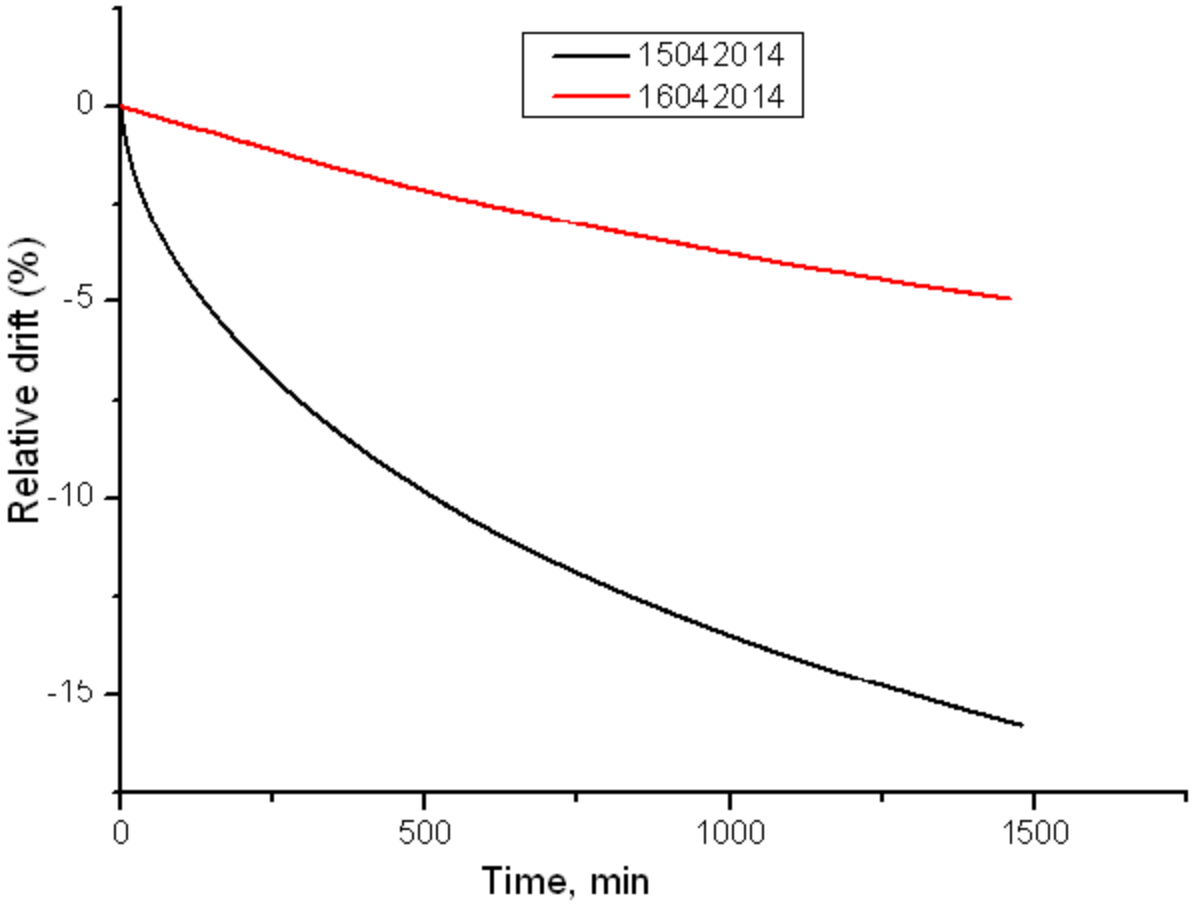

Figure 5-3: Relative drifts of sensor1 on exposure to carrier gas at room temperature (Drifts of sensor1 measured on 15.04.2014 and 16.04.2014 are represented by curves with colors black and red respectively.)

5.2.2 Drift under humid carrier gas

Most of the gas sensors perform in humid atmospheric condition; hence the measurement of drifts under humid condition was performed. The effect of humidity on the drifts of the graphene sensors were measured by examining their drifts upon exposure to carrier gas at the humidity level, RH=0.02% and 50%. A humidifier was used to vary the humidity levels of the carrier gas. With an equal duration of about 2 hours, 1 l/min flow of carrier gas (i.e. air) with humidity level RH=0.02%, RH=50% and RH= 0.02% respectively were passed over the sensors. The drifts of graphene sensors under these conditions are shown in figure 5-4.

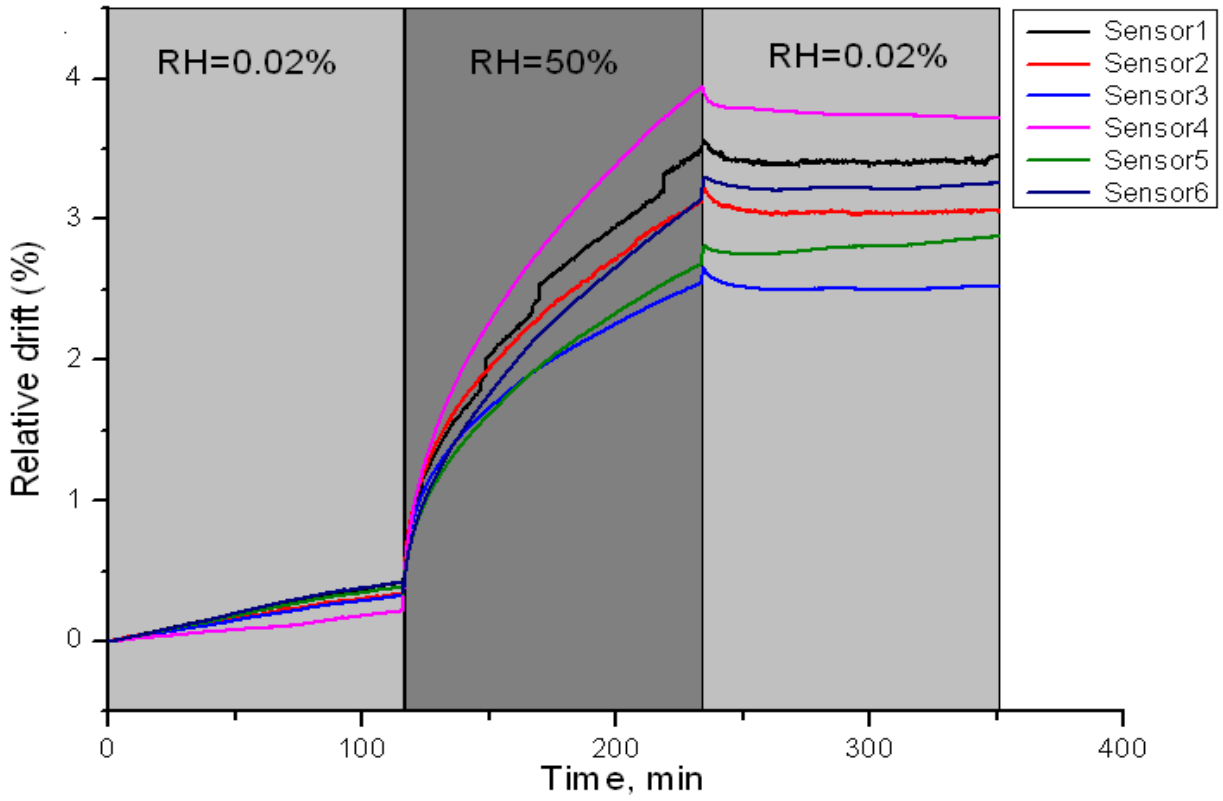

Figure 5-4: Relative drifts of all sensors on exposure to humid air with intervals of 2 hours at room temperature (Exposure periods with RH=0.02% humidity levels are marked by light grey bands and exposure periods with RH=50% as dark grey bands. Drifts of sensors 1-6 are represented by curves with colors black, red, blue, pink, green and violet respectively.)

Table 3: Drifts of sensors1-6 under carrier gas with relative humidity, RH =0.02% and RH=50% at room temperature

Sensor	Drift % (Humidity Drift)		
	RH=0.02% (before)	RH=50%	RH=0.02% (after)
Sensor1	0.4	3.5	-0.47
Sensor2	0.36	2.89	-0.15
Sensor3	0.31	2.32	-0.12
Sensor4	0.2	3.73	-0.22
Sensor5	0.38	2.41	0.08
Sensor6	0.4	2.88	-0.03

In the initial exposure to dry carrier gas with RH=0.02%, the drifts of graphene sensors showed a minor increase of 0.25% indicating withdrawal of electrons from graphene surface by the interfering gases in the air. Table 3 clearly shows that the drifts of the sensors increase by an

average of 2.96% under exposure of RH=50% humid air. The increment can be attributed to the adsorbed H_2O molecules acting as acceptors which withdraw electrons from the graphene layer and cause increase in its resistance. After adjusting humidity of carrier gas back to RH=0.02%, the drifts of the sensors decreased by an average of 0.17%. The direction of change in humidity drifts corresponds to desorption of water molecules from the graphene surface. The slower recovery exhibits the existence of strong bonding between the graphene layer and the adsorbed water molecules.

5.2.3 Drift at elevated temperature

The drifts of the gas sensors at elevated temperature become critical when they have to operate at high temperatures. To examine the effect of temperature on the drifts of the sensors, temperature was raised from room temperature to 110°C by supplying 10V DC voltage to the 100Ω Pt heater placed under the sample. Then 1 l/min flow of dry carrier gas was passed over the sensors and their drifts were measured. The drifts of graphene sensors at elevated temperature are shown in the figure 5-5 below.

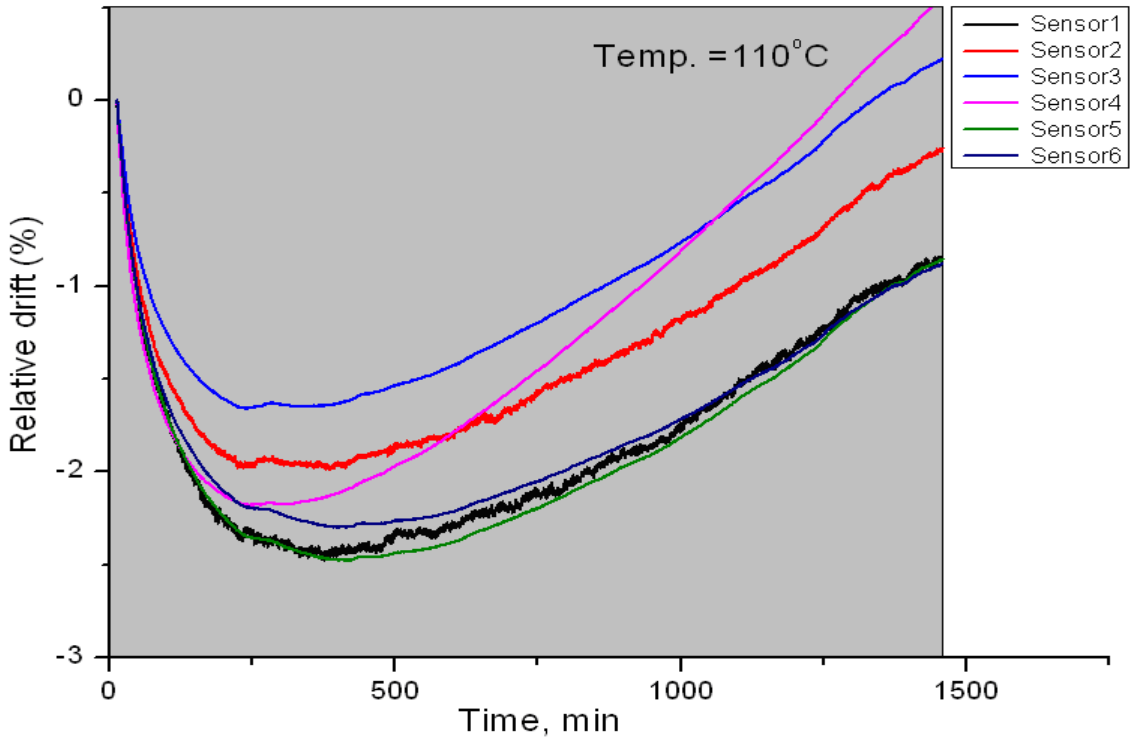

Figure 5-5: Relative drifts of all sensors on exposure to air at high temperature (Exposure period with temperature = 110°C is marked by light grey band. Drifts of sensors 1-6 are represented by curves with colors black, red, blue, pink, green and violet respectively.)

Initially, there is a sharp decrease in the resistances of the sensors and then, a much slower increase in their resistances until the end of the measurement cycle. The decrease in their resistances can be attributed to desorption of water molecules from the hot surface and thermal generation of electron hole pairs. However, the slow increase in their resistances is probably due to slow reaction of graphene surface with oxygen at elevated temperature.

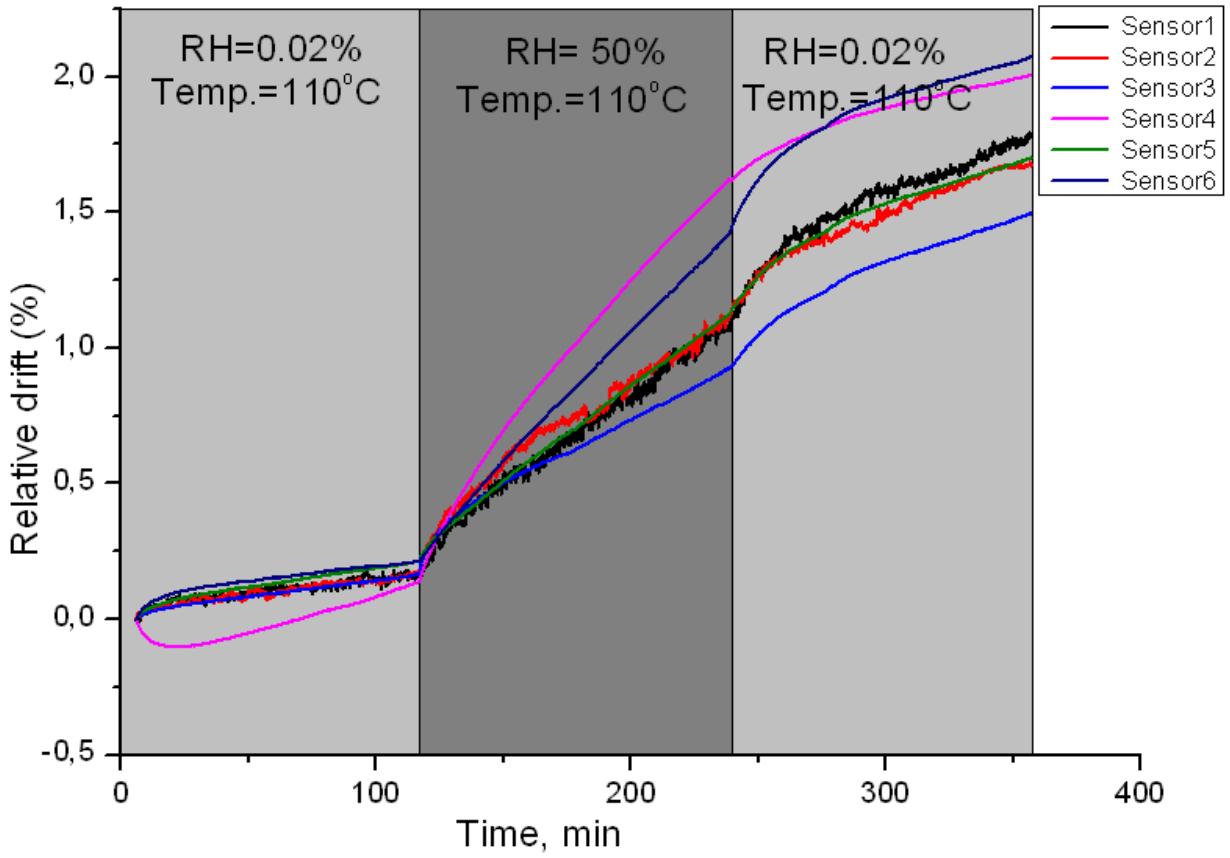

Figure 5-6: Relative drifts of all sensors on exposure to humid air with intervals of 2 hours at high temperature i.e. 110°C (Exposure periods under RH=0.02% humid conditions are marked by light grey bands and exposure periods under RH=50% humid condition as dark grey bands. Drifts of sensors 1-6 are represented by curves with colors black, red, blue, pink, green and violet respectively.)

The drifts of the sensors at elevated temperature under humid condition were also studied. The temperature of the sensors was raised by supplying 10V DC across the Pt resistors placed under the sample. 1 l/min flow of air with humidity level, RH=0.02%, RH=50% and RH=0.02% again was passed over the sensors, with equal duration of about 2 hours each and their corresponding

drifts were measured. The drifts of all the six sensors at elevated temperature under humid condition are shown in the figure 5-6.

At high temperature, the average drifts of the sensors under humidity level, RH= 0.02% (before), 50% and 0.02% (after) were calculated as 0.192%, 1.028% and 0.577% respectively. In comparison to the drifts of the sensors under humid condition at room temperature, the lower response to the water vapor exposure in the present condition may be due to lesser interaction of graphene surface with water molecules and the desorption of the adsorbed water molecules at high temperature.

Table 4: Drifts of sensors1-6 under carrier gas with relative humidity, RH =0.02% and RH=50% at high temperature (110^{o}C)

Sensor	Drift % (Temperature Drift under humid condition)		
	RH=0.02% (before)	RH=50%	RH=0.02% (after)
Sensor1	0.17	0.93	0.69
Sensor2	0.20	0.95	0.56
Sensor3	0.18	0.75	0.58
Sensor4	0.14	1.45	0.4
Sensor5	0.23	0.9	0.55
Sensor6	0.23	1.19	0.68

5.2.4 Response for low NO_2 concentration levels

Different low concentration levels of NO_2 i.e. 0.1ppb, 0.2ppb, 0.5ppb and 1ppb were applied over the graphene sensors to measure their responses at room temperature. It was done to extract the dependence of the response of a graphene sensor on the concentration of the test gas. In case of all the six sensors, an equal exposure time of 60 minutes was maintained for each concentration levels of NO_2 gas. After the exposure to each concentration level, an annealing period of 60 minutes was applied in order to obtain pristine graphene layer and improved responses for the subsequent concentration levels of NO_2. The responses of all the sensors at different concentration levels carried out in one particular measurement cycle are shown in the figure 5-7.

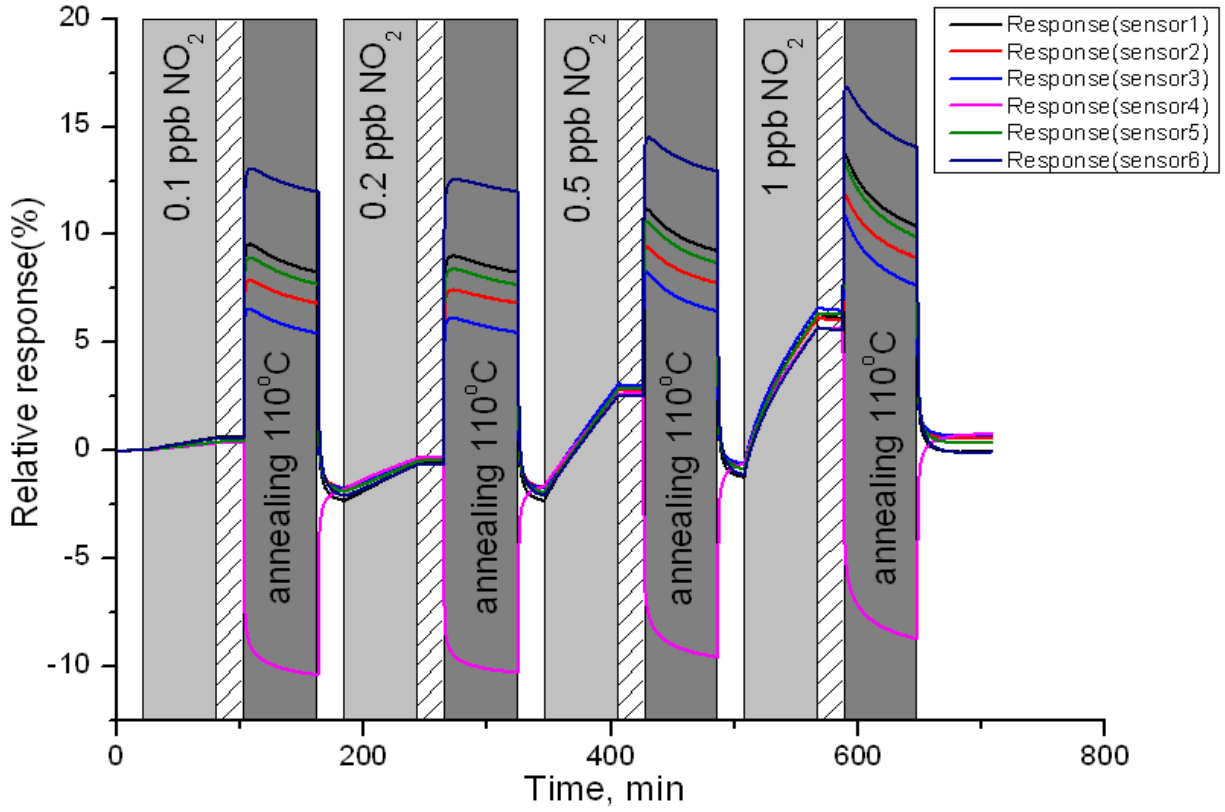

Figure 5-7: Responses of all sensors on exposure to gas mixture containing low concentration levels of NO_2 at room temperature (Exposure periods are marked by light grey bands, recovery periods as hatched bands and annealing periods as dark grey bands. Responses of sensors 1-6 are represented by curves with colors black, red, blue, pink, green and violet respectively.)

Table 5: Responses of sensors 1-6 at different concentrations of NO_2 at room temperature under RH=0.02% humid condition

Sensor	Response % (at NO_2 Concentration level)			
	0.1ppb	0.2ppb	0.5ppb	1ppb
Sensor1	0.56	1.6	4.84	6.88
Sensor2	0.36	1.52	4.5	6.78
Sensor3	0.38	1.37	4.56	6.85
Sensor4	0.4	1.65	4.85	6.93
Sensor5	0.38	1.33	4.45	6.68
Sensor6	0.43	1.31	4.14	6.09

The resistance of the graphene sensor increased upon the exposure to NO_2 gas. It confirmed the n-type conductivity of the monolayer epitaxial graphene. From table 5, it can be seen that the

response of the graphene sensor increases with increase in the concentration level of NO_2 gas. The response of sensor1 increased by 0.56%, 1.6%, 4.84% and 6.88% for concentration of 0.1ppb, 0.2ppb, 0.5ppb and 1ppb of NO_2 gas respectively. Such responses at low concentrations of NO_2 are significantly higher than the responses of gas sensors reported in various research papers. The response is lowest at 0.1ppb concentration level and highest at 1ppb concentration level. Hence, it is concluded that the response of the graphene sensor is proportional to the concentration level of NO_2. Response curves were almost horizontal during the recovery period, which indicates the strong bonding between graphene and NO_2 molecules. Annealing was used to clean the graphene surface due to the long desorption time at room temperature. The resistances of all the sensors increased rapidly at the start of annealing period and decreased sharply at the end of annealing due to positive thermal resistance. Sensor4 showed the opposite characteristics, the reason for which needs to be investigated.

The measurements were repeated for several times in order to validate the reproducibility of the responses of the sensors. The figure 5-8 shows that the rates of responses of the graphene sensors are linear at lower concentration levels of NO_2 gas. The bending of the responses after 0.5ppb is probably due to the saturation of graphene surface. Table 6 below contains the responses of sensor1 at different concentration levels of NO_2 at room temperature measured over several measurement cycles. The average responses of sensor1 for 0.1ppb, 0.2ppb, 0.5ppb and 1ppb of NO_2 gas were calculated as 0.65 %, 1.67%, 4.8% and 7.16 % respectively.

Table 6: Responses of sensor1 at different concentrations of NO_2 at room temperature under RH=0.02% humid condition. The responses are named after their measured date.

Measurement Name	Rate of response %/min of sensor 1 (at NO_2 Concentration level)			
	0.1ppb	0.2ppb	0.5ppb	1ppb
Res1_22042014	0.011	0.028	0.085	0.127
Res1_23042014	0.011	0.028	0.077	0.121
Res1_24042014	0.012	0.028	0.077	0.12
Res1_25042014	0.011	0.029	0.079	0.118
Res1_26042014	0.009	0.027	0.081	0.115
Res1_27042014	0.011	0.027	0.081	0.115

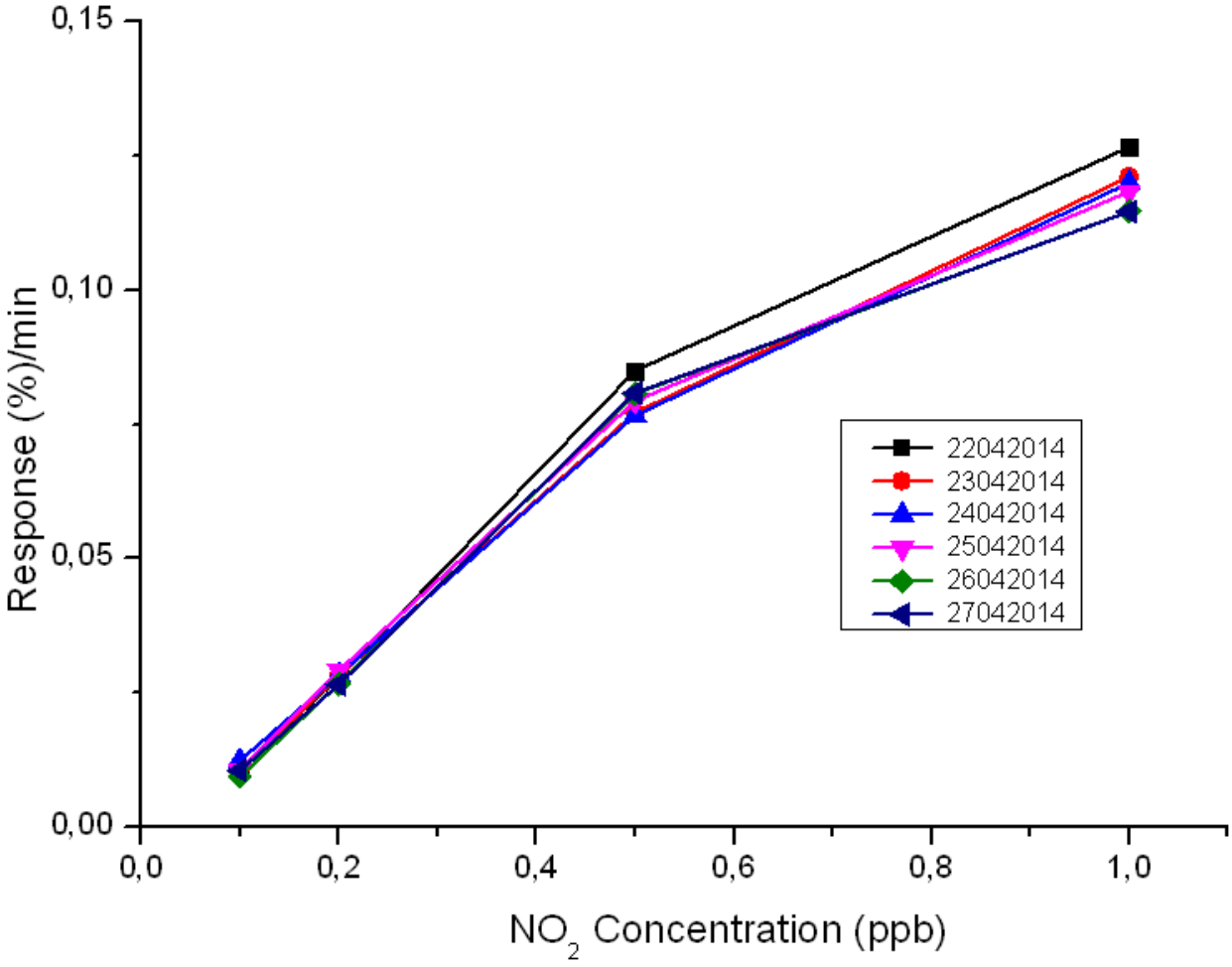

Figure 5-8: Dependence of the rates of responses of sensor1 on low NO_2 concentrations. The slope values were calculated for 60 minutes of exposure by the gas mixture containing NO_2. (Rates of responses of sensor1 during experiments on 22.04.2014, 23.04.2014, 24.04.2014, 25.04.2014, 26.04.2014 and 27.04.2014 are represented by black, red, blue, pink, green and violet colored curves respectively.)

The measurements of responses of sensors 2-6 under different concentration levels of NO_2 gas were repeated over several times at room temperature. They showed repeatability in their responses similar to the responses of sensor1 and have been attached in the Appendix 5.

5.2.5 Response for low NO_2 concentration levels under humid condition

With a constant humidity level (RH=50%), different concentration levels of NO_2 gas i.e. 0.1ppb, 0.2ppb, 0.5ppb and 1ppb were passed over the sensor samples and their responses were measured. The responses of sensors1-6 for different concentration levels of NO_2 gas under RH= 50% humidity level are shown in figure 5-9.

Table 7 contains the responses of the sensors for different concentrations of NO_2 gas under humid condition. The average responses of sensors under RH=50% humid condition were calculated as 0.72%, 1.44%, 5.62% and 9.89% for 0.1ppb, 0.2ppb, 0.5ppb and 1ppb NO_2 concentration levels respectively. In comparison to their responses under RH=0.02% humid condition, the corresponding responses of the sensors have increased under (RH=) 50% humidity level. As explained earlier, the adsorption of oxygen ions increases the defect density on the graphene surface which then increases the interaction rate of graphene surface with the NO_2 molecules. As a result, there is larger response upon exposure to NO_2 gas under humid condition. These results can be used to demonstrate the selectivity of graphene sensors to water molecules.

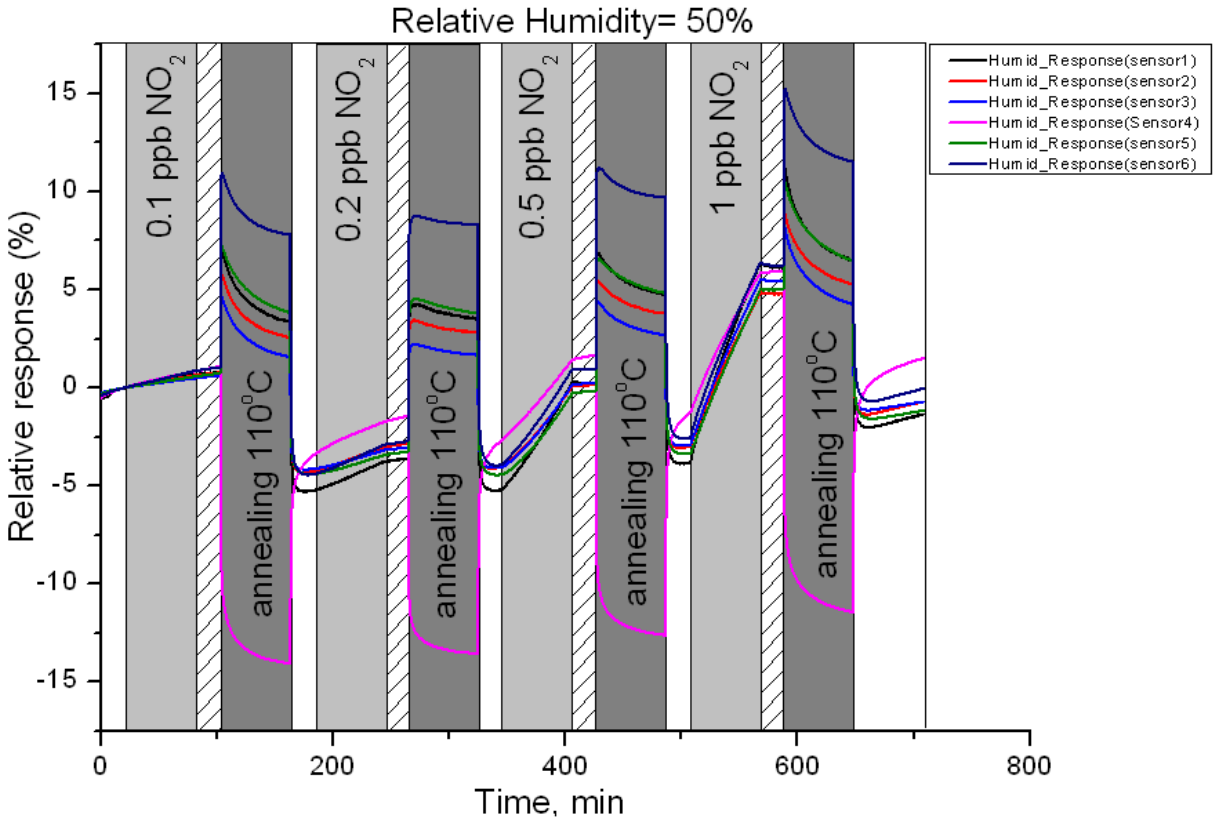

Figure 5-9: Responses of all sensors on exposure to gas mixture containing NO_2 at low concentration range at room temperature under RH=50% humid condition (Exposure periods are marked by light grey bands, recovery periods as hatched bands and annealing periods as dark grey bands. Responses of sensors 1-6 are represented by curves with colors black, red, blue, pink, green and violet respectively.)

Table 7: Responses of sensors1-6 at different concentrations of NO_2 at room temperature under RH=50% humid condition

Sensor	Response % (at NO_2 Concentration level under humid condition)			
	0.1ppb	0.2ppb	0.5ppb	1ppb
Sensor1	0.78	1.48	5.36	9.66
Sensor2	0.67	1.33	4.05	8.60
Sensor3	0.48	1.02	4.19	8.22
Sensor4	1.08	2.28	5	8.51
Sensor5	0.65	0.97	4.04	8.04
Sensor6	0.96	1.47	4.51	8.15

The comparison of dependence of the rates of responses for sensor1 under RH=0.02% and RH= 50% humidity level against different concentration levels of NO_2 gas is shown in figure 5-10. There is not much variation in the rates of the responses due to humidity at lower concentrations of NO_2, but only at higher concentration levels. Even at high concentration levels, the variation is itself very small. Hence the stable responses for the graphene sensors exit under humid condition.

During practical application, humid air is an important interfering component for the detection of NO_2 gas. The selectivity of a sensor to humidity is defined as the ratio of concentration of humidity to the concentration of NO_2 that gives the same response value. The selectivity of the graphene sensor1 was calculated to be 30,250,000. It shows that the fabricated graphene sensor is highly selective which is good for environmental implementation.

Table 8: Comparison of responses of sensor1 at different concentrations of NO_2 under RH=0.02%and RH=50% humidity level at room temperature. The responses are named after their measured date.

Measurement Name	Rate of response %/min of sensor 1 (at NO_2 Concentration level)			
	0.1ppb	0.2ppb	0.5ppb	1ppb
Res1_26042014	0.009	0.027	0.081	0.115
Humid_Res1_28042014	0.013	0.025	0.089	0.161
Humid_Res1_29042014	0.011	0.023	0.098	0.167

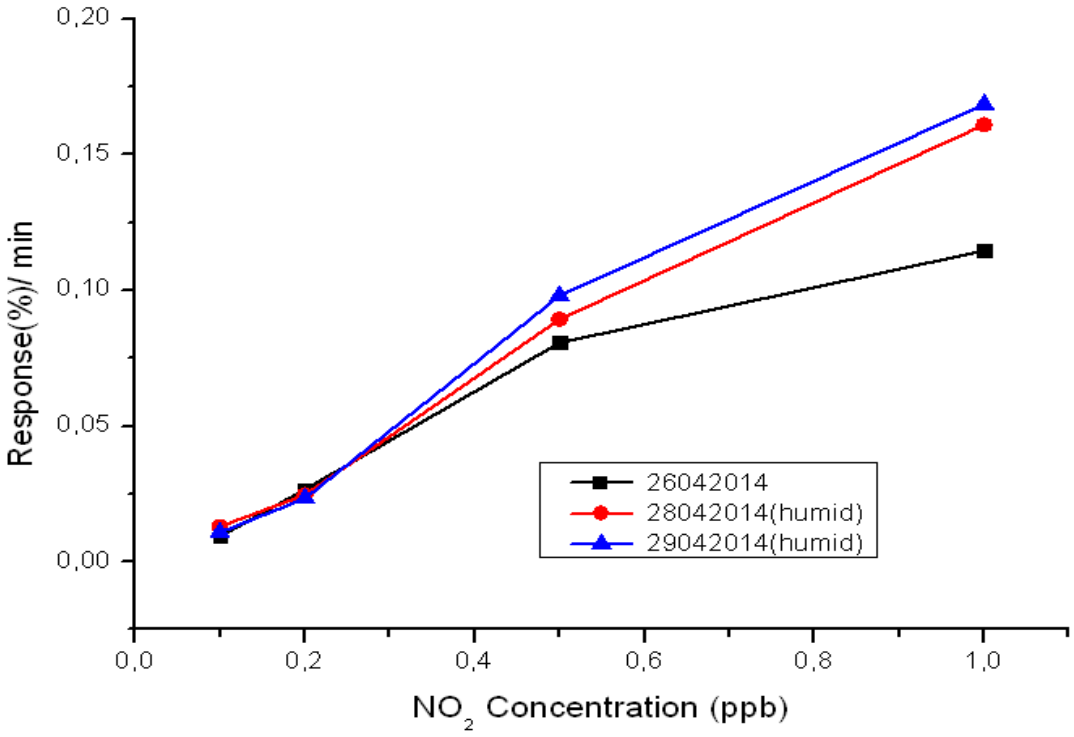

Figure 5-10: Comparison of the rates of responses of sensor1 under RH= 0.02% and RH=50% humid condition against low NO_2 concentrations. The rate values were calculated for 60 minutes of exposure by the gas mixture containing NO_2. (Rates of responses under RH=50% humidity condition are represented by red and blue curves while the black curve represents the rates of responses under RH=0.02% humidity condition.)

The comparison of the rates of responses for sensors 2-6 under RH= 0.02% and RH=50% humidity level against different concentration levels of NO_2 gas are attached in the Appendix 7.

5.2.6 Response for low NO_2 concentration levels at elevated temperature

The temperature of the sensors was raised by supplying 10V DC to the 100Ω Pt resistor placed under the sample. The different concentration levels of NO_2 i.e. 0.1ppb, 0.2ppb, 0.5ppb and 1ppb were passed over the sensors and their corresponding responses were collected. Exposure time for each concentration level was maintained as 60 minutes. As the temperature throughout the measurement cycle remained at 110°C, the non-exposure time intervals acted as recovery or annealing periods. The responses of graphene sensors under high temperature condition are shown in the figure 5-11.

The average responses of sensors at 110°C were 0.39%, 0.89%, 2.62% and 4.04% at 0.1ppb, 0.2ppb, 0.5ppb and 1ppb NO_2 concentration levels respectively. The reason for decreasing resp-

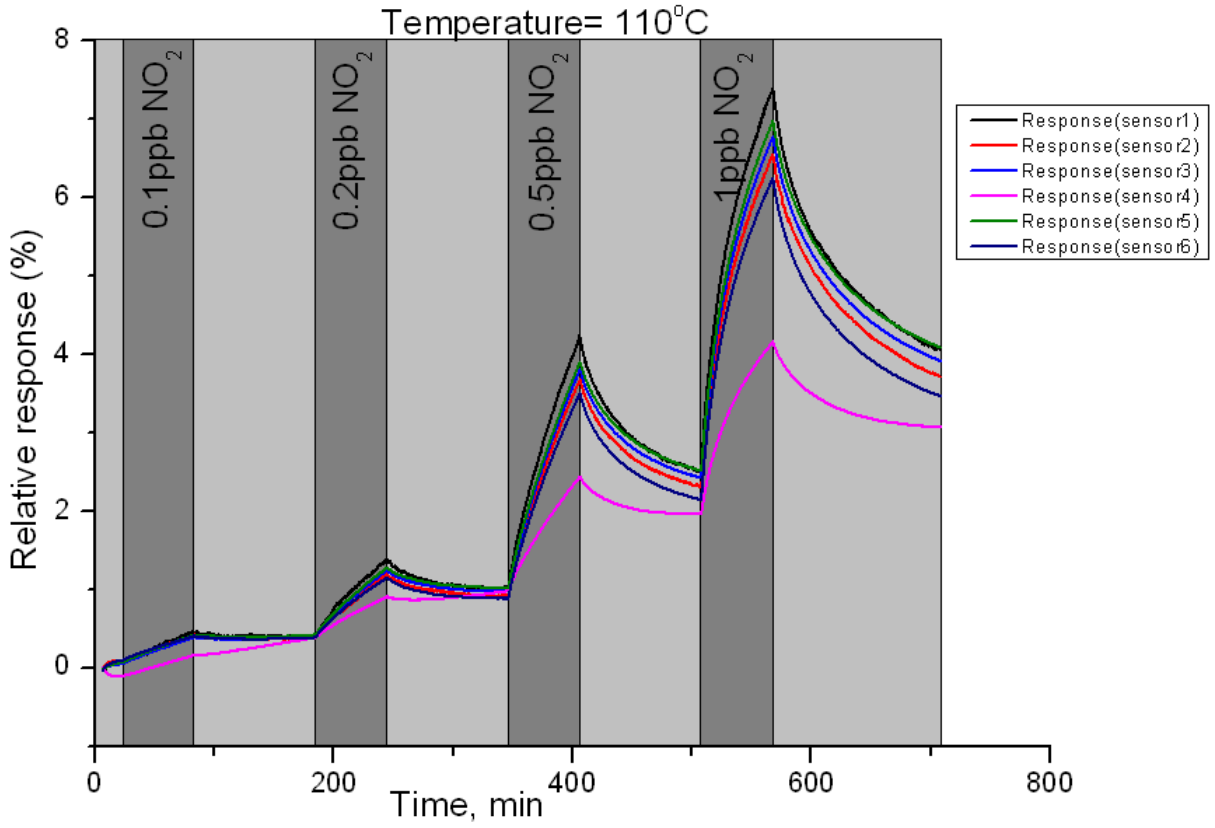

Figure 5-11: Responses of all sensors on exposure to gas mixture containing low concentration levels of NO_2 at elevated temperature i.e. 110°C (Exposure periods are marked by dark grey bands, remaining non-exposure time interval acts as both recovery and annealing periods marked as light grey bands. Responses of sensors 1-6 are represented by curves with colors black, red, blue, pink, green and violet respectively.)

Table 9: Responses of sensors1-6 at different concentrations of NO_2 at high temperature (110°C) under RH=0.02% humid condition

Sensor	Response % (at NO_2 Concentration level at high temperature)			
	0.1ppb	0.2ppb	0.5ppb	1ppb
Sensor1	0.48	1.02	3.24	4.9
Sensor2	0.44	0.82	2.76	4.25
Sensor3	0.41	0.86	2.82	4.34
Sensor4	0.17	0.56	1.47	2.19
Sensor5	0.43	0.87	2.87	4.46
Sensor6	0.42	1.19	2.58	4.09

onses of the sensors can be attributed to the weak C-N bonding at high temperature leading to less interaction between graphene and NO_2 molecules. The slow increment of the response

baseline of the sensors may be due to adsorption of oxygen at high temperature. Full recovery of the graphene surface did not occur due to the insufficient annealing period. The measurement of the responses of sensors1-6 for different concentration levels of NO_2 under high temperature condition was repeated again and has been attached in the Appendix 8.

Similarly, the sensors 1-6 were also exposed to different concentrations of NO_2 gas at high temperature under RH=50% humidity condition. Their responses were recorded as shown in figure 5-12. The average responses of sensors were calculated to be 0.48%, 0.71%, 2.43% and 3.12% at 0.1ppb, 0.2ppb, 0.5ppb and 1ppb NO_2 concentration levels respectively. The decrease in the responses may be again attributed to high temperature which allows lesser interaction of graphene layer with oxygen ions as well as NO_2 molecules.

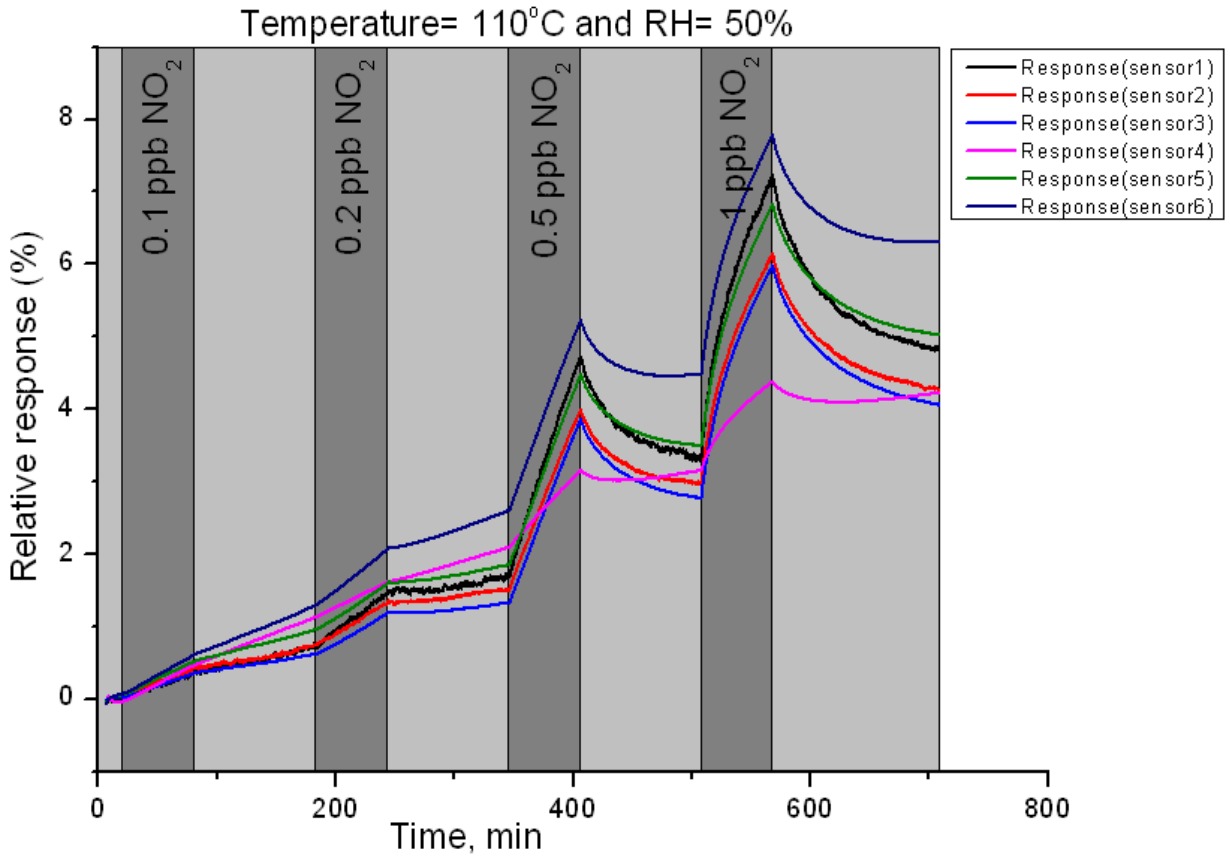

Figure 5-12: Responses of all sensors on exposure to gas mixture containing low concentration levels of NO_2 at elevated temperature i.e. 110°C under relative humidity of 50% (Exposure periods are marked by dark grey bands, remaining non-exposure time interval acts as both recovery and annealing periods marked as light grey bands. Responses of sensors 1-6 are represented by curves with colors black, red, blue, pink, green and violet respectively.)

Table 10: Responses of sensors1-6 at different concentrations of NO_2 at high temperature (110°C) under RH=50% humid condition

Sensor	Response % (NO_2 Concentration level at high temperature under humid condition)			
	0.1ppb	0.2ppb	0.5ppb	1ppb
Sensor1	0.41	0.83	3.04	3.93
Sensor2	0.44	0.65	2.51	3.18
Sensor3	0.37	0.61	2.56	3.21
Sensor4	0.49	0.59	1.12	1.75
Sensor5	0.54	0.71	2.66	3.33
Sensor6	0.64	0.89	2.69	3.3

The comparison of the rate of responses for sensor1 at room temperature, at high temperature, and at high temperature under RH=50% humidity level is shown against different concentration levels of NO_2 gas in the figure 5-13. At room temperature condition, the rates of responses for sensor 1 are 0.0063 %/min, 0.022 %/min, 0.074 %/min and 0.111 %/min for 0.1ppb, 0.2ppb, 0.5ppb and 1ppb of NO_2 concentration levels respectively. At high temperature condition, the average rates of responses for sensor 1 are 0.0067 %/min, 0.0115 %/min, 0.042 %/min and 0.065 %/min for 0.1ppb, 0.2ppb, 0.5ppb and 1ppb of NO_2 concentration levels respectively. Similarly, at high temperature condition under RH=50% humid condition, the rates of responses for sensor1 are 0.0087 %/min, 0.0103 %/min, 0.044 %/min and 0.056 %/min at 0.1ppb, 0.2ppb, 0.5ppb and 1ppb of NO_2 concentration levels respectively. There exits little variation between the rates of responses under these conditions. Hence, the responses of the graphene sensors for low concentrations of NO_2 gas at high temperature can be considered as stable.

Table 11: Comparison of responses of sensor1 at different concentrations of NO_2 at room temperature and, at high temperature (110°C) under RH=0.02%and RH=50% humid condition. The responses are named after their measured date.

Measurement Name	Rate of response %/min (at NO_2 Concentration level)			
	0.1ppb	0.2ppb	0.5ppb	1ppb
Response(sensor1)_26042014	0.009	0.027	0.081	0.115
High temp_Response(sensor1)_01052014	0.008	0.017	0.054	0.082
High temp_Response(sensor1)_05052014	0.013	0.014	0.044	0.062
Humid_High temp_Response(sensor1)_02052014	0.007	0.014	0.051	0.066

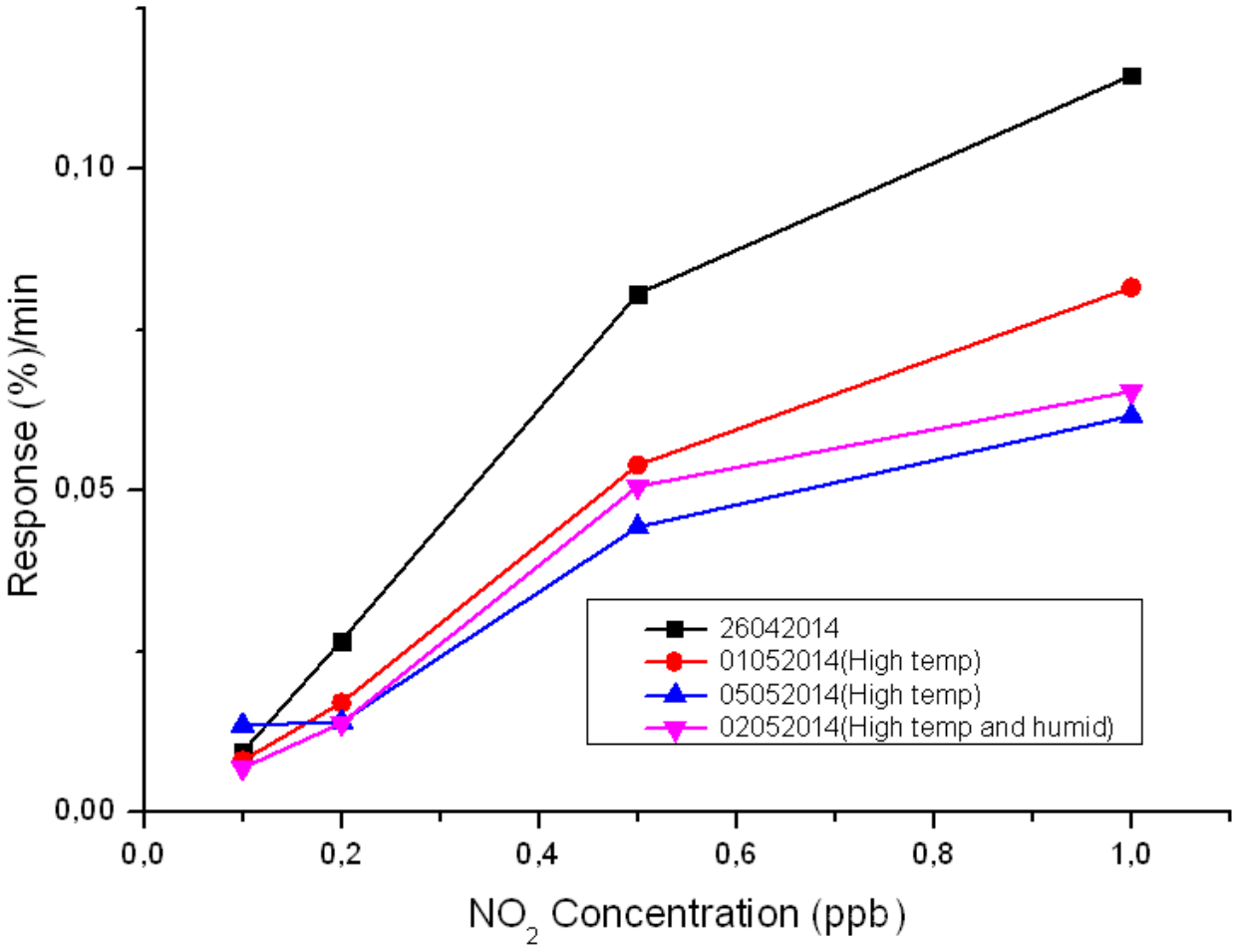

Figure 5-13: Comparison of the rates of responses of sensor1 at room temperature, at high temperature, and at high temperature under RH=50% humid condition against low NO_2 concentrations. The rate values were calculated for 60 minutes of exposure by the gas mixture containing NO_2. (Rates of responses at room temperature are represented by black curve; rates of responses at high temperature are represented by red and blue curves while the pink curve represents the rates of responses at high temperature under humid condition.)

The comparison of the rate of responses for sensors2-6 at high temperature and at high temperature under RH=50% humid condition against different low concentration levels of NO_2 were similar to sensor 1 and are attached in the Appendix 9.

6. Conclusions

Researchers are focused on exploiting the highly transparent, very flexible and atomically thin graphene layer on various platforms to realize ultra-sensitivity of gas sensors for NO_2 detection that is unimaginable from any other known material. This work demonstrates the high sensitivity of monolayer epitaxial graphene based gas sensor on low concentration levels of NO_2 gas and also studies the effects of temperature and humidity on its sensitivity.

In this work, simple resistive devices based on epitaxially grown graphene layer were fabricated. The effects of humidity and temperature on the drifts of the sensors were examined. Under humid air with RH=50%, there was an average 2.96% increase in the drifts of the sensors. At elevated temperature (110^oC), the sensors showed an initial sharp decrease in their drifts, followed by a slower increase in drift similar to their drifts at room temperature. However, the increase in the drift at elevated temperature is greater than that at room temperature (0.573 % > 0.342 %).

Responses of all the graphene sensors were measured to four different low concentrations of NO_2 gas i.e. 0.1ppb 0.2ppb, 0.5ppb and 1ppb. It was found that the sensitivities of the sensors were proportional to the concentration of NO_2 gas. The measurements of the responses of the sensors were repeated several times to check the validity of the obtained responses. At room temperature and relative humidity of 0.02%, the average responses of sensor1 at 0.1ppb, 0.2ppb, 0.5ppb and 1ppb concentrations of NO_2 gas were 0.65 %, 1.67%, 4.8% and 7.16 % respectively.

The effects of humidity on the sensitivity of the graphene sensors were evaluated by examining their responses towards NO_2 gas mixed with carrier gas at relative humidity of 0.02% and 50% respectively. The responses of the sensors increased upon detection of NO_2 under high humid condition. At relative humidity of 50%, there were 0.07%, -0.23%, 0.82% and 2.73% increment in the sensitivity of sensor1 at 0.1ppb, 0.2ppb, 0.5ppb and 1ppb NO_2 concentration respectively than their corresponding responses at relative humidity of 0.02%. Similarly, the effects of temperature on sensitivity of the graphene sensors were determined by testing their responses at room temperature (20^oC) and at an elevated temperature i.e. 110^oC. At elevated temperature, the sensors exhibited decrease in their responses compared to their responses at room temperature. In comparison to its responses at room temperature, there were 0.005%, 0.74%, 1.85% and 2.86%

decrease in the sensitivity of sensor1 at 0.1ppb, 0.2ppb, 0.5ppb and 1ppb NO_2 concentration respectively at elevated temperature.

Rate of change of responses were calculated to compare the responses of the sensors. There was little variation in the rate of change of responses under humid condition in comparison to the dry condition at lower concentrations of NO_2. Even at higher concentration levels, the variations in rate of change of responses were themselves very small. Similar cases were observed for elevated temperature condition and elevated temperature under humid condition. The responses of the sensors were, thus, considered as stable. The selectivity of the sensor to humidity (vapor), one of the important interfering gases, was calculated as 30,250,000. In summary, ultra-sensitive gas sensors with stable responses for NO_2 detection using monolayer epitaxial graphene have been demonstrated. Sensitivity down to sub-ppb level and high selectivity towards water vapor make these sensors suitable for environment pollution monitoring.

In future, the ultra sensitivity of the monolayer epitaxial graphene towards low concentrations of NO_2 gas can be extended to the detection of other gases such as CO, CO_2, NH_3, NO, N_2O, SO_2 etc. Using RHEED and LEED together with AFM helps for precise determination of graphene surface morphology. It can be used to determine the effects of graphene morphology on the sensitivity towards test gases. Similarly, Hall Effect measurements help to determine the mobility in monolayer graphene layer. The impact of mobility on the sensitivity of the graphene sensors on detection of the gases can also be tested. The chemical sensitivity of the sensor can be improved by functionalization of graphene surface. The doping of graphene layer helps to increase the defect sites for interaction with the test gases. Anupama Ghosh et al [2] examined the effect of doping of graphene layer prepared by arc-discharge of graphite in hydrogen (HG) and concluded the Nitrogen doped graphene layer is more sensitive than the Boron doped graphene layer for NO_2 detection. Also, Chung et al [10] studied NO_2 detection using ozone treated graphene sensor (OTG) and found that in comparison to a pristine graphene sensor, the use OTG sensor showed the percentage response improved by factor of 2 and response time by a factor of 8 when it was exposed to 200 ppm concentration of NO_2 at room temperature. So, this study can also be extended to examine the sensitivity of p-doped and n-doped epitaxial graphene layer on low concentrations of various test gases.

Bibliography

[1] T. Becker, S. Muhlberger, C. Braunmuhl, G. Muller, T. Ziemann, K. V. Hechtenberg, "Air pollution monitoring using tin-oxide-based microreactor systems", *Sensors and Actuators B: Chemical* 69(1-2) 108-119, September 2000 URL http://dx.doi.org/10.1016/S0925-4005(00)00516-5.

[2] Ghosh, Anupama ; Late, Dattatray J. ; Panchakarla, L. S. ; Govindaraj, A. ; Rao, C. N. R; "NO_2 and humidity sensing characteristics of few-layer graphenes", *Journal of Experimental Nanoscience* 4(4) 313-322, October 2009. URL http: //dx.doi.org/10.1080/17458080903115379.

[3] Sukju Hwang; Joon Hyong Cho; Juwhan Lim; Whan Kyun Kim; Hyunjin Shin; Choi, J.Y.; Choi, J.H.; Sang-Yoon Lee; Kim, J.M.; Jae Hun Kim; Seok Lee; Seong-Chan Jun. "Graphene based NO_2 gas sensor". *Nanotechnology Materials and Devices Conference (NMDC), 2010 IEEE* 18-21, October 2010. URL http: //dx.doi.org/10.1109/NMDC.2010.5649598.

[4] Chen, Gugang; Paronyan, Tereza M.; Harutyunyan, Avetik R.; "Sub-ppt gas detection with pristine graphene." *Applied Physics Letters* 101(5) 053119 - 053119-4, July 2012. URL http://dx.doi.org/10.1063/1.4742327

[5] M. Ettore, V. la Ferrara, M. Mara, T. Polichetti, N. Ivana, and G. di Francia, "Gas sensors based on graphene: comparison of two different fabrication approaches." *Chimica Oggi*, 29(1) 39-41, 2011.

[6] R. Pearce, T. Iakimov, M. Andersson, L. Hultman, A. Lloyd Spetz, R. Yakimova "Epitaxially grown graphene based gas sensors for ultra sensitive NO_2 detection." *Sensors and Actuators B: Chemical* 155(2) 451- 455, July 2011. URL http://dx.doi.org/10.1016/j.snb.2010.12.046

[7] S. Novikov, Joni Hämäläinen, J. Walden, I. Iisakka, N. Lebedeva and A. Satrapinski, "Characterization of epitaxial and CVD graphene with double metal-graphene contacts for gas sensing", *International Congress of Metrology 13003 (2013),* 13003(p1-p4), October 2013. URL http://dx.doi.org/10.1051/metrology/201313003

[8] Md.W.K. Nomani, Razib Shishir, Muhammad Qazi, Devendra Diwan, V.B. Shields, M.G. Spencer, Gary S. Tompa, Nick M. Sbrockey, Goutam Koley. "Highly sensitive and selective

detection of NO_2 using epitaxial graphene on 6H-SiC." *Sensors and Actuators B: Chemical* 150(1) 301-307, September 2010. URL http://dx.doi.org/10.1016/j.snb.2010.06.069

[9] F. Schedin, A. K. Geim, S. V. Morozov, E. W. Hill, P. Blake, M. I. Katsnelson, K. S. Novoselov. "Detection of individual gas molecules adsorbed on graphene." *Nature Materials* 6(9) 652-655, September 2007. URL http://dx.doi.org/10.1038/nmat1967

[10] M. G. Chung, D. H. Kim, H. M. Lee, T. Kim, J. H. Choi, D. K. Seo, J.-B. Yoo, S.-H. Hong, T. J. Kang, Y. H. Kim. "Highly Sensitive NO_2 Gas Sensor Based on Ozone Treated Graphene." *Sensors and Actuators B: Chemical 166-167* 172-176, May 2012. URL http://dx.doi.org/10.1016/j.snb.2012.02.036

[11] A. K. Singh, M. A. Uddin, J. T. Tolson, H. Maire-Afeli, N. Sbrockey, G. S. Tompa, M. G. Spencer, T. Vogt, T. S. Sudarshan, G. Koley, "Electrically tunable molecular doping of Graphene" *Applied Physics Letters,* 102(4) 043101(1-5), January 2013. URL http://dx.doi.org/10.1063/1.4789509

[12] Keun Soo Kim, Yue Zhao, Houk Jang, Sang Yoon Lee, Jong Min Kim, Kwang S. Kim, Jong-Hyun Ahn, Philip Kim, Jae-Young Choi, Byung Hee Hong, "Large-scale pattern growth of graphene lms for stretchable transparent electrodes", *Nature* 457(7230) 706-710, February 2009. URL http://dx.doi.org/10.1038/ nature07719

[13] M Scarselli, P Castrucci, M De Crescenzi. "Electronic and optoelectronic nano-devices based on carbon nanotubes." *Journal of Physics: Condensed Matter* 24(31) 313202(36pp), July 2012. URL http://dx.doi.org/10.1088/0953-8984/24/31/313202

[14] A. H. Castro Neto, F. Guinea, N. M. R. Peres, K. S. Novoselov, A. K. Geim. "The electronic properties of graphene" *Reviews of Modern Physics* 81(1) 109-162, January 2009. URL http://dx.doi.org/10.1103/RevModPhys.81.109

[15] Christopher John Borsa, "Large Area Graphene Synthesis" *Master's Thesis*, KTH Royal Institute of Technology 2012 URL http://kth.diva-portal.org/smash/get/diva2:523691/FULLTEXT01.pdf

[16] J Güttinger, F Molitor, C Stampfer, S Schnez, A Jacobsen, S Dröscher, T Ihn, K Ensslin. "Transport through graphene quantum dots." *Reports on Progress in Physics* 75(12) 126502(24pp), November 2012. URL http://dx.doi.org/10.1088/0034-4885/75/12/126502

[17] S. Basu, P. Bhattacharyya. "Recent developments on graphene and graphene oxide based solid state gas sensors." *Sensors and Actuators B: Chemical*, 173, 1-21, October 2012. URL http://dx.doi.org/10.1016/j.snb.2012.07.092

[18] S. Y. Zhou, G. H. Gweon, A. V. Fedorov, P. N. First, W. A. de Heer, D. H. Lee, F. Guinea, A. H. Castro Neto and A. Lanzara "Substrate-induced bandgap opening in epitaxial graphene." *Nature Materials* 6(10) 770-775, October 2007. URL http://dx.doi.org/10.1038/nmat2003

[19] F. Guinea. "Charge distribution and screening in layered graphene systems." *Physical Review B* 75(23) 235433(7pp), June 2007. URL http://dx.doi.org/10.1103/PhysRevB.75.235433

[20] O. Leenaerts, B. Partoens, F. M. Peeters. "Adsorption of H_2O, NH_3, CO, NO_2, and NO on graphene: a first-principles study." *Physical Review B* 77(12) 125416(6pp), March 2008. URL http://dx.doi.org/10.1103/PhysRevB.77.125416

[21] Joni Hämäläinen, "Characterization of epitaxial and CVD graphene films for evaluation of their applications for sensing NO_2", Master's Thesis, University of Jyväskylä 2013

[22] Wai-Leung Yim, X. G. Gong, Zhi-Feng Liu. "Chemisorption of NO_2 on Carbon Nanotubes: a first-principles study." *The Journal of Physical Chemistry B* 107(35), 9363-9369, July 2003. URL http://dx.doi.org/10.1021/jp0276471

[23] A. K. Geim, K. S. Novoselov, "The rise of graphene." *Nature Materials* 6(3) 183-191, March 2007. URL http://dx.doi.org/10.1038/nmat1849

[24] T. Ueda, M.M.H. Bhuiyan, H. Norimatsu, S. Katsuki, T. Ikegami, F. Mitsugi "Development of carbon nanotube-based gas sensors for NO_x gas detection working at low temperature." *Physica E: Low-dimensional Systems and Nanostructures* 40(7), 2272_2277, May 2008. URL http://dx.doi.org/10.1016/j.physe.2007.12.006

[25] T. Pustelny, M. Setkiewicz, S. Drewniak, E. Maciak, A. Stolarczyk,M. Procek, M. Urbanczyk, K. Gut, Z. Opilski, I. Pasternak and W. Strupinski, "The Influence of Humidity on the Resistance Structures with Graphene Sensor Layer." *Acta Physica Polonica, A.* 122(5), 870_873, November 2012. URL http://przyrbwn.icm.edu.pl/APP/PDF/122/a122z5p20.pdf

[26] T. Pustelny, S. Drewniak, M. Setkiewicz, E. Maciak, M. Urbanczyk, M. Procek, K. Gut, Z. Opilski, J. Jagiello, and L. Lipinska. "The sensitivity of sensor structures with oxide graphene exposed to selected gaseous atmospheres." *Bulletin of the Polish Academy of Sciences:*

Technical Sciences 61(3), 705_710, October 2013. URL http://dx.doi.org/10.2478/bpasts-2013-0075.

[27] E. Vesapuisto, W. Kim, S. Novikov, H. Lipsanen, P. Kuivalainen "Growth temperature dependence of the electrical and structural properties of epitaxial graphene on SiC(0001)." *Physica Status Solidi B* 248(8), 1908_1914, August 2011. URL http://dx.doi.org/10.1002/pssb.201046368

[28] Luxmi, Shu Nie, P. J. Fisher, R. M. Feenstra, Gong Gu and Yugang Sun. "Temperature dependence of Epitaxial Graphene Formation on SiC(0001)." *Journal of Electronic Materials* 38(6), 718-724, June 2009. URL http://dx.doi.org/10.1007/s11664-008-0584-3

[29] Michiko Sato, Shiori Shirai, Yoshihiko Seyama, Toru Itakur, "Analysis of Insulating Materials and Deep Interfaces by Auger Electron Spectroscopy." *Fujitsu scientific and technical journal* 46(3), 257-262, July 2010

[30] C. J. Powell, A. Jablonski, "Evaluation of Calculated and Measured Electron Inelastic Mean Free Paths near Solid Surfaces." *Journal of Physical and Chemical Reference Data* 28(1), 19-62, 1999 URL http://dx.doi.org/10.1063/1.556035

[31] Erkki Vesapuisto, "Growth and Characterization of Epitaxial Graphene on 4H-SiC(0001) substrate", *Master's Thesis*, Aalto University (2010).

[32] Ian Frank, "Shaping Graphene: An alternative approach" *Thesis*, Pomona College 2008 URL http://physastro.pomona.edu/wp-content/uploads/2012/09/Ian_Frank_Thesis.pdf.

[33] Aapo Varpula. "Modified vapor generation system." *Reports in Electron Physics*, Aalto University, 2010

Appendices

APPENDIX 1	Images of epitaxial graphene layer
APPENDIX 2	"Si:C Auger intensity ratio Vs number of graphene layers" curve
APPENDIX 3	Relative drifts of sensor2-6 on exposure to carrier gas at room temperature
APPENDIX 4	Responses of all sensors on exposure to gas mixture containing NO_2 at low concentration ranges at room temperature (Repeated measurements were performed on 23.04.2014, 24.04.2014 and 27.04.2014)
APPENDIX 5	Dependence of the rates of responses for sensors 2-6 on low NO_2 concentrations
APPENDIX 6	Responses of all sensors on exposure to gas mixture containing NO_2 at low concentration range at room temperature and 50% humid condition (Repeated measurements were performed on 29.04.2014)
APPENDIX 7	Comparison of the rates of responses for sensors 2-6 under RH=0.02% and RH=50% humid condition against low NO_2 concentrations
APPENDIX 8	Responses of all sensors on exposure to gas mixture containing NO_2 at low concentration range at elevated temperature (Repeated measurements were performed on 05.05.2014)
	Responses of all sensors on exposure to gas mixture containing NO_2 at low concentration range at elevated temperature i.e. 110°C and relative humidity of 50% (Repeated measurements were performed on 03.05.2014)
APPENDIX 9	Comparison of the rates of responses for sensors 2-6 at high temperature, and at high temp under RH=50% humid condition against low NO_2 concentrations

APPENDIX 1

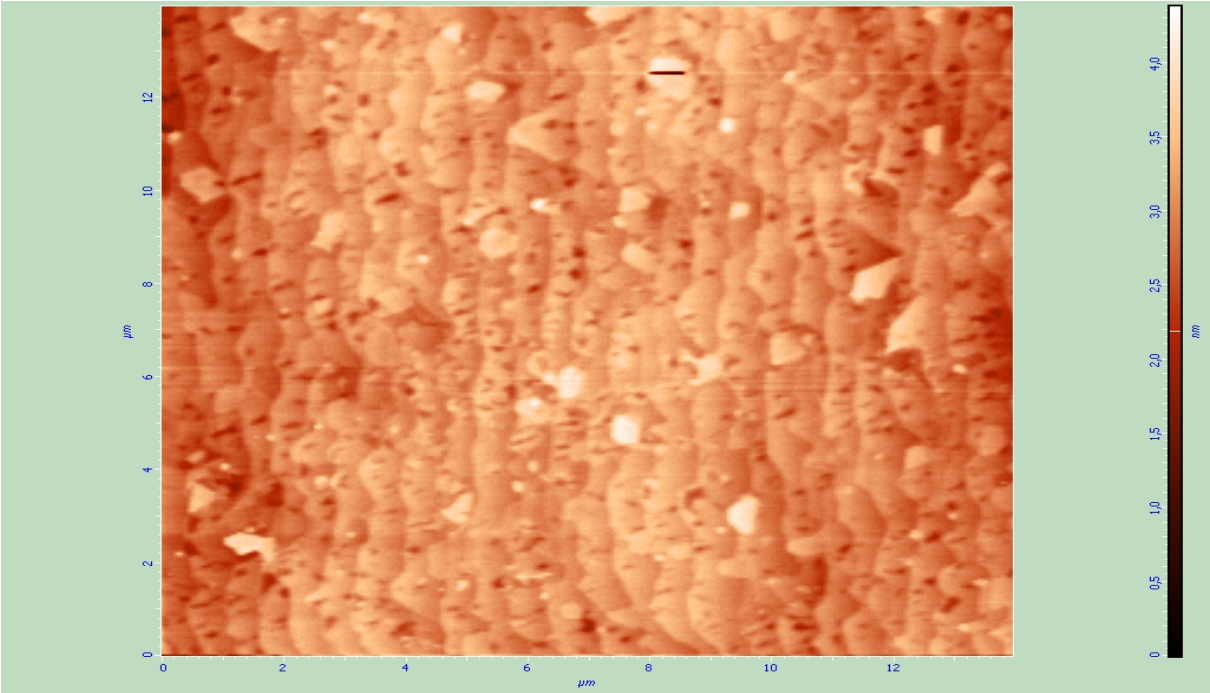

Figure A1: A 13µm*13µm image of monolayer epitaxial graphene fabricated using SiC substrate on 13.03.2014 which has been used in the current study.

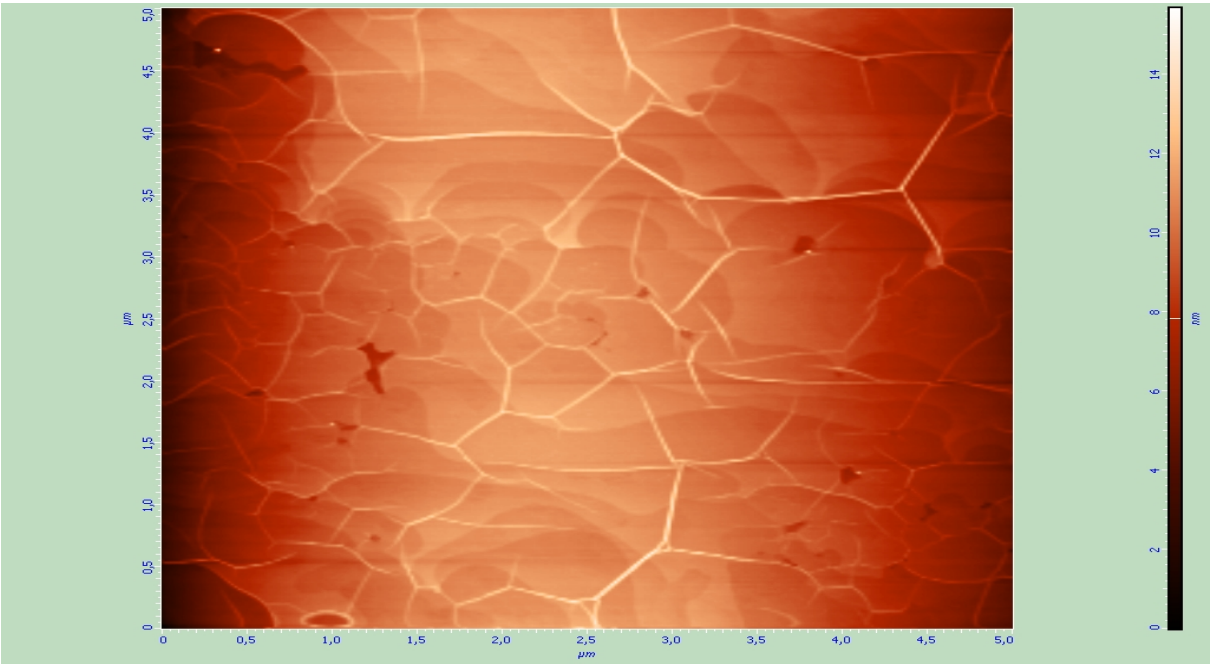

Figure A2: Few-layered epitaxial graphene fabricated on SiC substrate on 20.03.2014. This few-layered graphene was not used for study as the sensors fabricated using it showed poor sensors' drifts.

APPENDIX 2

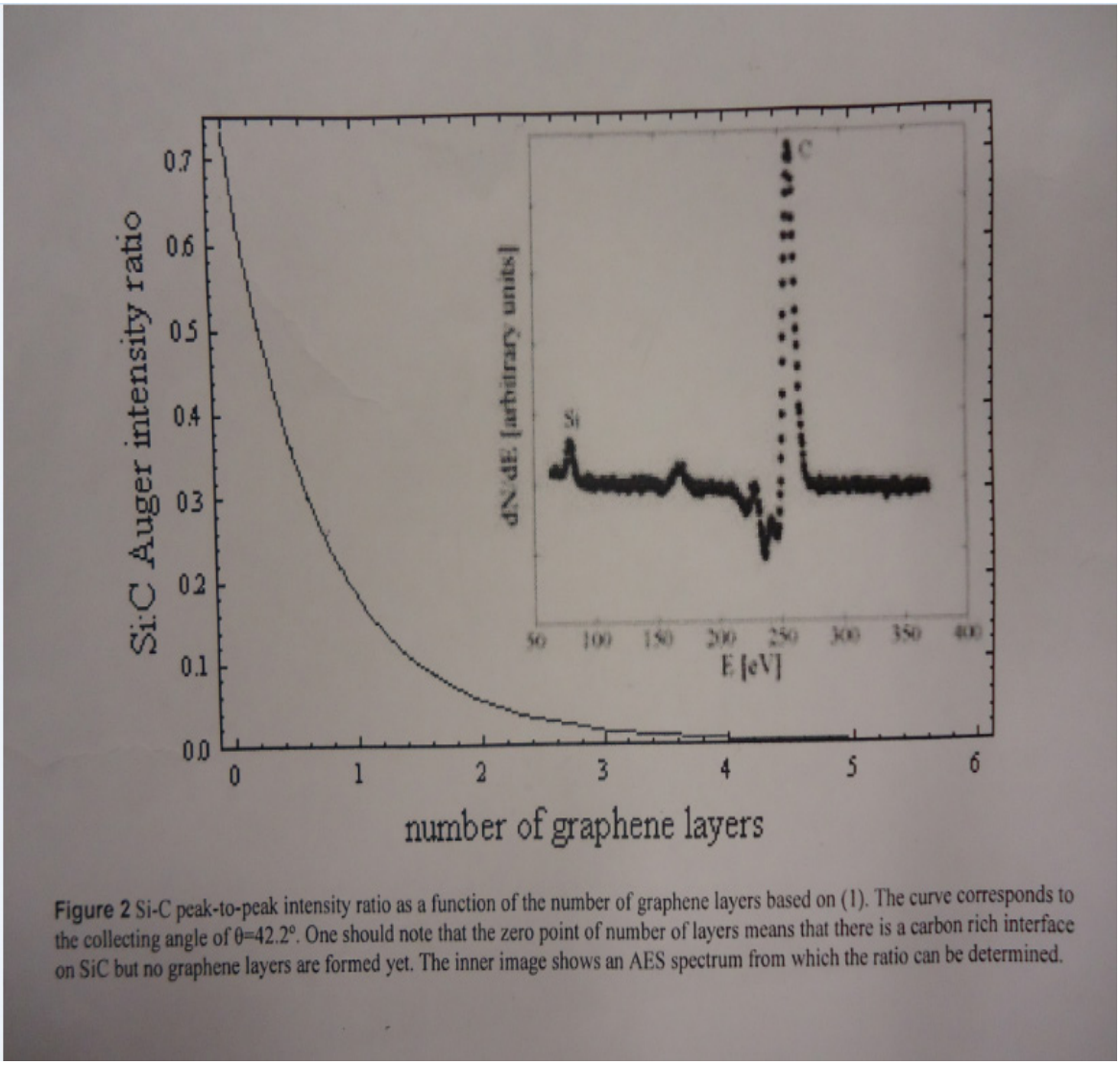

Figure 2 Si-C peak-to-peak intensity ratio as a function of the number of graphene layers based on (1). The curve corresponds to the collecting angle of θ=42.2°. One should note that the zero point of number of layers means that there is a carbon rich interface on SiC but no graphene layers are formed yet. The inner image shows an AES spectrum from which the ratio can be determined.

Figure A3: "Si:C Auger intensity ratio Vs number of graphene layers" curve [27]

APPENDIX 3

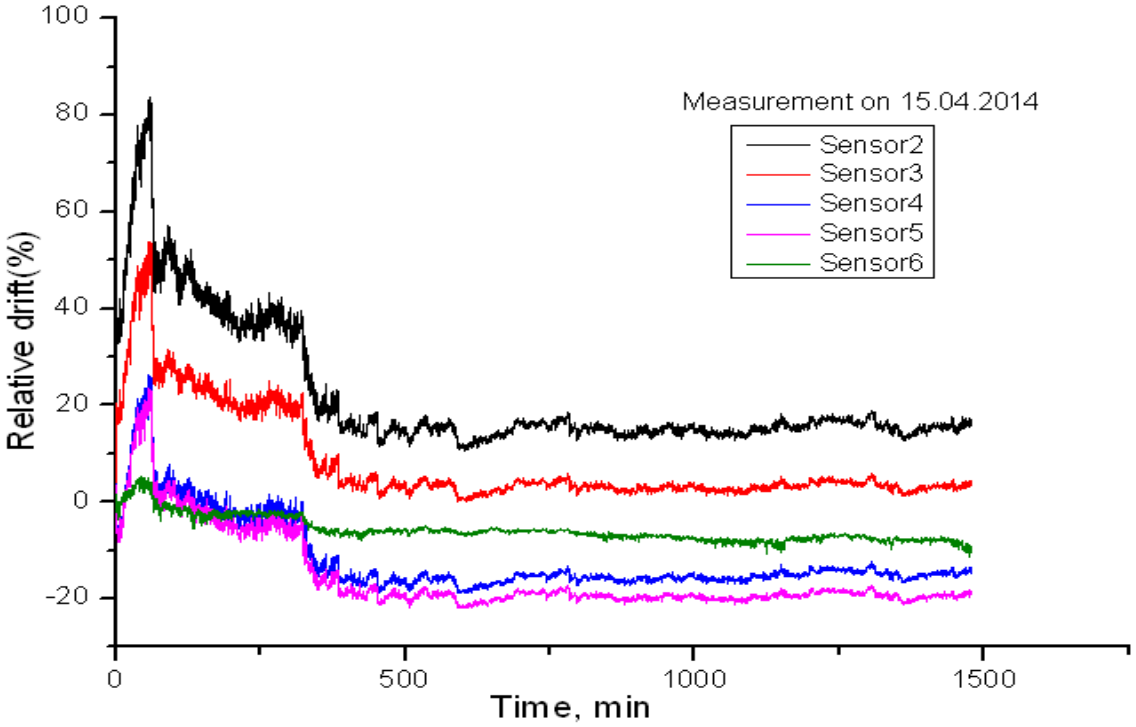

Figure A4: Relative drifts of sensors on exposure to gas mixture at room temperature measured on 15.04.2014 (Drifts of sensor2-6 are represented by curves with colors black, red, blue, pink and green respectively)

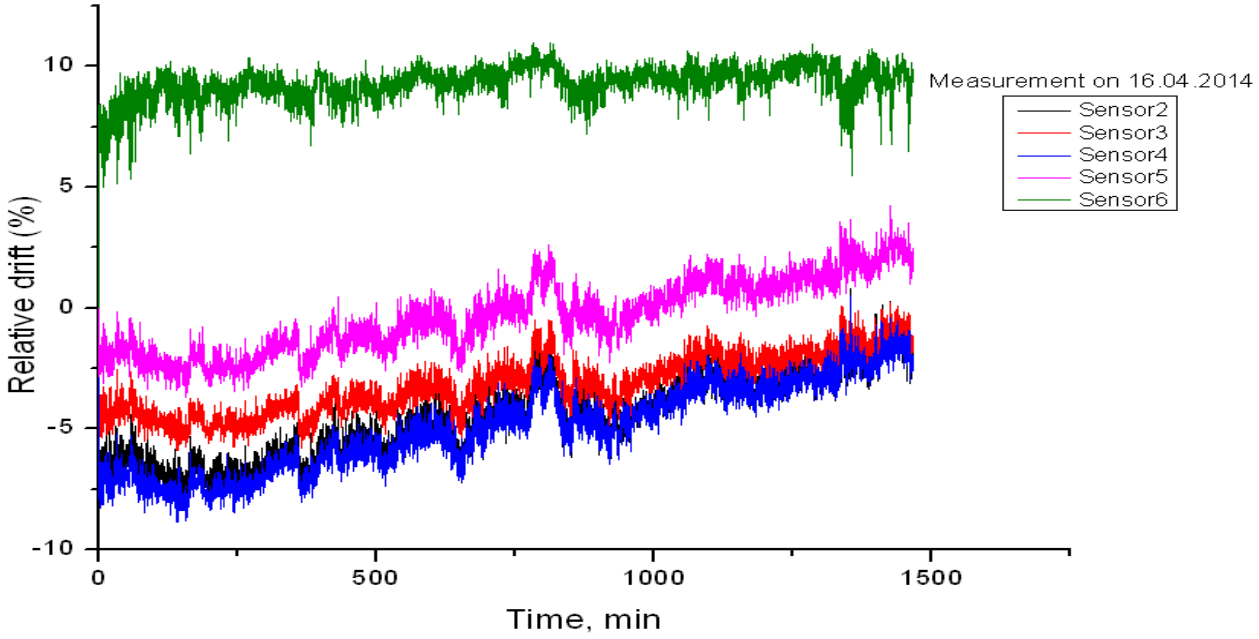

Figure A5: Relative drifts of sensors on exposure to gas mixture at room temperature measured on 16.04.2014 (Drifts of sensor2-6 are represented by curves with colors black, red, blue, pink and green respectively)

APPENDIX 4

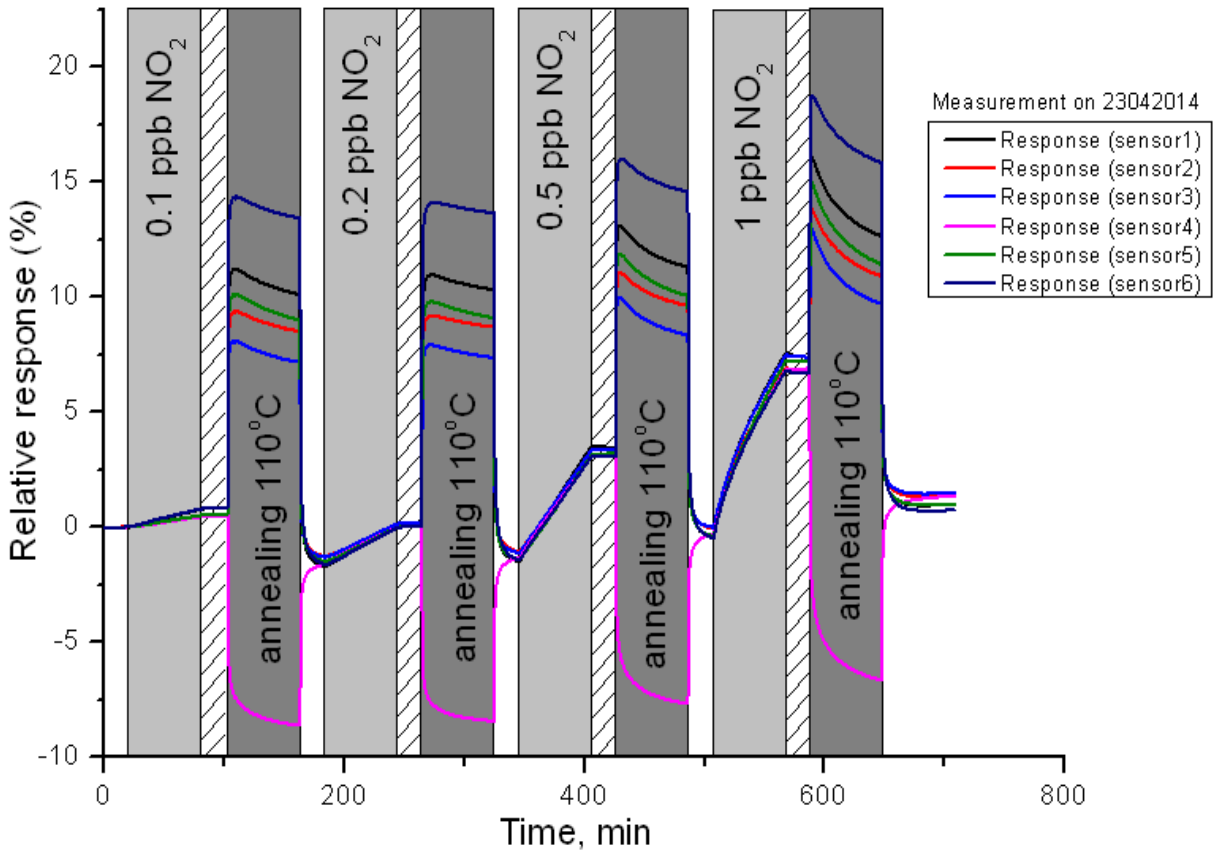

Figure A6: Responses of all sensors on exposure to gas mixture containing NO_2 at low concentration ranges at room temperature (Exposure periods are marked by light grey bands, recovery periods as hatched bands and annealing periods as dark grey bands. Responses of sensors 1-6 are represented by curves with colors black, red, blue, pink, green and violet respectively.) This repeated measurement was performed on 23.04.2014.

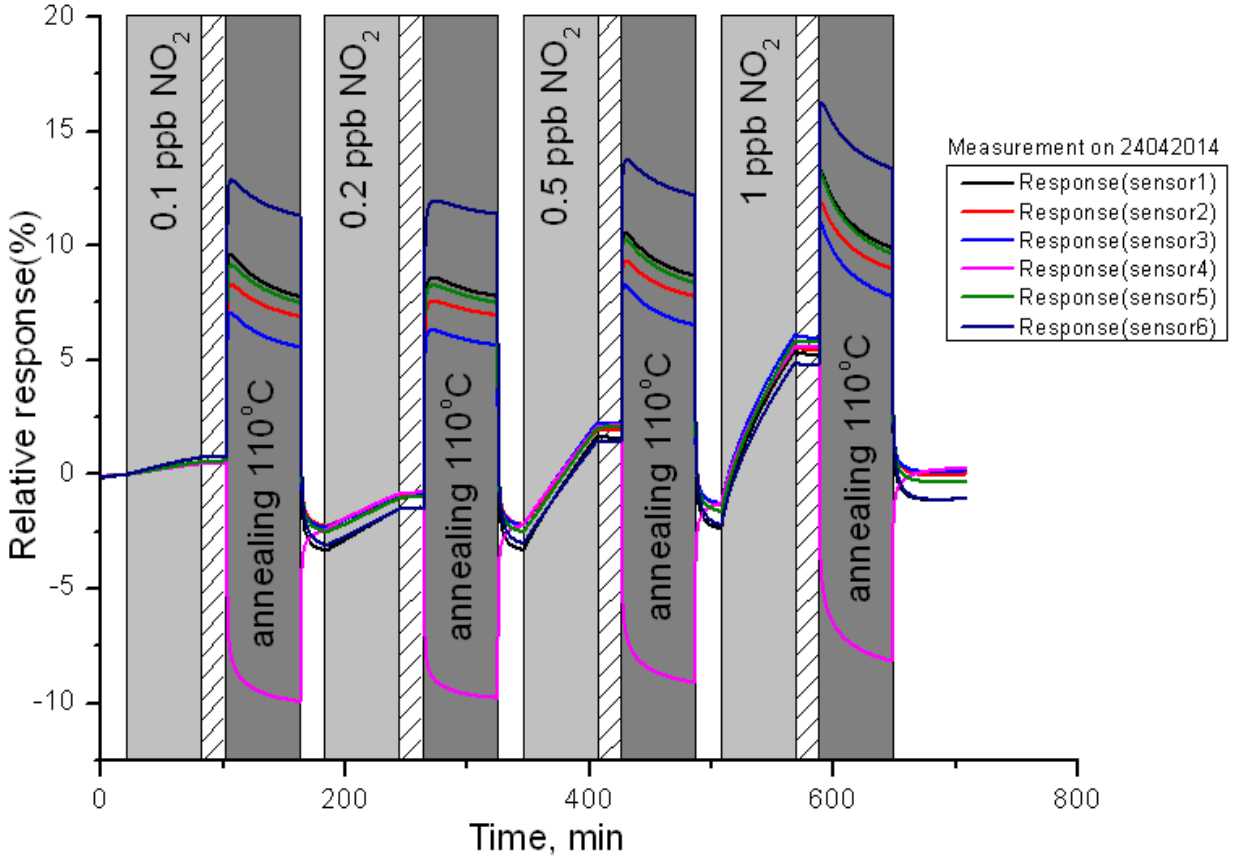

Figure A7: Responses of all sensors on exposure to gas mixture containing NO_2 at low concentration ranges at room temperature (Exposure periods are marked by light grey bands, recovery periods as hatched bands and annealing periods as dark grey bands. Responses of sensors 1-6 are represented by curves with colors black, red, blue, pink, green and violet respectively.) This repeated measurement was performed on 24.04.2014.

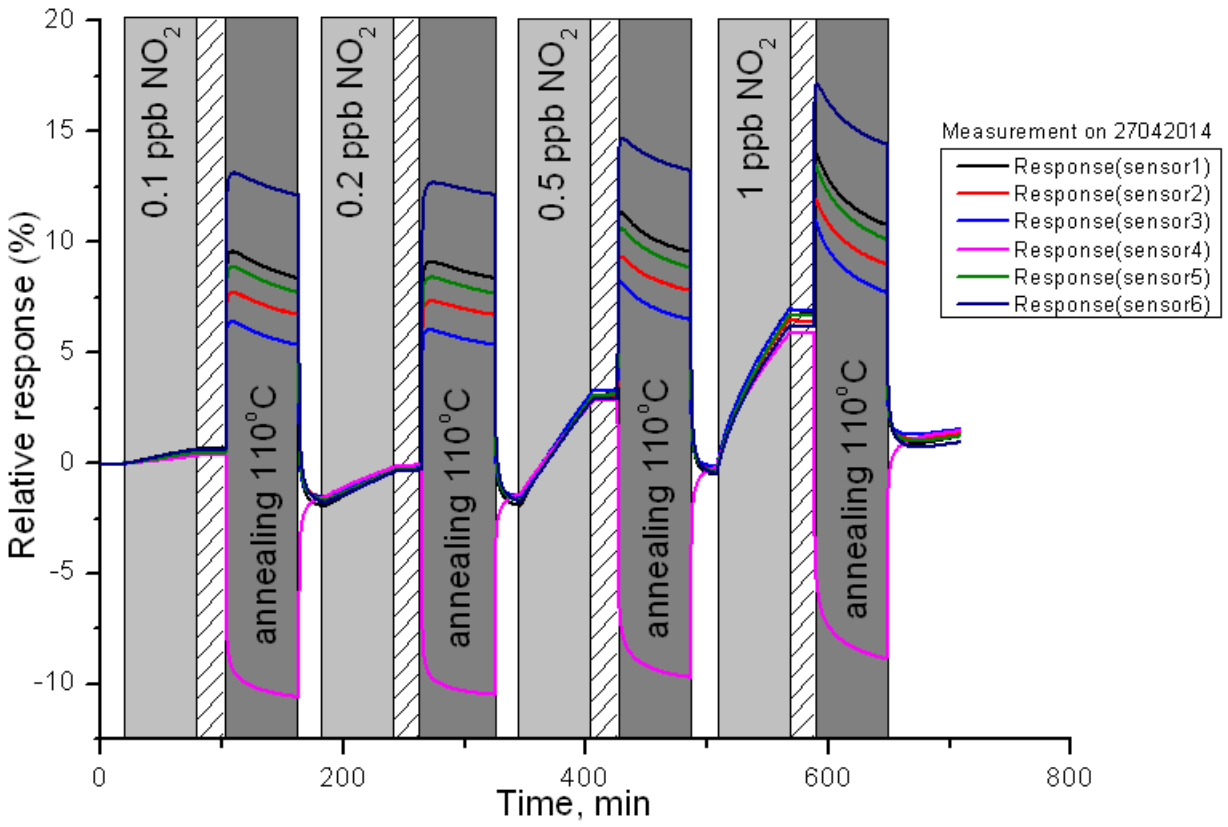

Figure A8: Responses of all sensors on exposure to gas mixture containing NO_2 at low concentration ranges at room temperature (Exposure periods are marked by light grey bands, recovery periods as hatched bands and annealing periods as dark grey bands. Responses of sensors 1-6 are represented by curves with colors black, red, blue, pink, green and violet respectively.) This repeated measurement was performed on 27.04.2014.

APPENDIX 5

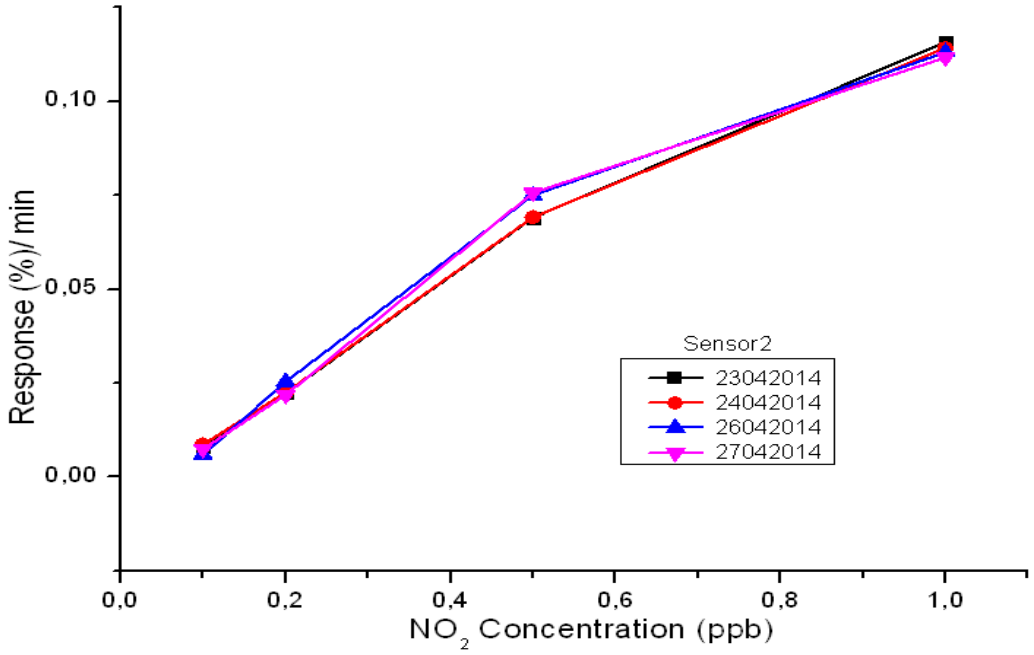

Figure A9: Dependence of the rates of responses for sensor2 on low NO_2 concentrations. The rate values were calculated for 60 minutes of exposure by the gas mixture containing NO_2. (Rates of responses of sensor2 for experiments on 23.04.2014, 24.04.2014, 26.04.2014 and 27.04.2014 are represented by black, red, blue and pink colored curves respectively.)

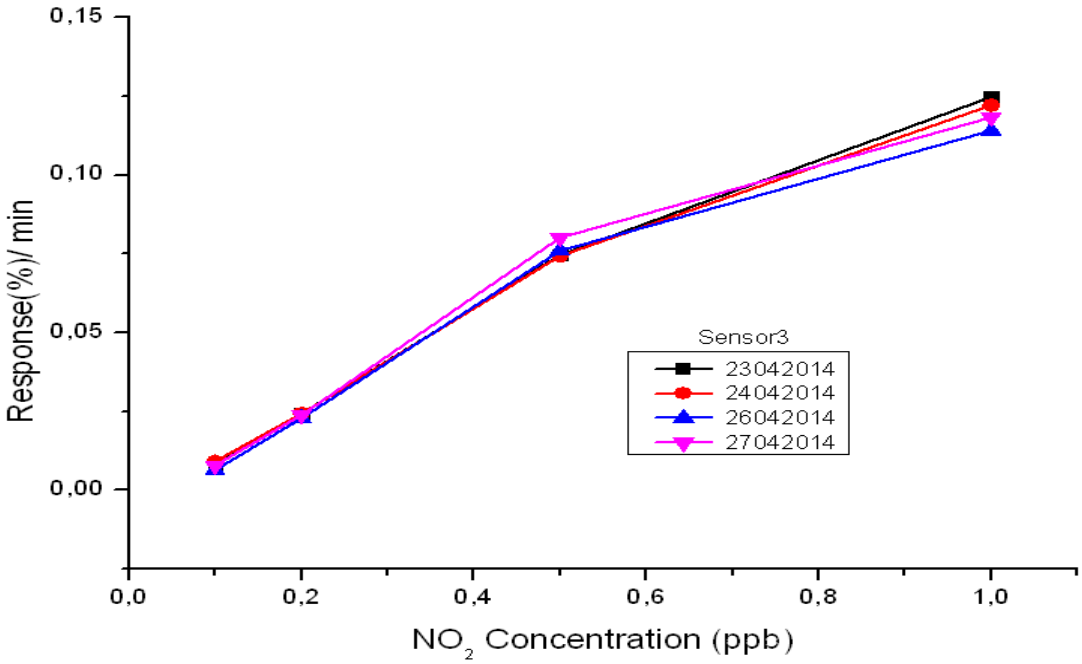

Figure A10: Dependence of the rates of responses for sensor3 on low NO_2 concentrations. The rate values were calculated for 60 minutes of exposure by the gas mixture containing NO_2. (Rates of responses of sensor3 for experiments on 23.04.2014, 24.04.2014, 26.04.2014 and 27.04.2014 are represented by black, red, blue and pink colored curves respectively.)

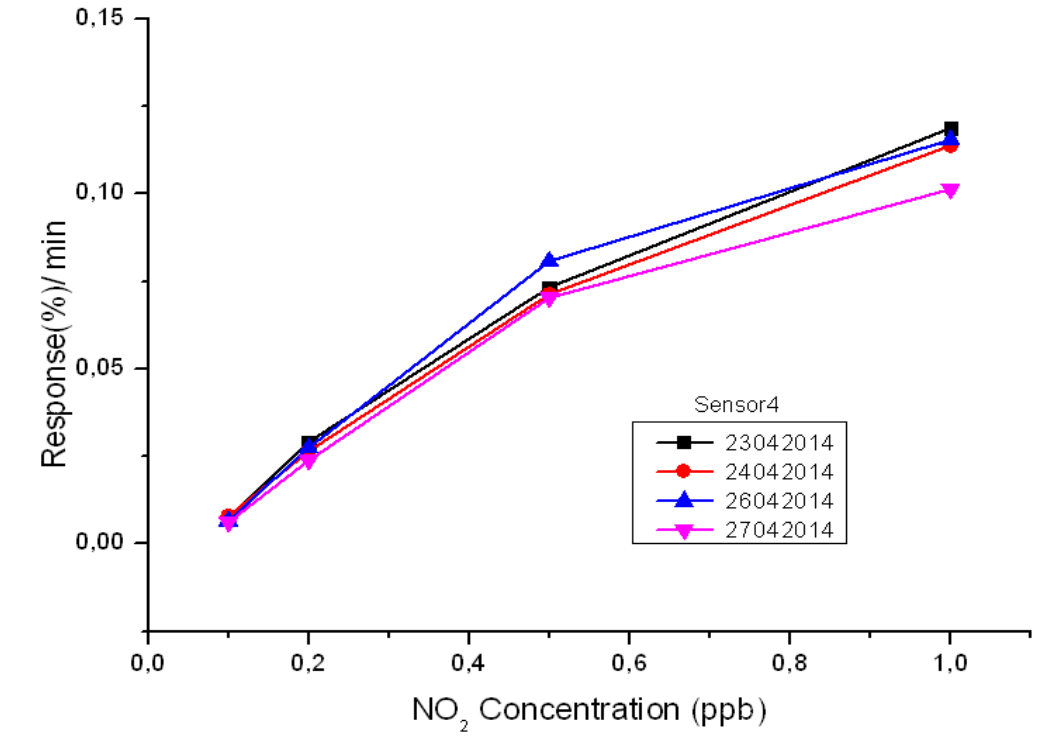

Figure A11: Dependence of the rates of responses for sensor4 on low NO_2 concentrations. The rate values were calculated for 60 minutes of exposure by the gas mixture containing NO_2. (Rates of responses of sensor4 for experiments on 23.04.2014, 24.04.2014, 26.04.2014 and 27.04.2014 are represented by black, red, blue and pink colored curves respectively.)

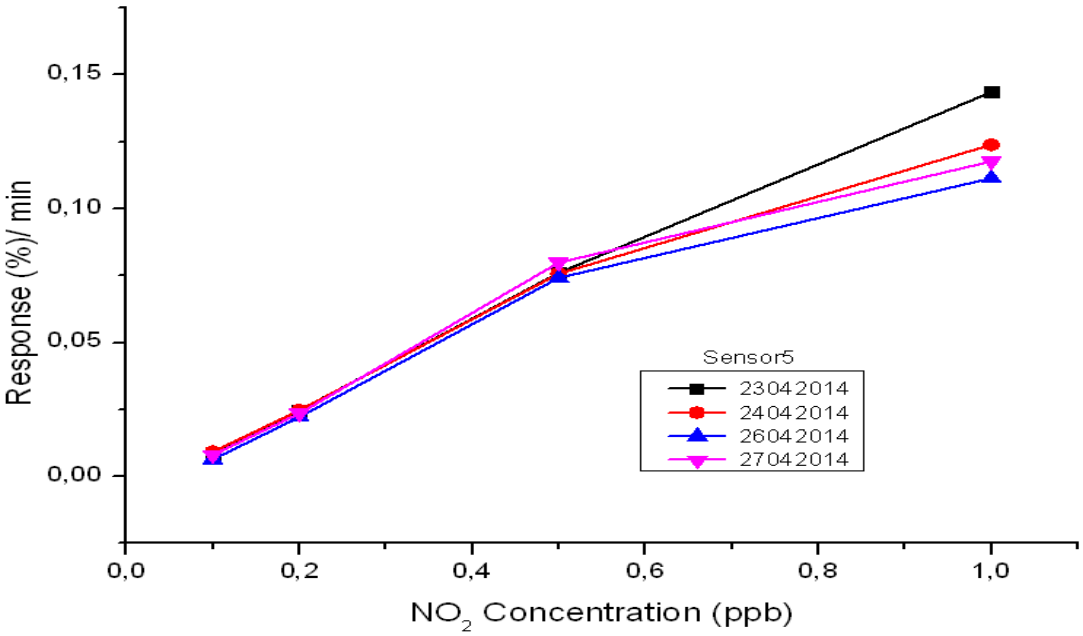

Figure A12: Dependence of the rates of responses for sensor5 on low NO_2 concentrations. The rate values were calculated for 60 minutes of exposure by the gas mixture containing NO_2. (Rates of responses of sensor5 for experiments on 23.04.2014, 24.04.2014, 26.04.2014 and 27.04.2014 are represented by black, red, blue and pink colored curves respectively.)

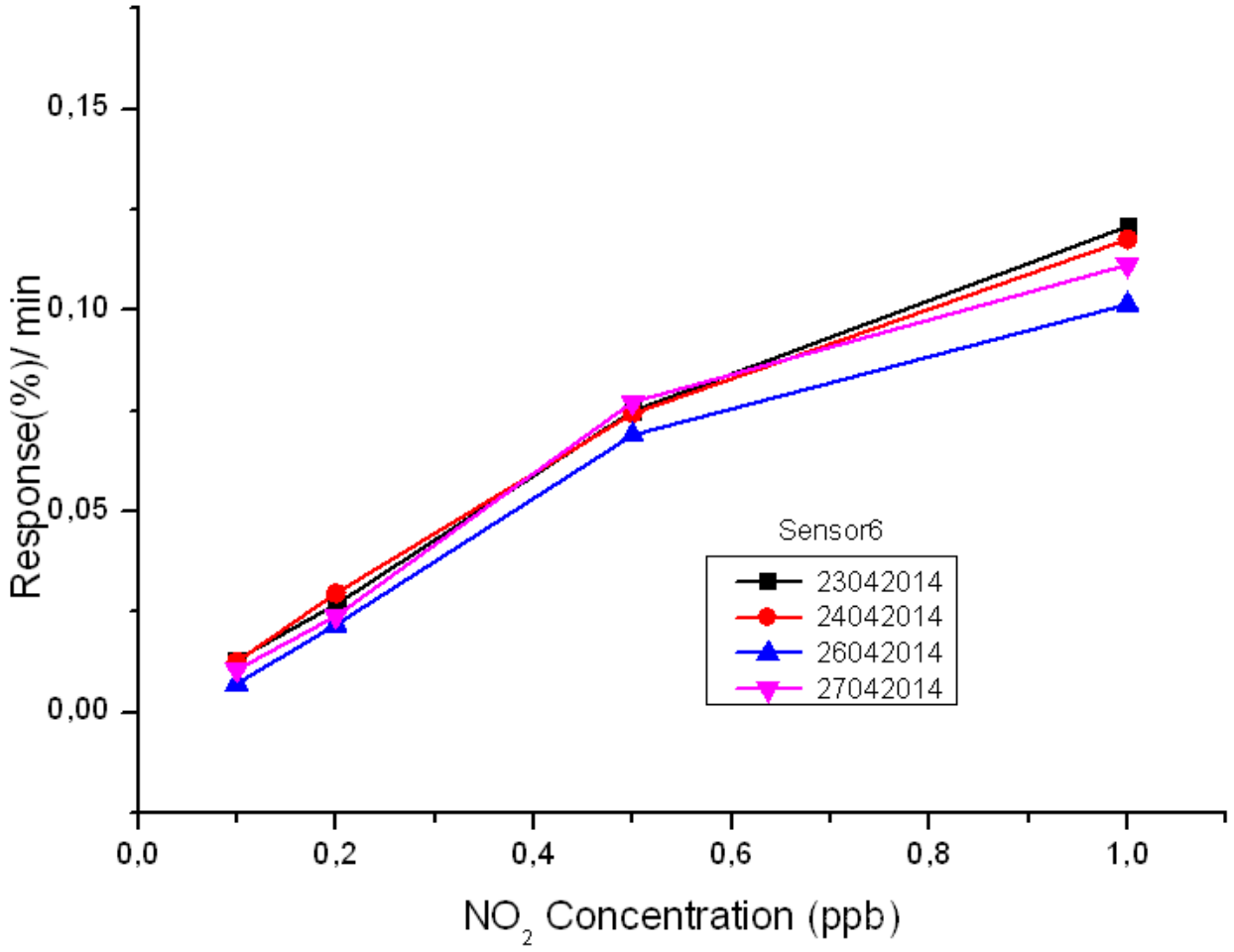

Figure A13: Dependence of the rates of responses for sensor6 on low NO_2 concentrations. The rate values were calculated for 60 minutes of exposure by the gas mixture containing NO_2. (Rates of responses of sensor6 for experiments on 23.04.2014, 24.04.2014, 26.04.2014 and 27.04.2014 are represented by black, red, blue and pink colored curves respectively.)

APPENDIX 6

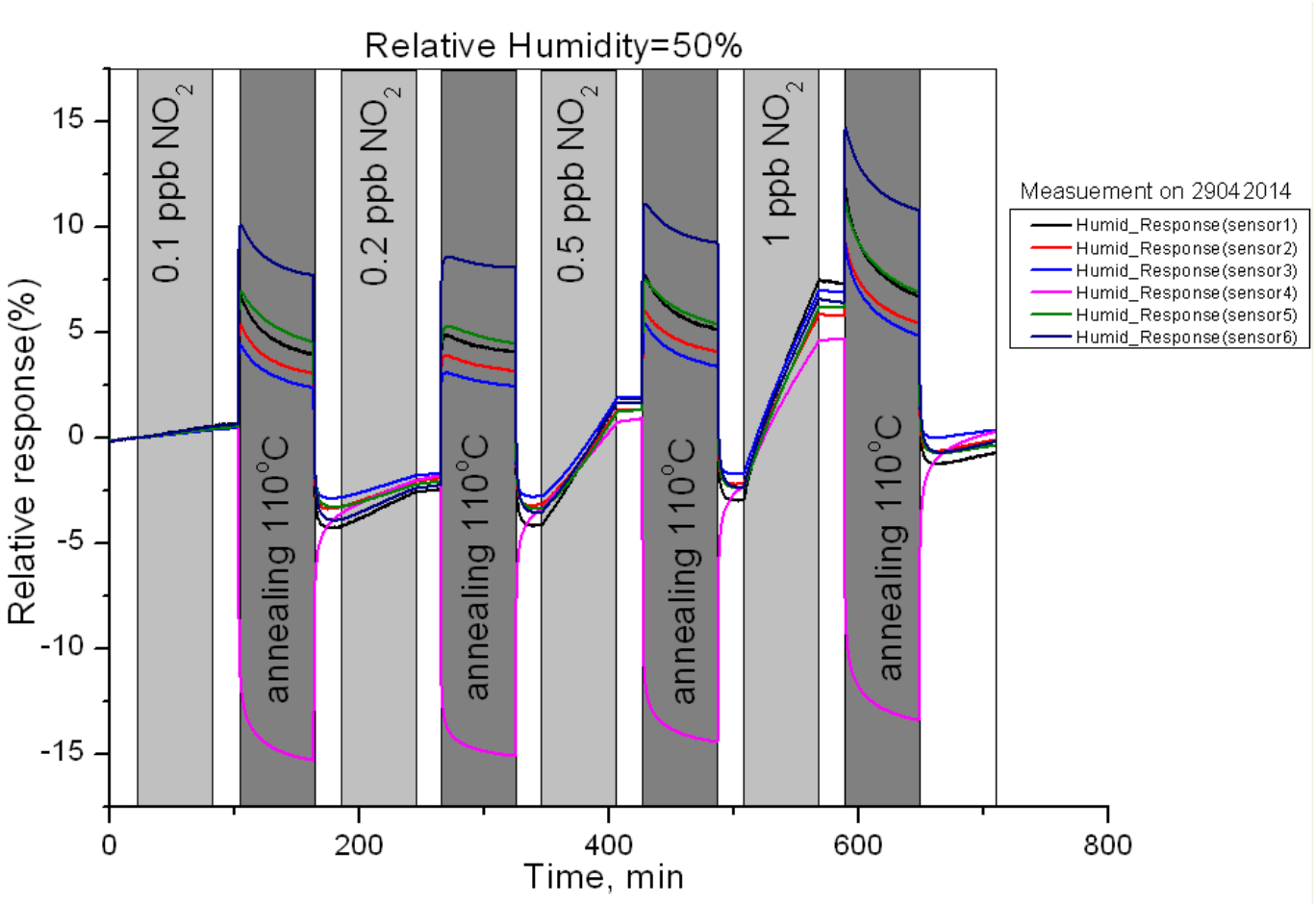

Figure A14: Responses of all sensors on exposure to gas mixture containing NO_2 at low concentration range at room temperature and RH=50% humid condition (Exposure periods are marked by light grey bands, recovery periods as hatched bands and annealing periods as dark grey bands. Responses of sensors 1-6 are represented by curves with colors black, red, blue, pink, green and violet respectively.) The repeated measurement was performed on 29.04.2014.

APPENDIX 7

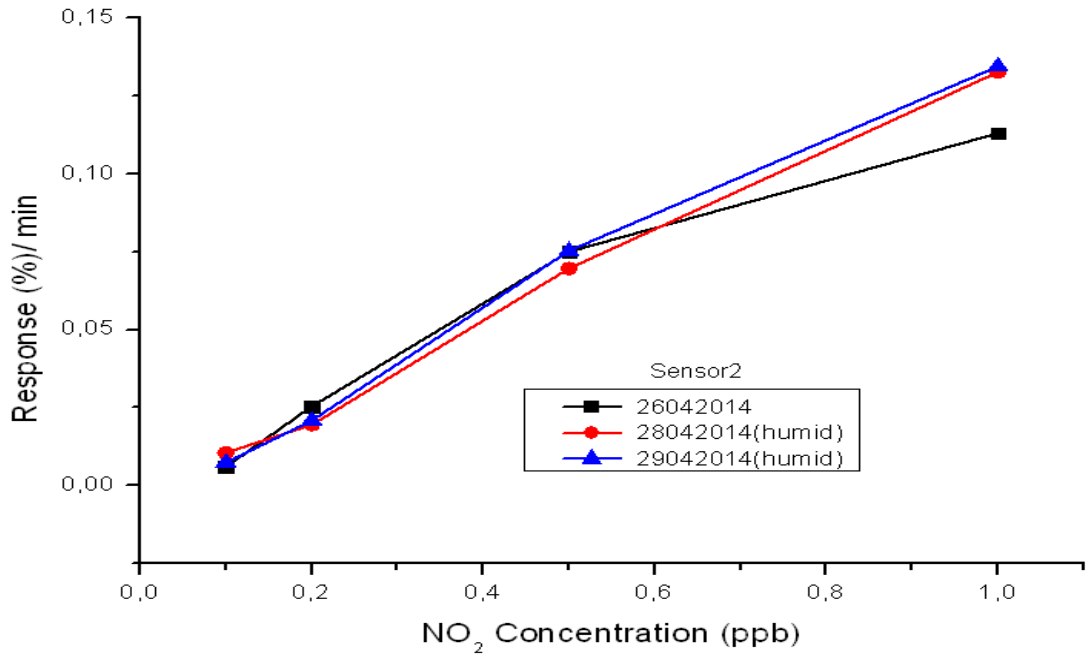

Figure A15: Comparison of the rates of responses for sensor2 under RH=0.02% and RH=50% humidity condition against low NO_2 concentrations. The rate values were calculated for 60 minutes of exposure by the gas mixture containing NO_2. (Rates of responses under RH=50% humidity condition are represented by red and blue curves while the black curve represents the rates of responses under RH=0.02% humidity condition.)

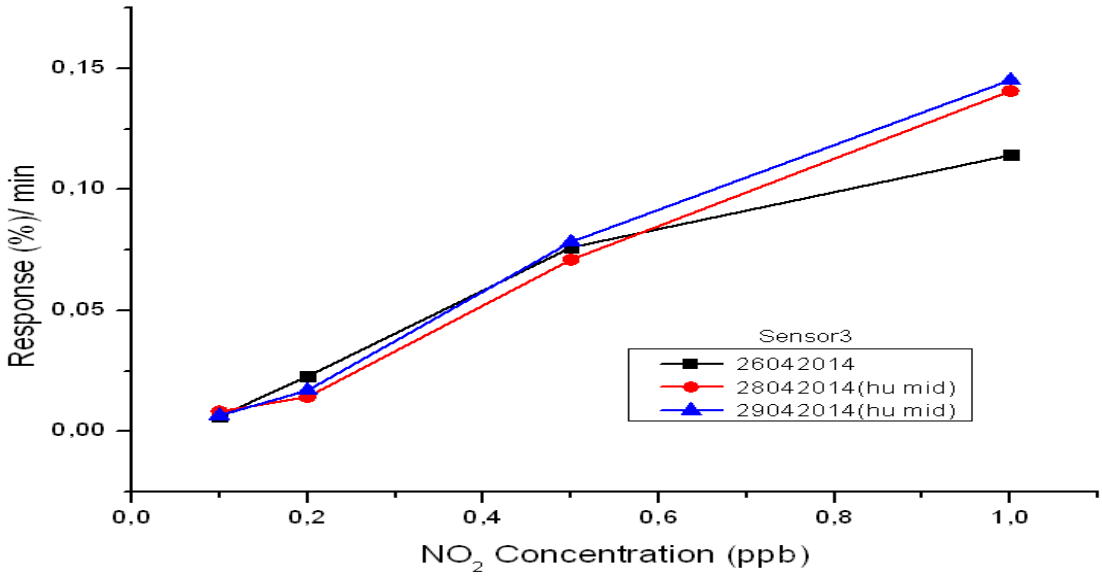

Figure A16: Comparison of the rates of responses for sensor3 under RH=0.02% and RH=50% humidity condition against low NO_2 concentrations. The rate values were calculated for 60 minutes of exposure by the gas mixture containing NO_2. (Rates of responses under RH=50% humidity condition are represented by red and blue curves while the black curve represents the rates of responses under RH=0.02% humidity condition.)

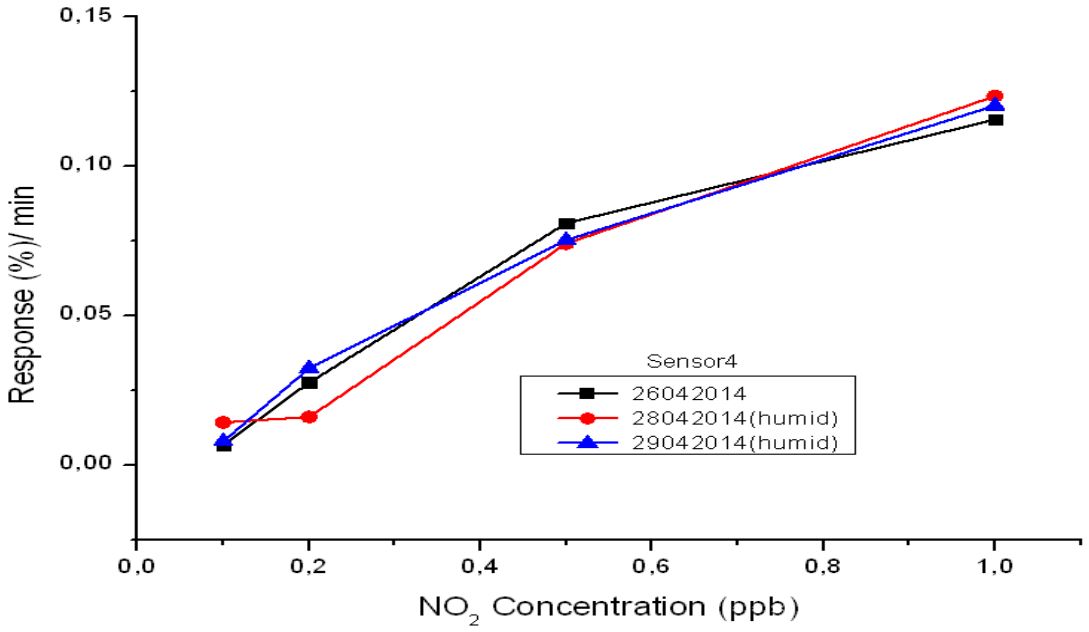

Figure A17: Comparison of the rates of responses for sensor4 under RH=0.02% and RH=50% humidity condition against low NO_2 concentrations. The rate values were calculated for 60 minutes of exposure by the gas mixture containing NO_2. (Rates of responses under RH=50% humidity condition are represented by red and blue curves while the black curve represents the rates of responses under RH=0.02% humidity condition.)

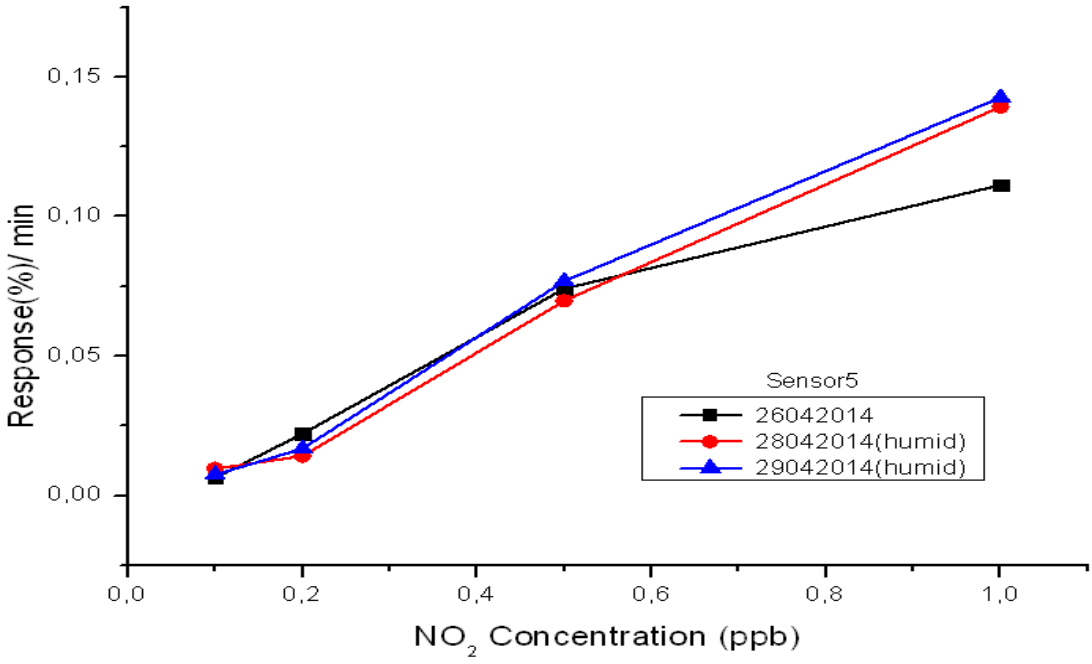

Figure A18: Comparison of the rates of responses for sensor5 under RH=0.02% and RH=50% humid condition against low NO_2 concentrations. The rate values were calculated for 60 minutes of exposure by the gas mixture containing NO_2. (Rates of responses under RH=50% humidity condition are represented by red and blue curves while the black curve represents the rates of responses under RH=0.02% humidity condition.)

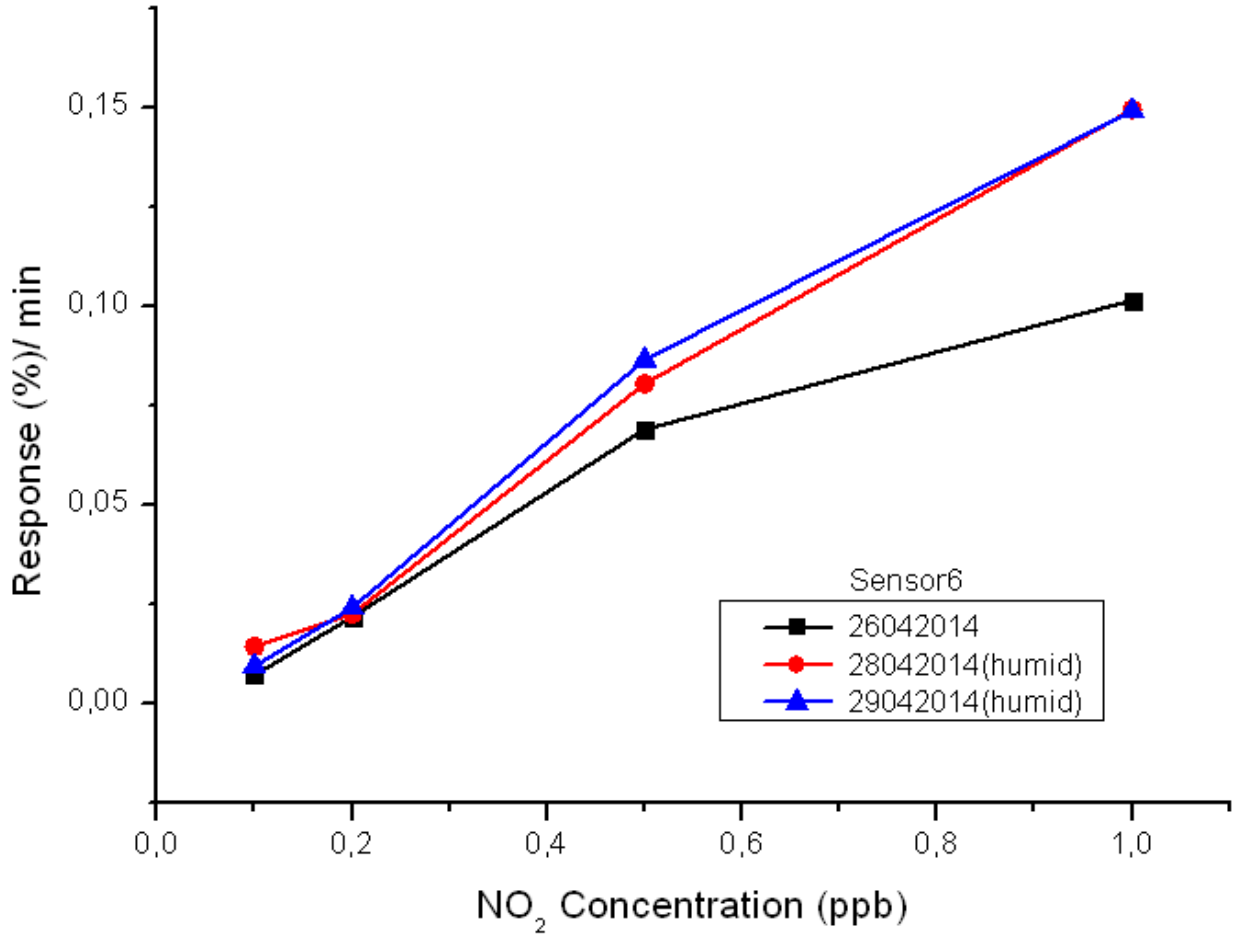

Figure A19: Comparison of the rates of responses for sensor6 under RH=0.02% and RH=50% humidity condition against low NO_2 concentrations. The rate values were calculated for 60 minutes of exposure by the gas mixture containing NO_2. (Rates of responses under RH=50% humidity condition are represented by red and blue curves while the black curve represents the rates of responses under RH=0.02% humidity condition.)

APPENDIX 8

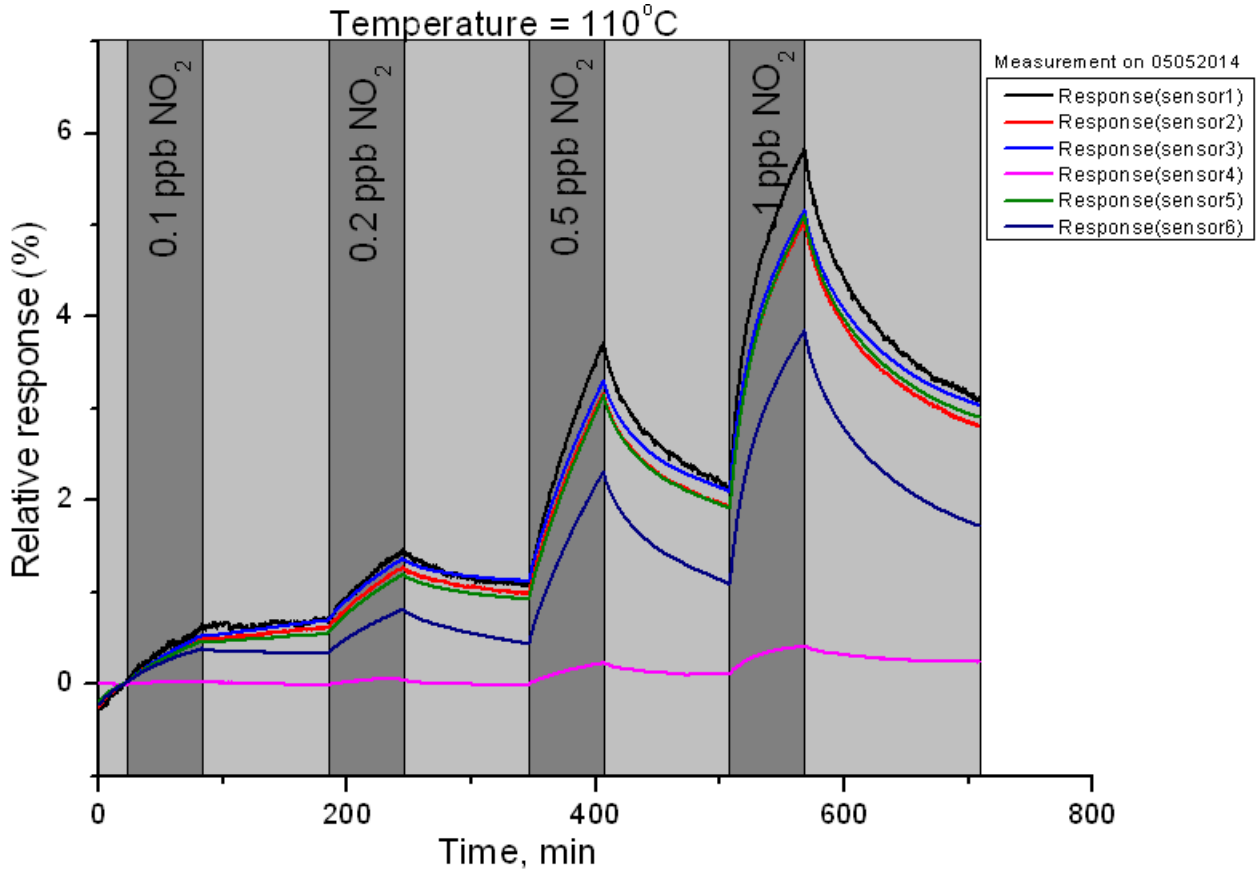

Figure A20: Responses of all sensors on exposure to gas mixture containing NO_2 at low concentration range at elevated temperature i.e. 110°C (Exposure periods are marked by dark grey bands, remaining non-exposure time interval acts as both recovery and annealing periods marked as light grey bands. Responses of sensors 1-6 are represented by curves with colors black, red, blue, pink, green and violet respectively.) The repeated measurement was performed on 05.05.2014.

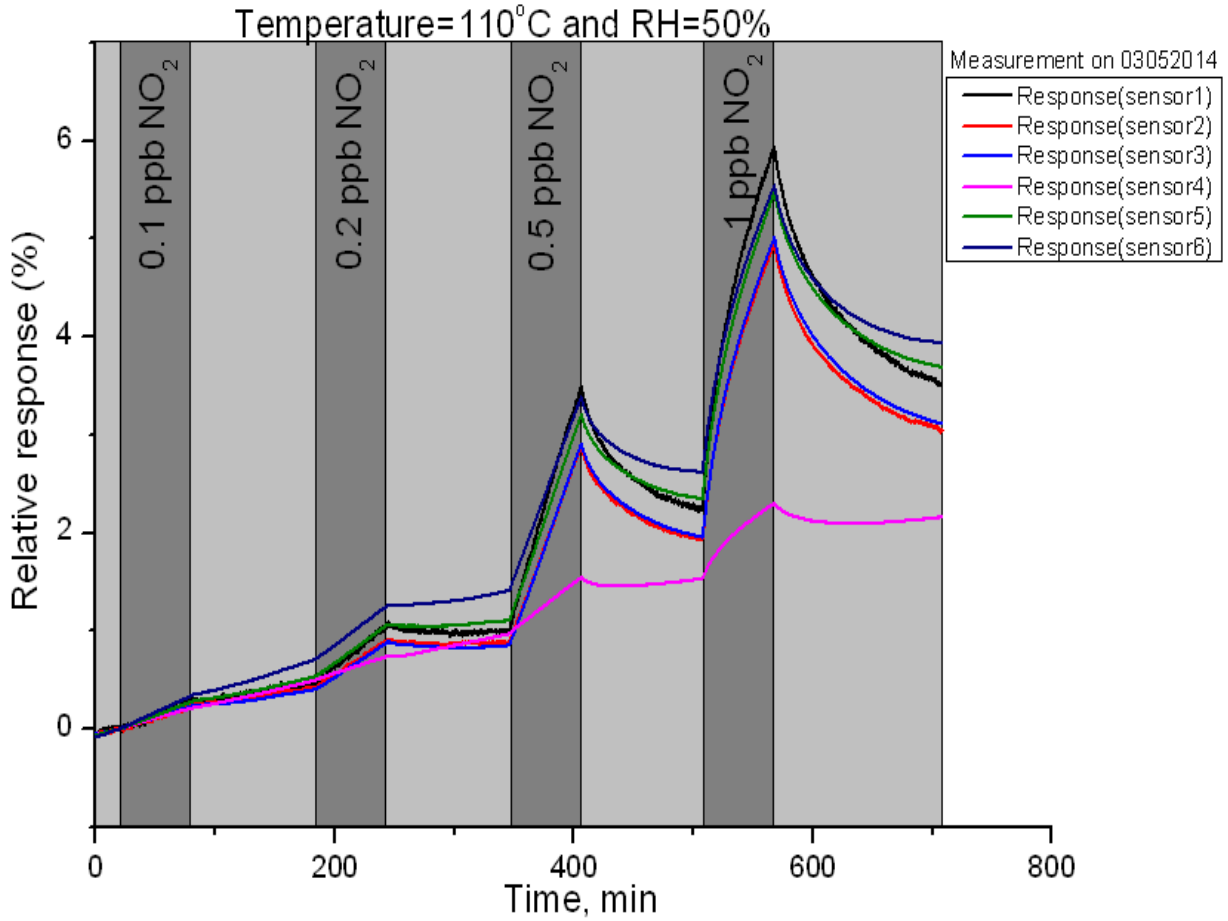

Figure 21: Responses of all sensors on exposure to gas mixture containing NO_2 at low concentration range at elevated temperature i.e. 110°C and relative humidity of 50% (Exposure periods are marked by dark grey bands, remaining non-exposure time interval acts as both recovery and annealing periods marked as light grey bands. Responses of sensors 1-6 are represented by curves with colors black, red, blue, pink, green and violet respectively.) The repeated measurement was performed on 03.05.2014.

APPENDIX 9

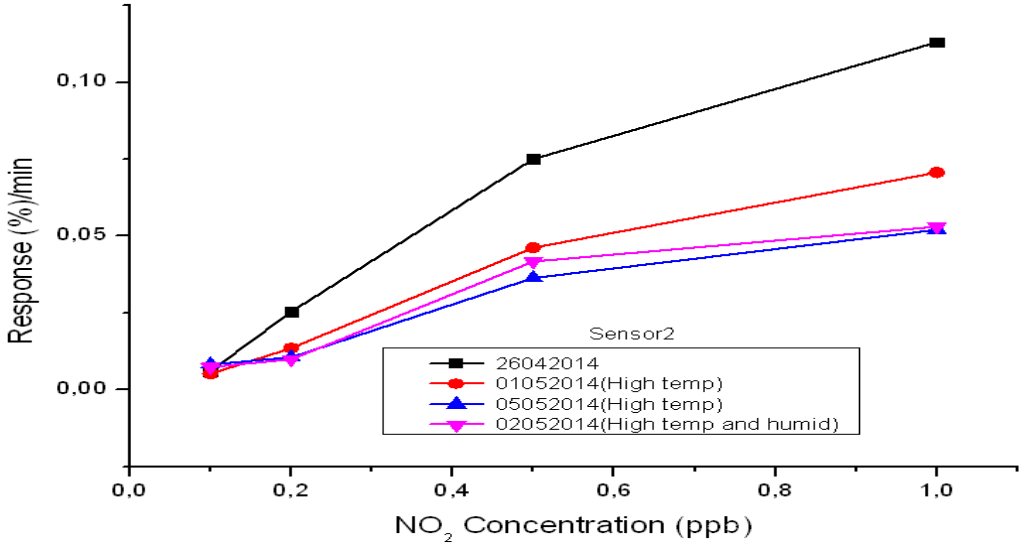

Figure A22: Comparison of the rates of responses for sensor2 at room temperature, at high temperature, and at high temp under RH=50% humid condition against low NO_2 concentrations. The rate values were calculated for 60 minutes of exposure by the gas mixture containing NO_2. (Rates of responses at room temperature are represented by black curve; rates of responses at high temperature are represented by red and blue curves while the pink curve represents the rates of responses at high temperature under humid condition.)

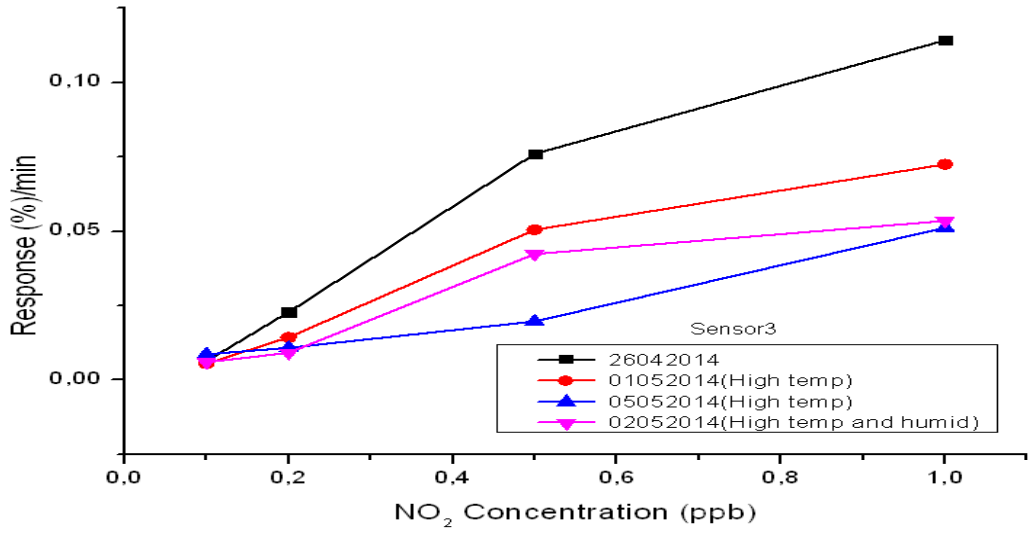

Figure A23: Comparison of the rates of responses for sensor3 at room temperature, at high temperature, and at high temp under RH=50% humid condition against low NO_2 concentrations. The rate values were calculated for 60 minutes of exposure by the gas mixture containing NO_2. (Rates of responses at room temperature are represented by black curve; rates of responses at high temperature are represented by red and blue curves while the pink curve represents the rates of responses at high temperature under humid condition.)

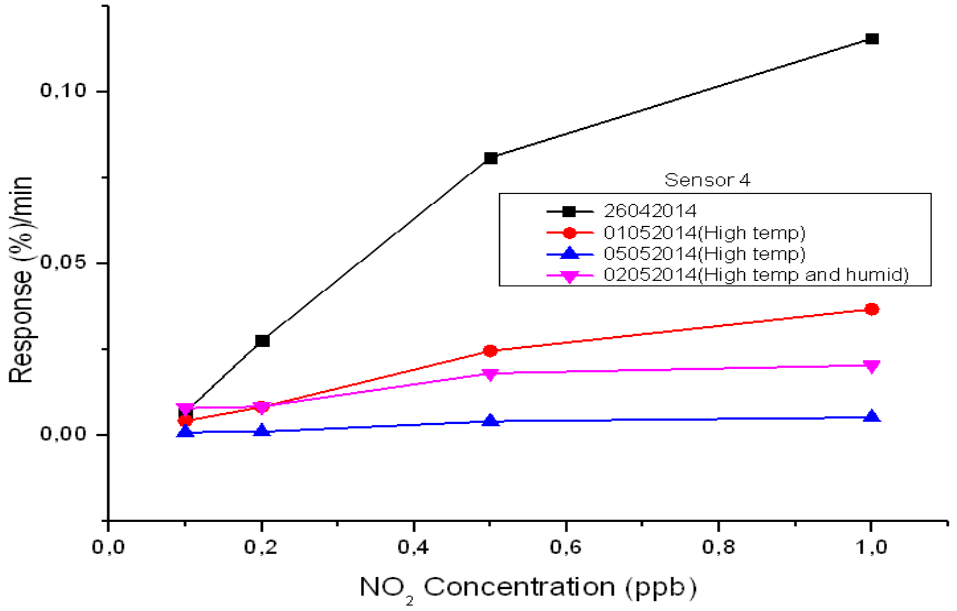

Figure A24: Comparison of the rates of responses for sensor4 at room temperature, at high temperature, and at high temp under RH=50% humid condition against low NO_2 concentrations. The rate values were calculated for 60 minutes of exposure by the gas mixture containing NO_2. (Rates of responses at room temperature are represented by black curve; rates of responses at high temperature are represented by red and blue curves while the pink curve represents the rates of responses at high temperature under humid condition.)

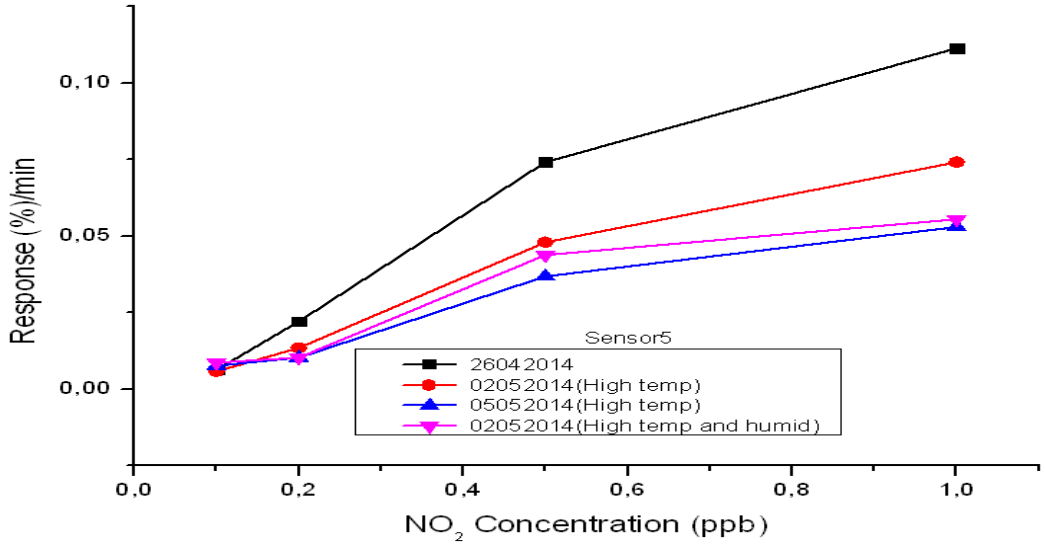

Figure A25: Comparison of the rates of responses for sensor5 at room temperature, at high temperature, and at high temp under RH=50% humid condition against low NO_2 concentrations. The rate values were calculated for 60 minutes of exposure by the gas mixture containing NO_2. (Rates of responses at room temperature are represented by black curve; rates of responses at high temperature are represented by red and blue curves while the pink curve represents the rates of responses at high temperature under humid condition.)

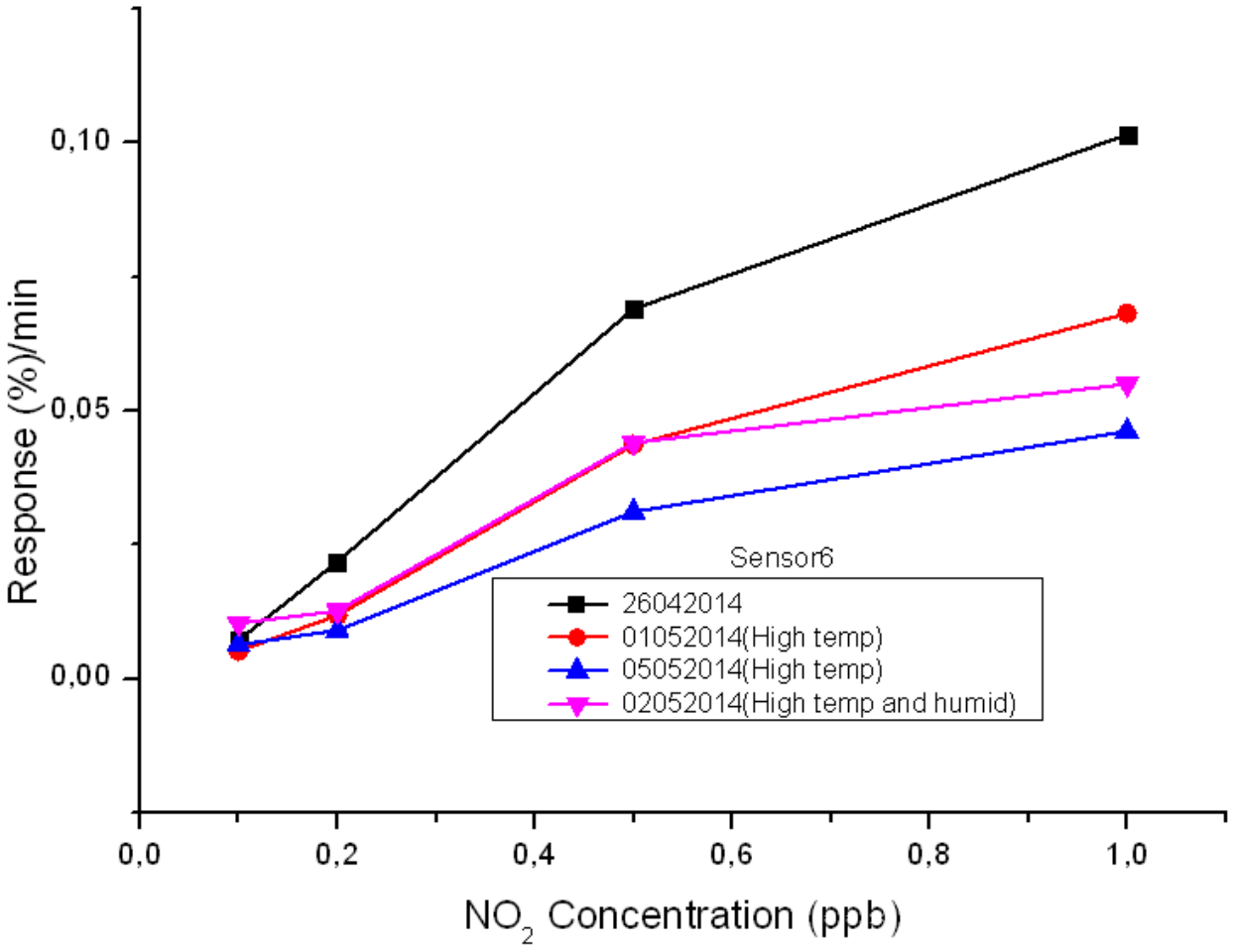

Figure A26: Comparison of the rates of responses for sensor6 at room temperature, at high temperature, and at high temp under RH=50% humid condition against low NO_2 concentrations. The rate values were calculated for 60 minutes of exposure by the gas mixture containing NO_2. (Rates of responses at room temperature are represented by black curve; rates of responses at high temperature are represented by red and blue curves while the pink curve represents the rates of responses at high temperature under humid condition.)